UNIVERSITY OF NAPLES "FEDERICO II"

DOCTORATE

MOLECULAR MEDICINE AND MEDICAL BIOTECHNOLOGY

XXIX CYCLE

Characterization of Hypoxia Inducible Factor HIF-1α function and identification of its targets to improve therapeutic intervention in Neuroblastoma malignancy.

TUTOR

Ch.mo Prof. Achille Iolascon

CANDIDATE

Marianna Avitabile

COORDINATOR

Ch.mo Prof. Vittorio Enrico Avvedimento

ACADEMIC YEAR 2016-2017

INDEX

Abbrevations

ATRA	All Trans Retinoic Acid
CNS	Cancer Stem Cell
CSC	Central Nervous System
GWAS	Genome Wide Association Studies
HYP	Hypoxia
IDRFS	Renamed Image-Defined Risk Factors
INRG	International Neuroblastoma Risk Group
INSS	International Neuroblastoma Staging System
IODs	Integral Optical Densitometry
MRD	Minimal Residual Disease
MTT	3-(4,5-Dimethylthiazol-2l),5-Diphenyltetrazolium Bromide
NB	Neuroblastoma
NX	Normoxia
RA	Retinoic Acid
RNA-seq	RNA sequencing
RT-PCR	Real Time Plymease Chain Reaction
SNP	Single Nucleotide Polymorphism
SNS	Sympathetic Nervous System
WES	Whole Exome Sequencing

ABSTRACT

Neuroblastoma (NB) is the most frequent malignant tumor in pediatric age derived from primitive cells of the sympathetic nervous system. It is composed of cells with different levels of neural differentiation and high tumor cell differentiation grade correlates with a positive outcome. Current NB treatments include surgery, the use of radio or cytotoxic therapies and the pro differentiating agents as retinoids to eradicate minimal residual disease (MRD). Nowadays there is no treatment that heals completely NB. Expression of the hypoxia inducible factors (HIFs) *HIF1A* and *EPAS1* and/or hypoxia-regulated pathways has been shown to promote the undifferentiated phenotype of NB cells. The first hypothesis of this study is that *HIF1A* and *EPAS1* expression represents one of the mechanisms responsible for the lack of responsiveness of NB to differentiation therapy.

Clinically, high levels of *HIF1A* and *EPAS1* expression were associated with inferior survival in two NB microarray datasets, and patient subgroups with lower expression of *HIF1A* and *EPAS1* showed significant enrichment of pathways related to neuronal differentiation. In NB cell lines, the combination of all-*trans* retinoic acid (ATRA) with *HIF1A* or *EPAS1* silencing led to an acquired glial-cell phenotype and enhanced expression of glial-cell differentiation markers. Furthermore, *HIF1A* or *EPAS1* silencing might promote cell senescence independent of ATRA treatment. Taken together, this data suggest that HIFs inhibition with ATRA treatment promotes differentiation into a more benign phenotype and cell senescence *in vitro*.

Between HIFs, *HIF1A* is the most promising factor to be silenced to induce differentiation in cotreatment with ATRA. *HIF1A* protein expression is changeble inside solid tumors because of oxygen levels. The second intent of this study has been to indentify *HIF1A* target genes whose expression is activated or repressed by *HIF1A* regardless microenviroment. The expression of these "*HIF1A* target genes" will be related to all tumor area and their silencing might lead solid tumor to be easily wiped out. Transcriptome analysis of *HIF1A* silenced NB cell lines and in silico analysis have suggested putative *HIF1A* targets to be used in combination with ATRA. These findings open the way for additional lines of attack in the treatment of NB minimal residue disease.

1 BACKGROUND

1.1 Neuroblastoma

Neuroblastoma (NB) is the most common extracranial solid tumor in childhood. The median age at diagnosis is ~19 months, but rarely, there are cases observed in utero or in patients older than 19 years [1]. The incidence of NB is 10.2 cases per million children under 15 years of age [2]. Tumors can arise anywhere along the sympathetic nervous system (SNS), with the majority occurring in the abdomen and are associated with the adrenal gland or sympathetic ganglia (Figure1). It is widely accepted, that the cell of origin for NB arises from the sympathoadrenal lineage of the neural crest during development. The neural crest is present only during embryogenesis and gives rise to several cell types including peripheral neurons, enteric neurons, glia, melanocytes, Schwann cells, cells of the craniofacial skeleton and adrenal medulla [3]. Cells arising in the adrenal medulla are postganglionic neurons that have lost their dendrites and axons. Preganglionic neurons from the central nervous system (CNS) connect directly to adrenal medulla cells and stimulate the release of catecholamines. Thus, the adrenal medulla is a ganglion of the SNS.

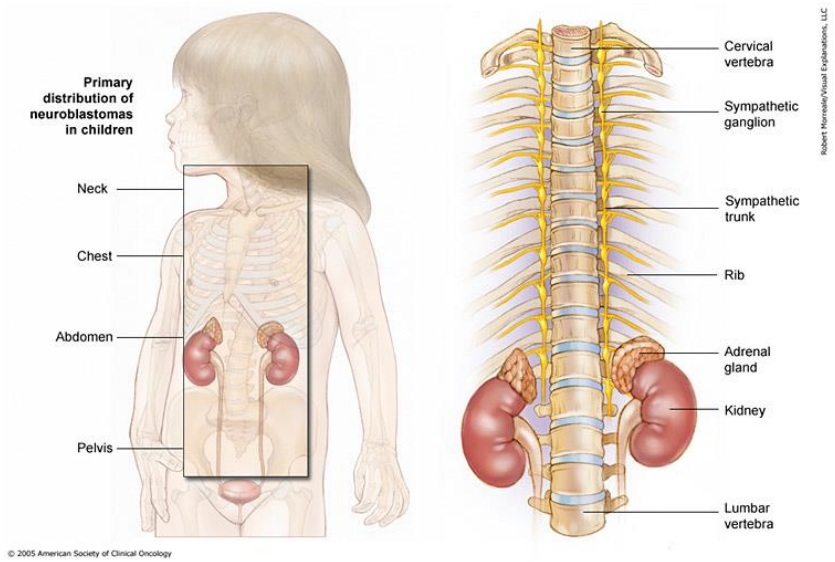

Figure 1. Clinical Presenations of Neuroblastoma (*American Society of Clinical Oncology 2005***)**

Similar to normal neuroblasts, NBs show variable amounts of differentiation along gangliocytic and schwannian lineages. In fact the undifferentiated form of NB can spontaneously differentiate in a less aggressive type such as the Ganglioneuroma or Ganglioneuroblastoma enriched in Schwannian stoma. The pathologic classification of the tumor is based on its differention grade, which reflectes the prognosis. For over a century, researchers observed that NBs exhibit diverse and often dramatic clinical behaviors. It accounts for disproportionate mortality among the cancers of childhood; but in the same time it is associated with one of the highest proportions of spontaneous and complete regression of all human cancers [4,5].

1.2 Staging

NB is distinguished from other solid tumors by its biologic heterogeneity and range of clinical behavior. Diagnosis and staging criteria are based on the International Neuroblastoma Staging System (INSS) first published in 1988, that allowed physicians to determine treatment plans based on patient risk [6] (Table 1).

Table 1: The international neuroblastoma staging system (INSS)

Stage 1	Localized tumour with complete gross excision, with or without microscopic residual disease; representative ipsilateral lymph nodes negative for tumour microscopically (nodes attached to and removed with the primary tumour may be positive).
Stage 2A	Localized tumour with incomplete gross excision; representative ipsilateral nonadherent lymph nodes negative for tumour microscopically.
Stage 2B	Localized tumour with or without complete gross excision, with ipsilateral nonadherent lymph nodes positive for tumour. Enlarged contralateral lymph nodes must be negative microscopically.
Stage 3	Unresectable unilateral tumour infiltrating across the midline (vertebral column) with or without regional lymph node involvement; or localized unilateral tumour with contralateral regional lymph node involvement; or midline tumour with bilateral extension by infiltration (unresectable) or by lymph node involvement.
Stage 4	Any primary tumour with dissemination to distant lymph nodes, bone, bone marrow, liver, skin and/or other organs (except as defined for stage 4S).
Stage 4S	Localized primary tumour (as defined for stage 1, 2A or 2B), with dissemination limited to skin, liver and/or bone marrow (limited to infants <1 year of age).

Table 1 The international neuroblastoma staging system (INSS)

Age and stage of disease are two criteria for risk classification. Children 18 months old or older with stage 4 (metastatic disease) are at high risk for death from refractory disease. In contrast, infants younger than 12 months with localized tumors (stage 1-2) almost always cured, often without cytotoxic therapy. Molecular analysis is a critical step in risk stratification and clinical care planning for NB. The challenge has been to identify which children may

benefit from treatment reduction versus intensified therapies. INSS staging, used for more than 20 years, was influenced by the location of the primary tumor (e.g., intrathoracic versus abdominal primary), access to experienced pediatric surgery and pathology teams, and access to detailed radiographic imaging. To compensate these variables, the European International Society of Pediatric Oncology, validated a set of surgical risk factors based on radiographic characteristics, that could be used preoperatively to assess resectability and risk of developing postoperative complications [7]. These characteristics, renamed image-defined risk factors (IDRFs), are incorporated into the (International Neuroblastoma Risk Group Staging System/INRGSS). The INRG classification system includes INRG stage, age, histology, tumor grade, *MYCN* status, 11q alteration status, and DNA ploidy. Based on this, clinically different pretreatment groups were described as: very low, low, intermediate, and high-risk in terms of 5-year event-free survivals (Table 2).

INRG stage	Age (months)	Histologic category	Grade of tumor, differentiation	MYCN	11q aberration	Ploidy	Pretreatment risk group
L1/L2	Any	GN maturing or GNB intermixed	Any	Any	Any	Any	A Very low
L1	Any	Any, except GN maturing or GNB intermixed	Any	NA Amp	Any	Any	B Very low K High
L2	<18	Any, except GN maturing or GNB intermixed	Any	NA NA	No Yes	Any	D Low G Intermediate
L2	>18	GN nodular; Neuroblastoma	Differentiating Differentiating Poorly differentiated or undifferen-tiated	NA NA NA Amp	No Yes	Any	E Low H Intermediate H Intermediate N High
M	<18 <12 12 to <18 <18 ≥18	Any	Any	NA NA NA Amp	Any	Hyperdiploid Diploid Diploid	F Low J Intermediate J Intermediate O High P High
MS	<18	Any	Any	NA NA Amp	No Yes	Any	C Very low Q High R High

Abbreviations and definitions: GN, ganglioneuroma; GNB, ganglioneuroblastoma; NA, nonamplified; Amp, amplified; diploid, DNA index ≤1.0; hyperdiploid, DNA index >1.0 and includes near-triploid and near-tetraploid tumors; very low risk, five-year event-free survival (EFS) >85%); low risk, five-year EFS >75% to ≤85%; intermediate risk, five-year EFS ≥50% to ≤75%; high risk, five-year EFS <50%.

Table 2 International Neuroblastoma Risk Group (INRG) consensus pretreatment classification schema *(Journal of Clinical Oncology 2009)*

These risk groups can be used to assign treatment recommendations or assess a patient's eligibility for participation in investigational studies [8]. Prospective implementation of the new INRG classification system will also allow improvements in collaborative efforts on international clinical trials.

1.3 Genetic basis

About thirty years of study on NB, some genetic alterations as prognostic factor of disease have been identified. The genetic aberration most consistently associated with poor outcome is genomic amplification of *MYCN* [9]. *MYCN* amplification occurs in roughly 20% of primary tumours and is strongly correlated with advanced stage disease and treatment failure [10]. Segmental chromosomal aberrations, most frequently found in 1p, 1q, 3p, 11q, 14q, and 17p, are associated or not with *MYCN* amplification, and are observed in almost all high-risk and/or stage 4 NBs [11].

Furthermore, copy number changes of whole chromosomes are also commonly observed in NB, and are closely associated with the ploidy of the tumors. In most cases, karyotypes of NB cells are either in the diploid ('near-diploid') or hyperdiploid ('near-triploid') range. These alterations have been associated with more favorable outcome if correlated to a younger age at diagnosis, and to lack of structural chromosomal aberrations of the patients [12,13].

Genome-wide association studies (GWAS) focused on single nucleotide polymorphisms (SNPs) that provided the basis for the identification of activating mutations in the Anaplastic Lymphoma Kinase (*ALK*) oncogene. These mutations appear to be responsible for most of the rare cases of hereditary NB, and might also be relevant for a smaller fraction (6-9%) of sporadic tumors [14,15].

GWAS studies have discovered common predisposing genetic variants, that are associated with tumor phenotype and NB susceptibility [16]. These findings suggest that genomic variation may underlie events that initiate tumorigenesis. Susceptibility to low-risk NB is associated with SNPs within *DUSP12* (at 1q23), *HSD17B12* (at11p11.2), *DDX4*, and *IL31RA* (both at5q11.2) and correlate with

less aggressive disease [17]. SNPs at *FLJ22536, FLJ44180* (6p22), *CASC15, CASC14, NEFL, BARD1, LM01, HACE1*, and LIN28B have been found in DNA copy number variants of high-risk NB and also represent a source of genetic diversity [18-21]. Common variant polymorphisms may work additively to activate NB tumor initiation. Several of these DNA variations influence gene and protein expression to promote tumorigenesis and tumor progression. This is exemplified by compelling evidence in *BARD1. It* is the most significant genetic contributor to NB risk and may promote tumor growth and progression [22].

High throughput sequencing-based studies have highlighted that recurrent mutations of single genes are infrequent in primary NB with activating mutation in *ALK* and inactivating mutations in *ATRX* and *TERT* being the most frequent. In latest years mutations in RAS-MAPK signaling associated genes as *NRAS, KRAS, HRAS, BRAF, PTPN11*, and *FGFR1* were detected in the relapsed samples and were absent in the samples at diagnosis [23-27]. These data suggest the oncogenic evolution of “low frequency” mutated genes from samples at diagnosis to relaps. The identification of somatic “driver mutations” raises a new challenge in the treatment of cancer that involves the use of a selection of therapies based on different genetic alterations in individual tumors.

1.4 Therapy and Differentiation

The biologic heterogeneity of neuroblastic tumors occurring in pediatric age leds to a disparity of used therapeutic approches. For tumors that have favorable biologic features, the clear trend has been to reduce therapeutic intensity. In contrast, the approach to tumors with adverse prognostic features has shifted toward an intensifying chemoradiotherapy and research of personalized cures [28].

The induction of differentiation seems one of the most promising approaches following cytotoxic treatment, in the minimal residual disease (MRD) therapy in high-risk NB patients. The beneficial effects of "differentiating treatment" are well-known in acute promyelocytic leukemia where the standard treatment

involves the use of All-Trans Retinoic Acid (ATRA) combined to chemotherapeutic agents [29].

Retinoids are signal molecules that together with their nuclear receptors activate signals for embryonic development and for the maintenance of the differentiated tissue state through the regulation of cell proliferation, differentiation and death. Furthermore, they have a substantial role in development and on physiological functions of nervous and reproductive systems [30, 31].

The action of retinoids is undertaken through two receptor types, belonging to the nuclear receptor family of Steroid Hormones: RAR (Retinoic Acid Receptor) and RXR (Rexinoic Receptor). Both receptors are expressed in three isoforms denominated with α, β and γ, which differ from each other for the space-time distribution and the affinity of ligands. RAR and RXR are transcription factors that function mostly as RAR RXR hetero-dimers and the isomer all-trans RA (ATRA) is the main ligand and activator of RAR but not of RXR. Retinoids offer great potential in cancer therapy by their ability to induce cell differentiation. Indeed, it has been proved that retinoic acid and its derivates are able to iduce differentiation and reduce the growth of NB cells [32].

So far outcomes for patients with high-risk NB remain poor despite recent improvements observed in randomized trials. Treatment options include in first phase an induction therapy with intensive cycle of chemotherapeutic agents. Subsequently, patients follow a consolidation phase with myeloablative therapy and stem cell transplantation (SCT) and radiation therapy to primary tumor and residual metastatic sites. To treat potential MRD following SCT, patients undergoing a post-consolidation phase, which involves the use of neuronal differentiating agent as isotretinoin (13-cis retinoic acid) and antibody anti-GD2 combined with with interleukin-2 (IL-2)/granulocyte-macrophage colony-stimulating factor (GM-CSF) [33,34]**.**

1.5 HIF-1 α e HIF-2 α (Hypoxia-Inducible Factor)

It's essential for the function and survival of aerobic organisms an adequate oxygen supply to cells and tissue. When oxygen supply fails to meet demand, it can occur a hypoxia condition. The definition of hypoxia is somewhat

ambiguous because normal oxygen pressure (PO_2) varies between different tissues. For in vitro studies 1% oxygen is commonly used to mimic a hypoxic environment [35]. Tumor hypoxia is due to the formation of non-functional blood vessels in neoplastic tissue and poorly vascularized areas. Tumor cells in low-oxygenated areas grow faster and are associated with aggressive tumor phenotypes, treatment resistance, and poor clinical patient prognosis [36,37].

The cellular response to hypoxia is mediated by the hypoxia-inducible factors (HIFs), which regulate the expression of multiple genes involved in adaptation and progression of cancer cells. Each HIF transcription factors is formed of two subunits: the α-subunit and the β-subunit, both belonging to the basic helix–loop-helix (HLH)-PER-ARNT-SIM (bHLH-PAS) protein family [38]. The α-subunit is oxygen sensitive, while the β-subunit (HIF-1β or ARNT) is ubiquitously expressed. In the presence of oxygen, conserved proline residues on the α-subunit, are hydroxylated by prolyl-4-hydroxylases PHDs (a set of oxygen-, iron-, and ascorbate-dependent enzymes belonging to the 2-oxoglutarate-dependent oxygenase superfamily) [39] and recognised from the von Hippel–Lindau (pVHL) tumor suppressor protein, that promotes its degradation via ubiquitin-proteasome pathway [40]. However, under hypoxia, PHDs cannot hydroxylate the α-subunit resulting in HIF-α protein stabilization, nuclear translocation, and dimerization with HIF-1β. There are three different α-subunit isoforms: HIF-1α, HIF-2α, and HIF-3α. HIF-1α (expressed by the *HIF1A* gene) and HIF-2α (expressed by the *EPAS1* gene) have been most studied, whereas few is known about HIF-3α. HIF-1α is thought to mediate the acute response to hypoxia and HIF-2α is stabilized longer in time also at normal physiological oxygen levels [41].

HIFs expression are essentiantial for SNS development, indeed they are expressed in human embryonal and fetal SNS cells [42] and are important regulators of the synthesis and secretion of catecholamines [43,44], which are key SNS neurotransmitters. Several studies report that hypoxia and HIFs substained stem cell-like features in cancer cells making them more aggressive.

It is important to mention that although low oxygen concentration is the major mode of HIFs stabilization, additional non-hypoxia-driven stimuli may also

regulate HIFs. Interestingly, factors such as nitric oxide [45], the cytokines interleukin-1beta (IL-1B), tumor necrosis factor α (TNF-α) [46], and trophic stimuli as serum and the insulin-like growth factors [47], might modulate HIFs up-regulation under normoxic conditions [48].

“Hypoxic” biomarkers such as HIF-1α and HIF-2α are associated with poor clinical prognosis in tumor patients. Tumor cells are also able to express these biomarkers under normoxic conditions [49] so they could be considered microenvironment independent prognostic factors for poor chemotherapeutic response and shortened patient survival time.

1.6 Hypoxia and chromatin remodelling.

Substantial evidences indicates that hypoxia induces epigenetic changes in the chromatin landscape, which consequently affect the transcriptional profiles of tissues. [50,51]. So far, it is not known how hypoxia generates chromatin changes. Interestingly, the stabilization of HIF-1α increases the expression of several histone lysine demethylases (KDM) which are crucial enzymes in the control of gene expression in hypoxia, but, with other chromatin modifiers, they can also affect heterochromatin structures, genome stability, and reprogramming of cellular senescence loci [52,53]. Histone demethylases control gene expression throw different mechanisms: they can enhance or repress the initiation of transcription, increase the rate of transcription elongation binding Pol II and remove methyl groups from the histones locati in gene bodies and recruit co-activators to the initiation complex in a demethylase-independent manner [54,55].

As previously mentioned, hypoxia is not the only reason that can stabilize the expression of HIFs. Interestingly, the expression of *HIF1* can be stabilized by several other signals, mostly related to stress (Figure 2). It’s clear that *HIF1A* and its target genes are crucial keypoints in epigenetic reprogramming and that normoxia microenviroment rather than hypoxia should be dissected to deepen knowledge of molecular mechanisms driven by *HIF1A* in solid tumors.

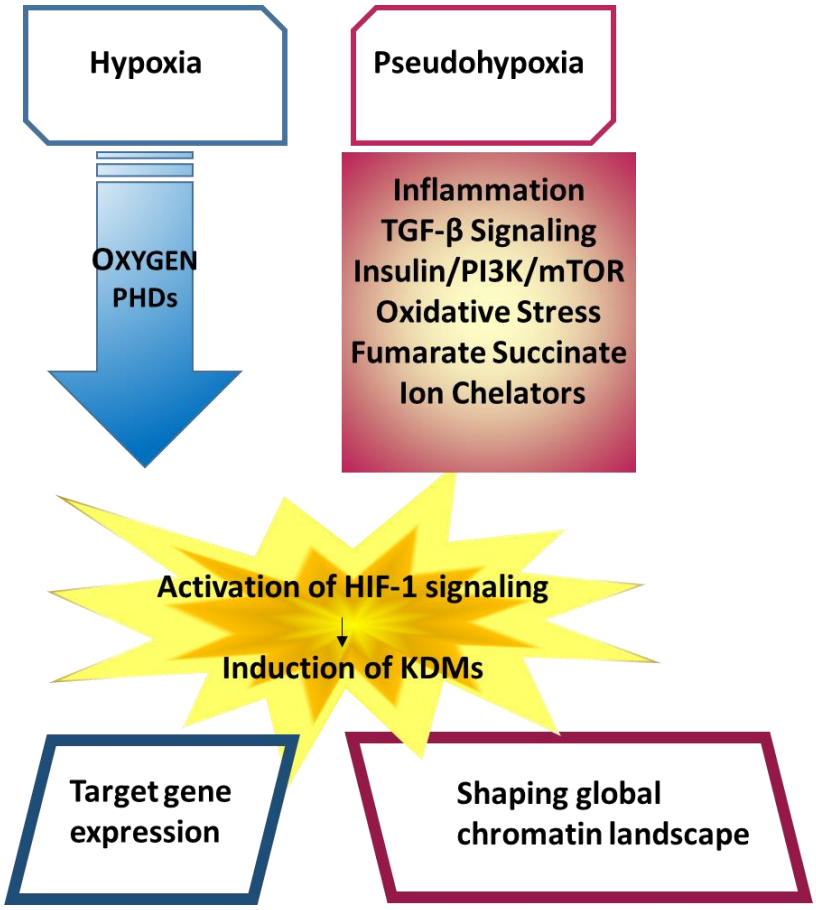

Figure 2. Representative scheme of HIF-1 regulation.

2. AIM

In NB cell lines, low oxygen tension might promote reductions in neuronal and neuroendocrine gene expression markers with the acquisition of an immature stem-like phenotype. The correlation between hypoxia and the grade of the differentiation status, suggests HIF and/or HIF-regulated pathways as one of the mechanisms behind the lack of cell responsiveness to differentiation therapy [56,57]. Therefore, inhibition of HIFs might provide more effective methods to enhance the NB cell propensity to differentiate.

Several studies *in vitro* have shown that in human NB cell lines, the use of differentiating agents like all-*trans* retinoic acid (ATRA) and 13-*cis* retinoic acid can cause arrest of cell growth, and can also induce neuronal differentiation [58,59]. The first aim of this study was to asses whether the combination of *HIF1A* or *EPAS1* silencing with ATRA treatment can provide major benefits over the use of the single agents. The proposed combination therapy can potentially help to reduce NB relapse through two main effects: differentiation into a more benign phenotype and induction of senescence.

HIF-1α expression is changeble inside different areas of solid tumors because of oxygen levels. This feature makes it hardly targetable by the use of direct drug compound, as *HIF1A* antibody. For this purpose the second intent of this study is to identify *HIF1A* target genes whose expression is activated or repressed by the presence of *HIF1A* regardless microenviroment. The expression of these *HIF1A* target genes will be related to all tumor area and their silencing might lead solid tumor to be easily wiped out.

3. MATERIALS AND METHODS

3.1 Microarray-KAPLAN SCAN.

R2 web tool (http://r2.amc.nl) was used to predict the association of *HIF1A*, *EPAS1* expression with survival of patients with NB. In brief, for each gene, R2 calculates the optimal cut-off in the expression level to divide the patients into 'good' and 'bad' prognosis cohorts. Samples within a dataset are sorted according to the expression of the investigated genes, and are divided into two groups. All of the cut-off expression levels and their resulting groups are analyzed according to patient survival. For each cut-off level and grouping, the log-rank significance of the projected survival is calculated. The best P value and the corresponding cut-off are selected. The cut-off level is reported and was used to generate the Kaplan-Meier curves. These depict the log-rank significance (raw P) as well as the P value corrected for multiple testing (Bonferroni correction) of the cut-off levels for each gene. Kaplan scan analysis was performed to estimate the overall survival and relapse-free survival according to *HIF1A* and *EPAS1* in the two microarray datasets: the Seeger dataset that included 102 International Neuroblastoma Staging System stage 4 patients without *MYCN* amplification; and the Versteeg dataset that included 88 patients with different clinical characteristics. The same analysys were reproduced for *FGFR1 FZD1* and *SYT13.*

3.2 Correlation of genes involved in development and *HIF1A* and *EPAS1* mRNA levels.

Differential expression of genes involved in development was tested between the two groups of patients divided according to their median values of expression of *HIF1A* and *EPAS1*. This analysis was performed using the R2 web tool (http://r2.amc.nl) and the gene expression data of the Versteeg and Seeger datasets. The list of genes for both of these datasets is shown in appendices Table 7.1 and 7.2. The coefficient of correlation (R-value) between the gene expression values and the two subgroups ('High' and 'Low' *HIF1A* or *EPAS1* espression) is also reported. The statistical differences in the gene expression values betweenthe patient groups with 'High' and 'Low' *HIF1A* or *EPAS1* expression were evaluated by ANOVA tests implemented in the R2

web tool. The p-values were corrected for multiple testing according to the false discovery rate. The significant threshold was established at a false discovery rate of 30%. Kegg pathway analysis was independently performed on the two lists (appendices tables 7.1-7.2) of the significant genes obtained from the two datasets (i.e., Versteeg, Seeger).

3.3 Cell culture.

The human SHSY5Y, SKNBE2c, SKNAS and HEK293T cell lines were grown in Dulbecco's modified Eagle's medium supplemented with 10% heat-inactivated fetal bovine serum (Sigma), 1 mM L-glutamine, penicillin (100 U/ml) and streptomycin (100 µ g/ml) (Invitrogen), at 37 °C, under 5% CO2 in a humidified atmosphere. The NB cells were plated at 60% to 70% confluence and treated with 5 µM and 10 µM ATRA (Sigma) dissolved in dimethyl sulfoxide. During the *HIF1A* and *EPAS1* silencing and the ATRA treatments, the cells were grown under normoxic conditions. The cells under hypoxia were grown at 1% oxygen for 6 h.

3.4 Production of lentiviral particles and infection of cell lines.

To knock-down *HIF1A* and *EPAS1* expression, the pGIPZ lentiviral shRNAmir that targets human *HIF1A* and *EPAS1* were purchased from Open Biosystems (Thermo Fisher Scientific, Inc.). We used two different shRNAs for each gene. The shRNAs against *EPAS1* were: V2LHS113750 (RHS4430-98894439) and V2LHS-113750 (RHS4430- 98851126). The shRNAs against *HIF1A* were: V2LHS_132152 (RHS4430-98513964) and V2LHS_236718 (RHS4430-98513880). A non-silencing pGIPZ lentiviral shRNAmir was used as the control (RHS4346). HEK293T were transfected using 10 µg shRNA plasmid DNA, 30 µl Trans-Lentiviral Packaging Mix (OpenBiosystem), and 25 µl TrasFectin (Bio-Rad), in 10-mm plates. The supernatants (10 ml per condition) were harvested after 24 h, centrifuged at a low speed to remove cell debris, and filtered through 0,45-µm filters. *In-vitro* transduction and determination of the lentivector titre were performer as reported previously [60]. After 48 h of incubation, the transduced cells were examined microscopically for the presence of TurboGFP expression (70%–90%). To obtain 100% GFP-positive cells, puromycin was added into the medium for an additional 10 days. The reported

data are representative of the experiments performed and confirmed using both lentiviral vectors for each gene.

3.5 Fractionation of nuclear proteins and Western blotting.

Cell pellets were resuspended in a hypotonic buffer (10 mM HEPES-K+, pH 7.5, 10 mM KCl, 1.5 mM MgCl2, 0.5 M dithiothreitol) in the presence of a protease inhibitors cocktail (Roche). The cells were lysed by addition of ice-cold 0.5% NP-40 for 10 min. The nuclei were pelleted at 1,000 x *g* for 2 min at 4 °C. The nuclear pellets were washed twice with 0.2 mM EDTA, 1.5 mM MgCl2, 0.5 M dithiothreitol, 25% glycerol) with protease inhibitors. The nuclei were incubated on ice for 30 min and vortexed periodically. The supernatants containing the nuclear proteins were collected by centrifugation at 16,000 x *g* for 5 min at 4 °C. The protein concentrations were determined by Bradford assays (Bio-Rad). Thirty micrograms of protein were loaded and separated using 8% polyacrylamide gels, and transferred onto polyvinylidene difluoride membranes (Bio-Rad). The membranes were blocked with 5% non-fat dried milk (Applichem) in phosphate-buffered saline (PBS) with 0.2% Tween (PBS-T) for 1 h, and then probed with anti-HIF-1α (610959; BD Biosciences) or anti-HIF-2α (ab8365; Abcam) antibodies. After a wash in PBS-T, the membranes were incubated with horseradish-peroxidase-conjugated anti-mouse secondary antibody (1:4000 dilution; ImmunoReagent), and then the positive bands were visualized using the ECL kit SuperSignal West Pico Chemiluminescent Substrate (Pierce). A goat anti lamin-β antibody (1:100 dilution; sc-6216; SantaCruz) was used as the control for equal loading. The protein band images were acquired with a GelDoc 2000 system (Bio-Rad), and the densitometry measurements were performed using the Quantity One 4.5 tool (Bio-Rad).

3.6 Colony formation assay in soft agar.

The colony formation assay was performed to analyze anchorage-independent cell growth. Two hundred thousand cells were plated in 0.35% agar on a bottom layer of 1% agar in the 35-mm dishes of 6-well plates (Corning). The plates were incubated at 37 °C for 4 weeks, and then stained with 0.01%

crystal violet. Colonies with 20 cells or more were counted. The means and standard deviations were calculated from three independent experiments.

3.7 Cell cycle distributions.

Cells were seeded in cell culture 10-mm × 20-mm dishes (Corning) at a density of 1 × 10^6 cells. After 8 h of serum starvation, the cells were treated with 5 μM and 10 μM ATRA for 24 h and 48 h. For the cell cycle analysis, 1 × 10^6 cells were washed in PBS and resuspended in 20 μl propidium iodide (50 μg/ml in PBS; Sigma), plus 50 μl RNaseA solution (100 μ g/ml in water; Sigma) and 0/004% NP40 in PBS. The cells were incubated at 37 °C for 3h in the dark. The cell-cycle distribution was then analyzed using flow cytometry, by fluorescence-activated cell sorting analysis (BD FACS, Canto II, BD Biosciences). The means and standard deviations were calculated from two independent experiments.

3.8 Caspase-3 activity assay.

Caspase-3 activity was evaluated using Caspase Fluorescent (AFC) Substrate/ Inhibitor QuantiPak (ENZO Life Sciences), following the manufacturer protocol. Briefly, cell lysates (total protein, 100 μg) were added to reaction mixtures (final volume, 100 μl) containing fluorigenic substrate peptides that are specific for caspase 3 (DEVD-AFC). The reaction was performed at 37 °C for 1 h. Fluorescence was measured with a fluorescence microplate reader (Microplate Imaging System, Bio-Rad), at 530 nm.

3.9 Cell viability assay.

Cells were grown in the presence of ATRA for a total of 6 days. After 2 days, the cells were seeded as six replicates into 96-well plates at a density of 104 cells per well. After 3, 4, 5, and 6 days of treatment, the metabolic activities of the samples were assessed as a surrogate marker for cell proliferation, using the 3-(4,5-dimethylthiazol-2l),5-diphenyltetrazolium bromide assay, according to the manufacture protocol (Promega).

3.10 Quantification of neurite outgrowth.

Neurite outgrowth was defined as neurite processes that were equal to or greater than two times the length of the cell body [61]. Neurites as single, dispersed cells were measured from the cell body to the furthest tip of the process using the LeicaApplicationSuite/AF software and a DMI4000B microscope (Leica Mycrosystem). The means and standard deviations of the neurite populations were calculated from three independent experiments.

3.11 Real-time RT-PCR.

The expression levels of genes were analyzed using real-time, quantitative PCR. Total RNA extraction using TRIzol LS Reagent (Invitrogen) and cDNA retrotranscription using the High Capacity cDNA Reverse Transcription Script (Applied Biosistem) was performed according to the manufacturer protocol. The cDNA samples were diluted to 20 ng/μ l. Gene-specific primers were designed by using PRIMEREXPRESS software (Applied Biosystems).

GENE	PRIMER FORWARD	PRIMER REVERSE
HIF1A	CCCATAGGAAGCACTAGACAAAGT	TGACCATATCACTATCCACATAAA
EPAS1	GACCCAAGATGGCGACATG	TGTCCTGTTAGCTCCACCTGTG
TUJ-1	TATGAGGGAGATCGTGCACATC	TGACTTCCCAGAACTTGGCC
MAP-2	TCTCTTCTTCAGCGCACCGGCG	GGGTAGTGGGTGTTGAGGTACC
NEFL	AAGCATAACCAGTGGCTACTCCCA	TCCTTGGCAGCTTCTTCCTCTTCA
GFAP	GGTTGAGAGGGACAATCTGGC	GCTTCCAGCCTCAGGTTGG
S100	GCTGAAAGAGCTGCTGCAGA	TTCATACACCTTGTCCACAGCAT
β-Actin	CGTGCTGCTGACCGAGG	GAAGGTCTCAAACATGATCTGGGT
NAV2	ACTTGGCCTCTATACCCGTC	GAGGTATTTCGTTGCAGGGTCT
CDH7	GGACTGTCAGGAACTACATCAGTCA	ATAAGACCTTCGAGGAAAGCGA
PCDH17	GGGAGGCACTCAAGATGAAAACTA	CTGTGCAATTAACACACTCTTCTGG
DACH1	TTCCATCTCCTTTTCTGTTTCCTG	CAACTTTCAACAGCCCCTGTATG
SH3RF3	CAACGTGTACCTGGCGCTCTA	ACCCGGTACATCTCTCCCTTG
SPON1	GGCTCTCTGACCAAGAAACTTTGT	GGCACAGCAGTCTAAGATGGGT
LAMA4	ACCGGAGAATGCTTGGAAGAA	CCAGACGCACTTATCACAGCTTAT
TMEM45A	AACCATTGTCATCGTTGGAATG	TCTGAGGAGCAGAGCCTCTTAAGT
PARP4	TGTGGTGCCGGAGTATTTGAA	CCTGGTCATTTGGTCTTCTATCTGT
GABRB3	TCTGGAAATTGAAAGCTATGGCTAC	ACTCCGGTAACAGCCTTGTCC
SLC35F3	AGTCCACAGAGAAGCAGTCTGTGA	CCTTCAAAGTCAAGCCATTGTCT
KIF26B	CGATGCAGTTTTTCCACAAGAC	GTTGACCACAGACTGGATCACCT

Real-time PCR was performed using SYBR Green PCR Master Mix (AppliedBiosystems). All real-time PCR reactions were performed using the 7900HT Fast Real-Time PCR System (Applied Biosystems). The experiments were carried out in triplicate for each data point. The housekeeping gene β -actin was used as the internal control. Relative gene expression was calculated using the $2^{-\Delta CT}$ method [62], where the ΔCT was calculated using the differences in the mean CT between the selected genes and the internal control (β -actin). The mean fold change of 2−(average ΔΔCT) was determined using the mean difference in the ΔCT between the gene of interest and the internal control.

3.12 Immunofluorescence.

Cells were placed on the chambers of polystyrene vessel tissue culture treated glass slides (BD Falcon), fixed in 4% paraformaldehyde, permeated with 0.2% Triton X-100, and blocked with 1% bovine serum albumin. The anti-GFAP (SAB4100002, Sigma) primary antibody was incubated for 1 h to 3 h, and the AlexaFluor 546 donkey anti-mouse (A10036, Invitrogen) secondary antibody for 45 min. Nuclear staining was obtained using 4',6-diamino-2-phenylindole (DAPI, Roche) (1:10,000 dilution in methanol). Confocal microscopy images of cells were acquired using a point-scanning confocal microscope (Zeiss LSM 510 Meta; Zeiss, Germany) with a 40 × EC Plan-Neofluar oil-immersion objective. Digital images were acquired using the LSM 510 Meta software60. All of the instrumental parameters for the fluorescence detection and image analyses were held constant to allow cross-sample comparisons.

3.13 Senescence analysis.

Senescence of cells during differentiation experiments was analyzed using Senescence β -Galactosidase Staining kits (Cell Signaling Technology). Briefly, the cells were fixed in 2% glutaraldehyde/ 20% formaldehyde and then stained at 37 °C overnight with the X-gal staining solution. The blue cells were considered positive. The means and standard deviations were calculated from three independent experiments.

3.14 RNA-sequencing.

Total RNA was isolated from NB cell line using TRIzol LS Reagent (Invitrogen) according to manufacturer's instructions, samples quality is assessed with Agilent 2100 Bioanalyzer RNA Nano chip device (Agilent, Santa Clara, CA, USA), and total RNA concentrations were determined using a NanoDrop ND-1000 spectrophotometer (Nano-Drop, Wilmington, DE, USA). RNA with an OD260/280 between 1.8 and 2.2 and an OD260/230 ≥ 1.8 was used for the construction of cDNA libraries.

3.15 cDNA library construction and sequencing.

The mRNA content was concentrated from total RNA using RNase-free DNase I (TaKaRa) and magnetic oligo (dT) beads. The mRNA was mixed with the

fragmentation buffer and broken into short fragments (~200 bp long). Then, the first strand of cDNA was synthesized with a random hexamer primer. The second strand was synthesized using the SuperScript Double-Stranded cDNA Synthesis kit (Invitrogen, Camarillo, CA) and was purified via magnetic beads. The ends were repaired and tailed with a single 3' adenosine. Subsequently, the cDNA fragments were ligated to sequencing adapters. Sequencing was accomplished using an Illumina HiSeq™ 2000 platform according to the manufacturer's protocols (Analysis performed by BIOGEM facillity).

3.16 RNA-seq data analysis

The analysis started from cleaned data previously filtred by adapter sequencies, low quality reads and from reads with more than 10% of unknown bases. Quality assessment on cleaned FASTQ files was performed using FastQC [63]. Sequencing data were analysed with the set of open source software programs of the Tuxedo suite: TopHat v2.0.14 and Cufflinks, following the analysis pipeline pubblished in nature protocol 2012.TopHat is a fast splice junction mapper for RNA-Seq reads. It aligns RNA-Seq reads to the reference genome using the ultra high-throughput short read aligner Bowtie2 v2.2.6.0, and then analyzes the mapping results to identify splice junctions between exons. TopHat was ran with default options by providing the reference genome (assembly GRCh37/hg19 downloaded from UCSC and indexed with Bowtie2) and its related RefSeq reference transcriptome (downloaded from UCSC) along with the couple of FASTQ files (forward and reverse reads) for each sample. Next, Cufflinks was used to assemble the mapped reads (in the BAM file format) into possible transcripts and to generate a final transcriptome assembly. The tool Cuffmerge was exploited to merge transcriptomes from all samples and generate a common transcriptome file. Cuffdiff was finally used to detect differentially expressed genes and transcripts. It takes mapped reads from two or more biological conditions (provided as two or more biological replicates) and analyzes their differential expression of genes and transcripts, thus aiding in the investigation of their transcriptional and post transcriptional regulation under different conditions. The program was ran by providing all the obtained BAM files (specifying the experimental condition and the replicate to which they belonged), the merged

transcriptome assembly and the sequence of the reference genome. The software returned: FPKM counts (Fragments Per Kilobase Of Exon Per Million Fragments Mapped) for each replicate, averaged FPKM counts for each experimental condition, and pairwise comparisons from the different experimental conditions (reporting the differences in expression levels). The set of output files obtained by Cuffdiff, reporting was then inspected and explored using the R-Bioconductor package CummeRbund v2.16.0, which provides functions to read, subset, filter and plot results.

3.17 RNA-seq Differential expression analysis

Genes were considered as differentially expressed in each of the pairwise comparisons if the comparison Bonferroni adjusted P-value was under 0.05 and if the fold change was greater than +0,5 (overexp) or lower than -0,5 (underexp). The lists of these genes were used to query Pathway and Gene Ontology databases.

3.18 Statistical analysis. The differences between the groups were analyzed using unpaired student's t-test. Probability values <0.05 were considered to be statistically significant. * $P \leq 0.05$, ** $P \leq 0.01$, *** $P \leq 0.001$.

4. RESULTS

4.1 Association of *HIF1A* and *EPAS1* expression with clinical outcomes in patients with NB.

In NB cell lines, hypoxia-regulated pathways and/or HIF expression have been shown to promote an undifferentiated phenotype, either through dedifferentiation or through inhibition of differentiation. So it can be considered that *HIF1A* and *EPAS1* overexpression in patients with high-risk NB will contribute to differentiation therapy resistance and to tumor cell aggressiveness. Firtsly was evaluated the association of *HIF1A* and *EPAS1* expression with clinical outcomes in NB patients using two datasets that are deposited in the R2 microarray web tool: the Seeger dataset that included 102 patients; and the Versteeg dataset that included 88 patients. The Seeger dataset includes patients with high-risk NB (i.e., stage 4 disease), whereas the Versteeg dataset includes patients with different stages and ages at diagnosis. As shown in figure 4.1.1, high mRNA levels of *HIF1A* were significantly associated with lower overall survival and relapse-free survival in both sets of patients, whereas high expression levels of *EPAS1* showed significant association with lower overall survival and a trend toward an association with lower relapse-free survival, although this did not reach statistical significance.

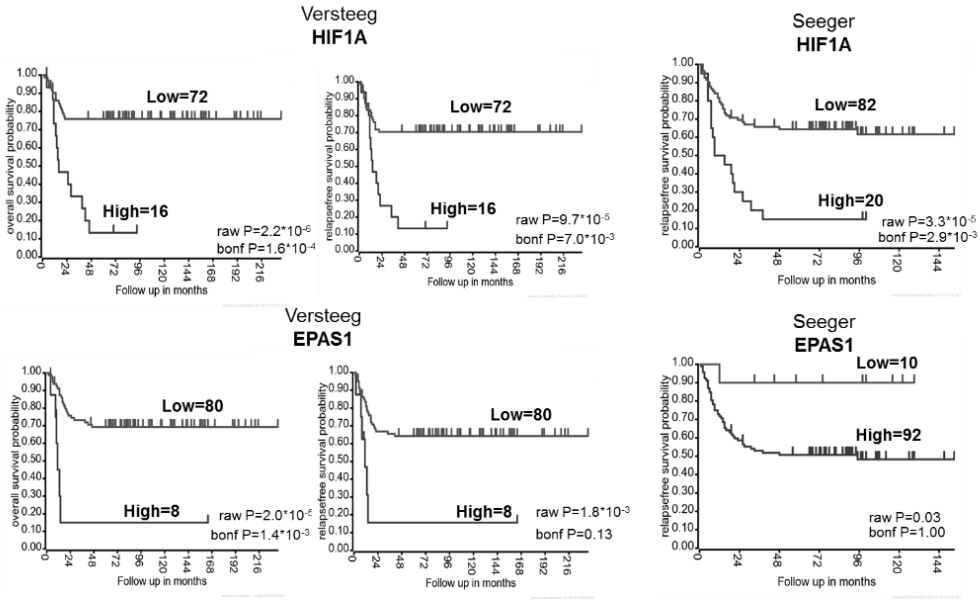

Figure 4.1.1. *HIF1A* and *EPAS1* gene expression is associated with poor survival in patients with NB. Kaplan-Maier analysis with patients grouped by the optimal cut-off (calculated using the R2 web tool) of expression of *HIF1A* and *EPAS1* for overall survival and relapse-free survival rates, in 88 patients with NB (Versteeg dataset) and 102 International Neuroblastoma Staging System stage 4 patients with MYCN not amplified (Seeger dataset).

The overall survival data of the Seeger dataset were not available. The “raw P” indicates the uncorrected p-value, whereas the “bonf P” indicates the p-value corrected for multiple tests according the Bonferroni method.

In both of these datasets, two patient subgroups were identified with different expression levels of *HIF1A* and *EPAS1*, in terms of their ‘High’ and ‘Low’ expression levels. So it was investigated whether, the different expression of these genes, between the two subgroups can influence the neuronal differentiation pathways.

Genes differentially expressed between ‘High’ and ‘Low’ *HIF1A* or *EPAS1* (mRNA expression levels), were filtred selecting only which included in the category “Development”and submitted for gene ontology analysis. As shown in figure. 4.1.2, the neuronal differentiation pathways were more represented in the patient group for ‘Low’ *HIF1A* or *EPAS1* expression than for ‘High’ *HIF1A* or *EPAS1* expression (P ≤ 0.05).

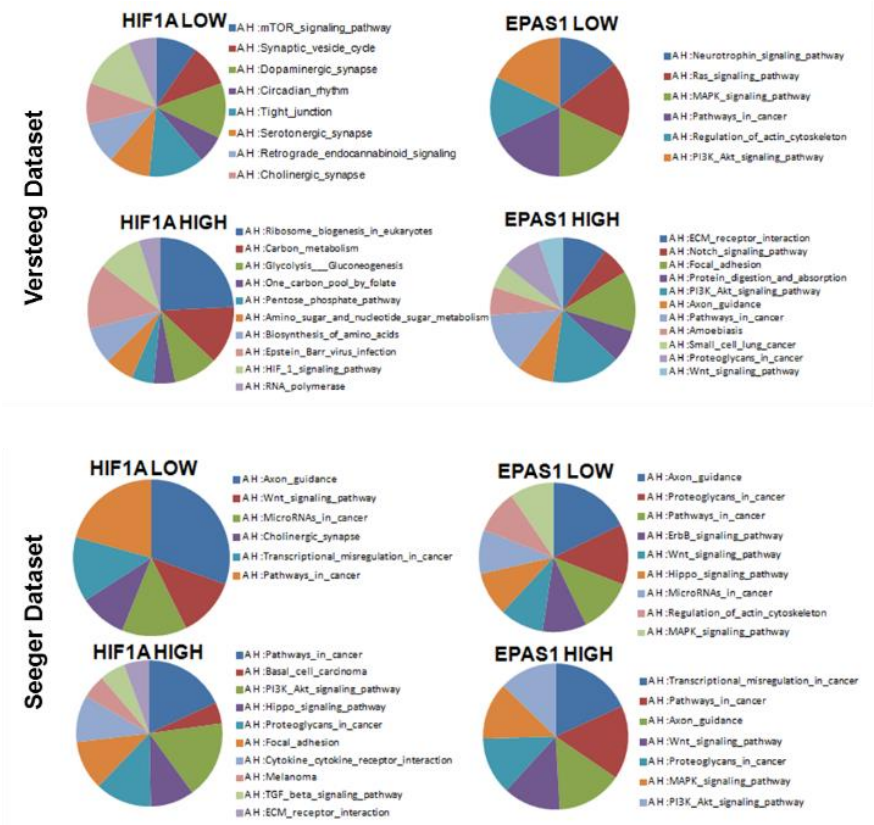

Figure 4.1.2. Pathway analysis of the genes involved in development that were differentially expressed between patients with ‘High’ and ‘Low’ levels of *HIF1A* and *EPAS1* expression. Results of the pathway analysis for the genes involved in development in patients with ‘High’ and ‘Low’ mRNA levels of *HIF1A* and*EPAS1* (P ≤ 0.05).

Furthermore MAPK PI3K-AKT signaling pathways were represented in the ‘High’ and ‘Low’ *EPAS1* expression subgroups in both datasets [64].

Interestingly, the IL-1B, IKBKB, RELA and NFKB1 genes were more expressed in the 'High' (*HIF1A* and *EPAS1*) expression subgroups in the Versteeg dataset, while the same factors were overexpressed only in the 'High' *HIF1A* expression subgroup in the Seeger dataset (Figure 4.1.3)

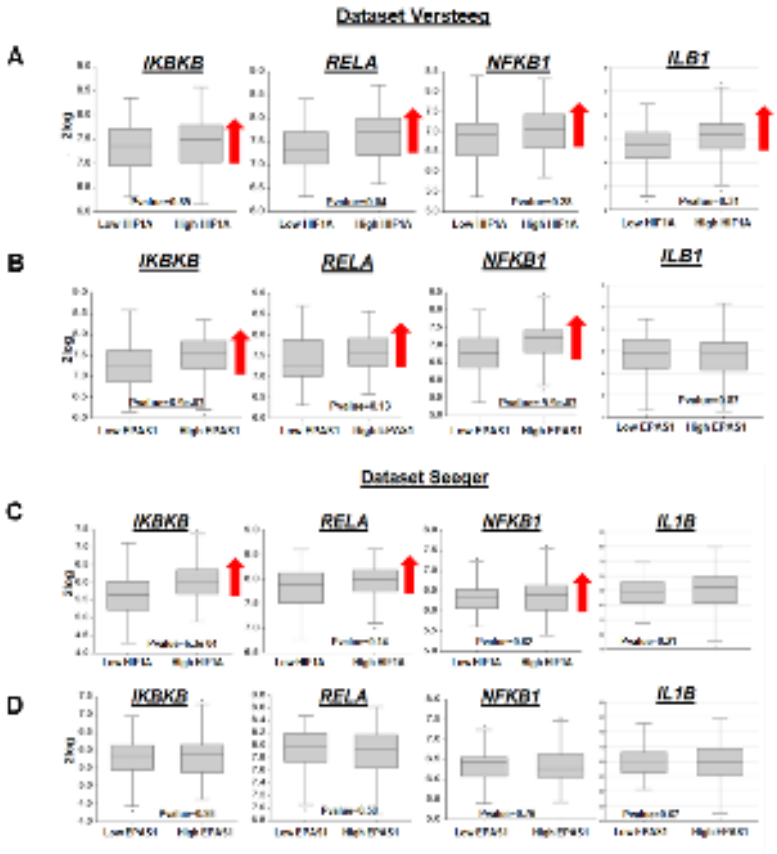

Figure 4.1.3. *IKBKB*, *RELA*, *NFKB1* and *ILB1* expression in the subgroups of patient with NB. Box plots showing the expression levels (Log2) of *IKBKB*, *RELA*, *NFKB1* and *ILB1* in the patient subgroups of 'Low' *HIF1A* and 'High' *HIF1A* expression in the Versteeg (A) and Seeger (C) datasets, and in the 'Low' *EPAS1* and 'High' *EPAS1* expression in the Versteeg (B) and Seeger (D) datasets.

4.2 *HIF1A* and *EPAS1* silencing in NB cells

For the next experiments three NB cell lines were selected: SHSY5Y, SKNBE2c and SKNAS cells. The SHSY5Y and SKNBE2c cell lines have biochemical features of neuronal cells, and these are believed to represent embryonic precursors of sympathetic neurons. These cells differentiate toward a neuronal phenotype upon RA treatment. The SKNAS cells have the flat phenotype of glial cells, and they do not differentiate [58,59]. These three cell lines showed different basal levels of *HIF1A* and *EPAS1* expression, as shown by their $2^{\wedge-\Delta CT}$ values, which represent their relative gene expression.

The SHSY5Y and SKNAS cells had higher levels of *HIF1A* expression than the SKNBE2c cells. *EPAS1* expression was higher in the SHSY5Y cells with respect to the SKNBE2c and SKNAS cells. The SKNBE2c cells showed the lowest levels of both *HIF1A* and *EPAS1* expression, with respect to the SHSY5Y and SKNAS cells (Figure 4.2.1 A). In the same cells grown under hypoxic conditions, these *HIF1A* and *EPAS1* relative mRNA levels ($2^{-\Delta CT}$) were decreased with respect to those in the cells grown under normoxic conditions (Figure 4.2.1 A, HYP, NX, respectively). As shown by the Western blotting in (Figure 4.2.1 B), the expression levels of the HIF-1α and HIF-2α proteins (as determined by the integral optical densities [IODs], and normalized with respect to lamin-β expression) were stabilized in these NB cells grown under hypoxic conditions. HIF-1α protein expression was more stabilized than HIF-2α protein expression. These data suggest that the *HIF1A* and *EPAS1* mRNA levels decreased probably because the increases in the HIF-1α and HIF-2α protein levels would result in negative feedback on their mRNA production

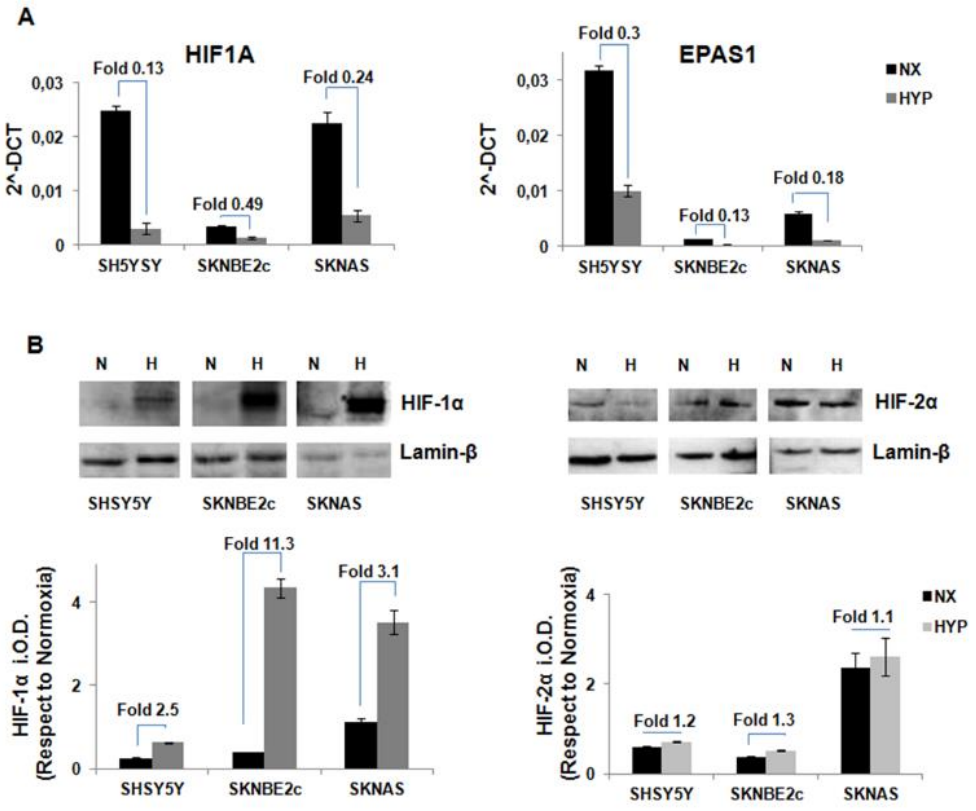

***Figure 4.2.1. HIF1A* and *EPAS1* and HIF-1α and HIF-2α protein expression under normoxia and hypoxia conditions.** The three cell lines (SHSY5Y, SKNBE2c, SKNAS) were grown in normoxia (NX) and hypoxia (HYP) (1%

oxygen for 6 h). The relative mRNA expression of *HIF1A* and *EPAS1* normalized to β –actin expression as determined ($2^{-\Delta CT}$) from the RT-PCR analysis (**A**). Western blotting of nuclear extract from the cells grown under normoxia (N) and hypoxia (**H**) conditions shows HIF-1α and HIF-2α changes under hypoxia. The bands were quantified by densitometry. The bar graphs shows the integral optical density (IOD) for each band, normalized with respect to lamin-β expression (**B**). Data are means of three experiments.

The *HIF1A* and *EPAS1* silencing in these NB cell lines under normoxic conditions was mediated using lentiviral delivery of short hairpin (sh)RNAs directed against *HIF1A* and *EPAS1* (i.e., sh*HIF1A* and sh*EPAS1*, respectively). A non-silencing shRNA was delivered using the lentivirus in the control cells (shCTR). The efficiency of silencing was determined by RNA expression (RT-PCR), as shown in (Figure 4.2.2 A), where the gene expression is given as percentages relative to the shCTR cells (at 100%). In the gene silencing here, *HIF1A* mRNA expression was significantly decreased in the SHSY5Y (by 33.8% ± 1.9%), SKNBE2c (by 42% ± 5.1%) and SKNAS (by 28% ± 1.3%) sh*HIF1A* cells. *EPAS1* mRNA expression was also significantly decreased in the SHSY5Y (40% ± 4.8%), SKNBE2c (48% ± 12.0%) and SKNAS (46% ± 4.1%) sh*EPAS1* cells. These decreases in *HIF1A* and *EPAS1* mRNA were enough to influence the transcription of the target genes downstream of HIF, as shown in the appendices (Figure 7.1). The efficiency of the silencing was also determined by Western blotting in these three cell lines. As shown in Figure 4.2.2 B there were decreases in the HIF-1α and HIF-2α protein levels upon *HIF1A* and *EPAS1* mRNA silencing, respectively. The decrement of *HIF1A* and *EPAS1* gene expressions were sufficient to reduce the oncogenic potential of NB cells, as shown by soft agar assays. Figure 4.2.2 C shows that there were decreases in the colony formation numbers in the SHSY5Y sh*HIF1A* (54 ± 7.7 colonies) and sh*EPAS1* (52.5 ± 9.2 colonies) cells compared to the SHSY5Y shCTR cells (84 ± 4 colonies). Similarly for the SKNBE2c sh*HIF1A* (45 ± 8.4 colonies) and sh*EPAS1* (38.5 ± 0.7 colonies) cells compared to the SKNBE2c shCTR cells (71 ± 2.8 colonies). The SKNAS cells showed weaker growth than the SHSY5Y and SKNBE2c cells, and *HIF1A*/*EPAS1* mRNA depletion did not affect their growth (data not shown).

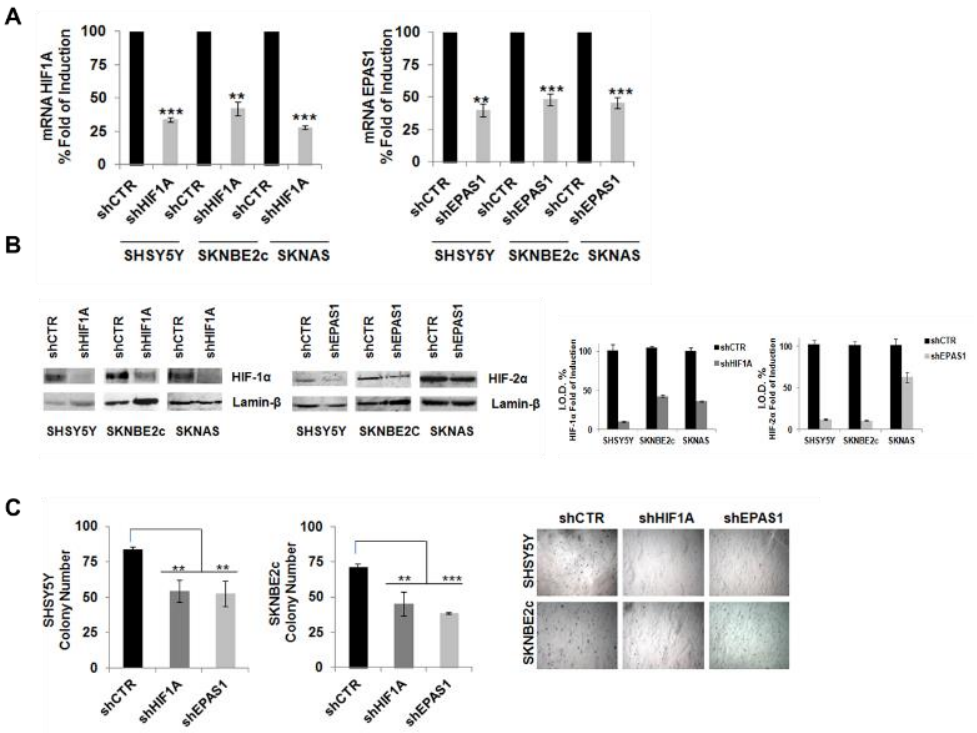

Figure 4.2.2. *HIF1A* and *EPAS1* silencing in NB cells and the effects on cell growth in the colony formation assay. (**A**) Efficiency of gene silencing mediated by lentiviral delivery of hairpin RNAs directed against *HIF1A* and *EPAS1* (sh*HIF1A*, sh*EPAS1*, respectively) in the three NB cell lines (SHSY5Y, SKNBE2c, SKNAS) was assessed using RT-PCR. Data are means of three experiments and are represented as percentages with respect to the NB shCTR cells, which were infected by lentivirus-mediated delivery of non-silencing hairpin RNA. (**B**) Western blotting of nuclear extracts from *HIF1A* and *EPAS1* silenced cells showing the decreases in the HIF-1α and HIF-2α proteins. The bands were quantified by densitometry. The bar graphs show the integral optical density (IOD) for each band, normalized with respect to lamin-β expression. (**C**) *HIF1A* and *EPAS1* silencing in SHSY5Y and SKNBE2c cells affects cell growth in the soft agar colony formation assay. The graft bars show decreased colony numbers in the NB sh*HIF1A*/sh*EPAS1* cells compared to the NB shCTR cells. The SKNAS cells are not shown (** P ≤ 0.01; *** P ≤ 0.001).

4.3 Combination of ATRA with *HIF1A* or *EPAS1* silencing enhances the Schwann cell-like phenotype.

The initial purpose was to determine the effects of *HIF1A* and *EPAS1* silencing on cell differentiation induced by ATRA in NB cells: SHSY5Y and SKNBE2c RA responsive and SKNAS RA unresponsive. These cell lines were silenced for *HIF1A* or *EPAS1* expression and then treated for 6 days with 5 μM and 10 μM ATRA. As reported in the literature, these ATRA concentrations can induce differentiation in diverse NB cells without any toxicity resulting from such prolonged treatments [58,59,64,65].

It is known that ATRA treatment increases the expression of HIF-1α in acute promyelocitic leukemia and in other cell types [29], and more remarkably, that HIF-1α inhibition cooperates with ATRA in the reduction of APL disease [66]. Here, we investigated the levels of the HIF-1α and HIF-2α proteins in these ATRA-treated NB cells. ATRA treatment alone induced increases in the HIF-

1α protein levels, as expected, and *HIF1A* silencing combined with ATRA treatment prevented this ATRA-induced HIF-1α increase (Figure 4.3.1). No increases in the HIF-2α protein were observed here. According to these data, inhibition of HIF in ATRA-treated tumors might synergize with ATRA, and so improve the success of this therapy.

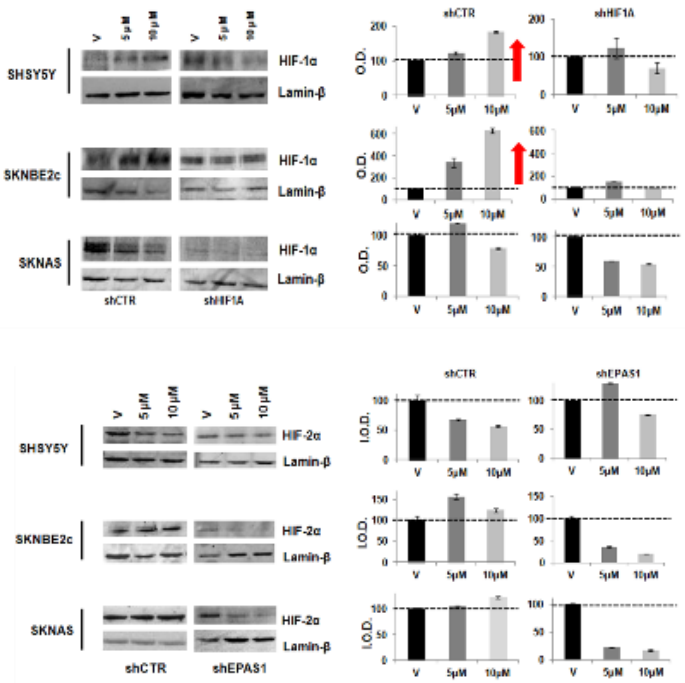

Figure 4.3.1. HIF-1α and HIF-2α protein expression upon ATRA treatment. SHSY5Y, SKNBE2c and SKNAS shCTR, sh*HIF1A*, and sh*EPAS1* cells were treated with 5 µM or 10 µM ATRA or vehicle (V) for 6 days. (A) Western blotting shows HIF-1α protein levels (A) and HIF-2α protein levels upon ATRA treatment. Bar graphs show the integral optical density (IOD) for each band normalized respect to lamin-β expression. The IOD are expressed in percentages with respect to vehicle treated cells.

ATRA can induce differentiation in numerous NB cell lines, which forces the cells out of the cell cycle. We examined the proportions of SHSY5Y, SKNBE2c and SKNAS cells at each stage of the cell cycle, through their caspase activities and their cell proliferation upon ATRA treatment and *HIF1A* or *EPAS1* silencing. Flow cytometry revealed that in the SHSY5Y shCTR, sh*HIF1A*, and sh*EPAS1* cells and in the SKNBE2c shCTR, sh*HIF1A*, and sh*EPAS1* cells, ATRA generated a modest accumulation of cells in G0/ G1, with depletion of the cells in the S-phase and the G2 phase (Figure 4.3.2 A and appendices 7.2). This depletion in the S-phase in response to ATRA treatment also showed increased caspase activities and reduced cell proliferation rates (Figure 4.3.2 B-C). Interestingly, the caspase activities in the SHSY5Y and SKNBE2c cells

were similarly increased with ATRA treatment for the SHSY5Y and SKNBE2c shCTR, sh*HIF1A* and sh*EPAS1* cells, which suggested that this co-treatment does not promote any increase in apoptosis. The absence of G1 accumulation and any increase in caspase activity, as well as the unvaried rate of proliferation in the treated SKNAS shCTR, sh*HIF1A*, sh*EPAS1* cells indicated the failure of ATRA-induced cell differentiation in these cells.

A

SHSY5Y		G1 (%)	S (%)	G2 (%)
shCTR	V	49 ± 1.5	41.3 ± 3	9.54 ± 1.5
	5µM	59 ± 2	34.7 ± 4	5.8 ± 1.7
	10µM	62.2 ± 1.5	31.4 ± 4	6.44 ± 2
shHIF1A	V	52.2 ± 5.2	40.7 ± 2.2	7.1 ± 1.6
	5µM	57.6 ± 3.9	34.7 ± 2.5	7.7 ± 2.1
	10µM	62.5 ± 2.5	30.7 ± 1.2	6.9 ± 1.5
shEPAS1	V	48.1 ± 2.5	41 ± 1.5	10.8 ± 1.5
	5µM	69 ± 2	24.7 ± 2	6.7 ± 2.5
	10µM	69 ± 3	24 ± 1	6.7 ± 3

SKNBE2c		G1 (%)	S (%)	G2 (%)
shCTR	V	67.5 ± 7	23.5 ± 5.5	8.9 ± 2
	5µM	86 ± 5	7.6 ± 3	6.3 ± 3
	10µM	83.5 ± 5	8.6 ± 2	7.8 ± 3.5
shHIF1A	V	66.2 ± 2	22.1 ± 2.7	11.7 ±
	5µM	74 ± 3	12.2 ± 1.3	13.7 ±
	10µM	84 ± 3	11.5 ± 1.6	4.4 ±
shEPAS1	V	62 ± 2	24.9 ± 3	13 ± 1.5
	5µM	73.1 ± 1.5	9.3 ± 2	17.5 ± 2.5
	10µM	82.9 ± 2	7.9 ± 3	9.1 ± 3

SKNAS		G1 (%)	S (%)	G2 (%)
shCTR	V	70.3 ± 2.2	21 ± 2	8.6 ± 1.3
	5µM	71.3 ± 1.5	21.7 ± 1.2	6.8 ± 1.5
	10µM	74.3 ± 2	18.3 ± 3.2	7.3 ± 1.4
shHIF1A	V	64.7 ± 2	24.6 ± 2.2	10.5 ± 0.4
	5µM	69.5 ± 1	20.9 ± 2.5	9.5 ± 1.2
	10µM	71.1 ± 2	18.4 ± 2	10.3 ± 1
shEPAS1	V	62.9 ± 2.5	24.6 ± 0.4	12.5 ± 1.2
	5µM	65.3 ± 1	21.3 ± 1	13.3 ± 1.1
	10µM	69.9 ± 1	18.3 ± 2.1	11.7 ± 2

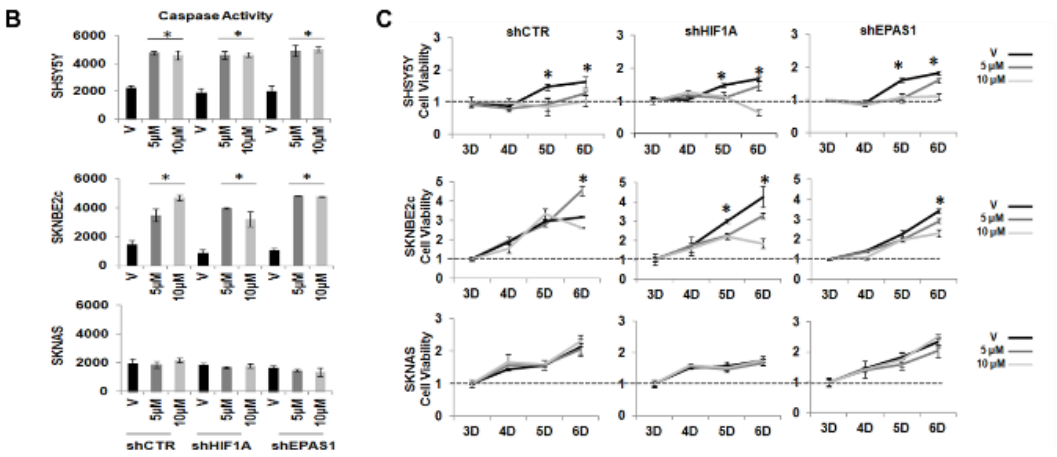

Figure 4.3.1. ATRA treatment: cell cycle and caspase activity. (**A**) Cells silenced for *HIF1A* or *EPAS1* expression were treated for 6 days with 5 µM or 10 µMATRA and processed for flow cytometry using propidium iodide. The proportion of cells at each stage of the cell cycle were calculated. (**B**) Caspase-3 activity was assessed in the same cells (V, vehicle; 5 µM and 10 µMATRA), and the data were normalized with respect to the negative control. (**C**) Cell viability was measured using the MTT assay, after 3, 4, 5, and 6 days (**D**) of ATRA treatment. Significances between the vehicle and the ATRA-treated cells are shown. The data are means of two experiments (* P < 0.05).

To estimate the neuronal differentiation under these treatments, a phenotype analysis was carried out, where the number of neuronal and flat cells were counted [67]. These data are expressed as percentages (Figure. 4.4.1A). In the SHSY5Y shCTR cells, with the 5µM and 10 µM ATRA treatments, there were more neuronal cells (75% ± 5%; 85% ± 5%; respectively) than flat cells (25% ± 5%; 16.6% ± 5.5%; respectively) (Figure. 4.1.1B). In contrast, upon 10 µM ATRA treatment in the SHSY5Y shHIF1 A and sh*EPAS1* cells, there were significant increases in the numbers of flat cells that were paralleled by

decreases in the neuronal cells, compared to the SHSY5Y shCTR cells (Figure. 4.4.1B; P ≤ 0.05). In particular, in the SHSY5Y shHIF1 A cells, there were 49% ± 6.3% neuronal cells and 51% ± 7.0% flat cells, and in the SHSY5Y sh*EPAS1* cells there were 55% ± 1.5% neuronal cells and 37% ± 7.5% flat cells (Figure. 4.4.1B). These decreases in the neuronal-like cells at 5 µM and 10 µM ATRA treatment were accompanied by shorter mean neurite lengths in the SHSY5Y sh*HIF1A* cells (38 ± 0.4 µm; 49 ± 13.0 µm) and the SHSY5Y sh*EPAS1* cells (44 ± 3.0 µm; 48 ± 10.8 µm), compared to the SHSY5Y shCTR cells (65 ± 16.0 µm; 63 ± 17.3 µm), (P ≤ 0.05) (Figure. 4.4.1C). In the SKNBE2c shCTR cells, there were increased numbers of neuronal cells with 5 µM ATRA (68% ± 3.8%) and 10 µM ATRA (73% ± 13.0%) treatment, with respect to the flat cells with 5 µM ATRA (32% ± 5.4%) and 10 µM ATRA (27% ± 4.3%) treatment. In the SKNBE2c sh*HIF1A* and sh*EPAS1* cells, instead, there were significantly increased numbers of flat cells with respect to a decrease in the number of neuronal cells, when compared to the SKNBE2c shCTR cells (P ≤ 0.005). In particular, for the SKNBE2c sh*HIF1A* cells, upon 5 µM ATRA treatment there were 19% ± 3.7% neuronal cells and 81% ± 2.7% flat cells, and upon 10 µM ATRA treatment there were 26% ± 5.3% neuronal cells and 73% ± 0.1% flat cells. For the SKNBE2c sh*EPAS1* cells, upon 5 µM ATRA treatment there were 33% ± 3.2% neuronal cells and 68% ± 10.0% flat cells, and upon 10 µM ATRA treatment there were 32% ± 5.0% neuronal cells and 68% ± 20.0% flat cells. The neuronal cell population did not show substantial differences in mean neurite length (Figure. 4.4.1B-C) The SKNAS shCTR, sh*HIF1A*, and sh*EPAS1* cells did not show an obvious phenotypic responses to ATRA (Figure. 4.4.1A).

4.4 Combination of ATRA with *HIF1A* or *EPAS1* silencing affects neuronal marker expression in NB cells

To determine the neuronal differentiation, NB shCTR, sh*HIF1A* and sh*EPAS1* cells were treated these for 6 days with 10 µM ATRA and multiple factors that are known to be involved in axon guidance were investigated: beta-III-tubulin (TUJ-1) and microtubule-associated protein 2 (MAP-2), which are involved in microtubule assembly; neuronal light intermediate filament (NEFL), which is expressed during neuronal differentiation; glial fibrillary acidic protein (GFAP),

which is expressed by astrocytes, and S100, which is expressed in cells derived from the neural crest (Schwann cells, melanocytes), both of which are implicated in the dynamics of cytoskeleton constituents. As determined by RT-PCR, after 10 µM ATRA treatment, in the SHSY5Y shCTR cells there was increased expression of the neuronal markers that was not seen in the SHSY5Y sh*HIF1A* and sh*EPAS1* cells (except for MAP-2, the expression of which increased in the treated SHSY5Y sh*HIF1A* cells) (Figure 4.4.1 D). Furthermore, all of these three SHSY5Y cells did not express glial markers at that time of treatment (*data not shown*). In the SKNBE2c shCTR cells, there were increases in neuronal marker expression, and in the SKNBE2c sh*HIF1A* and sh*EPAS1* cells there were increases in glial marker expression. Although *HIF1A* or *EPAS1* silencing appeared to enhance the ATRA-induced glial marker expression, the glial markers were more highly expressed in the SKNBE2c sh*HIF1A* cells than the SKNBE2c sh*EPAS1* cells. There were no differences in the expression of the neuronal and glial markers between the SKNAS shCTR, sh*HIF1A*, and sh*EPAS1* cells (except for TUJ-1, the expression of which decreased in the ATRA-treated SKNAS shCTR cells compared to the ATRA-treated SKNAS sh*HIF1A* and sh*EPAS1* cells).

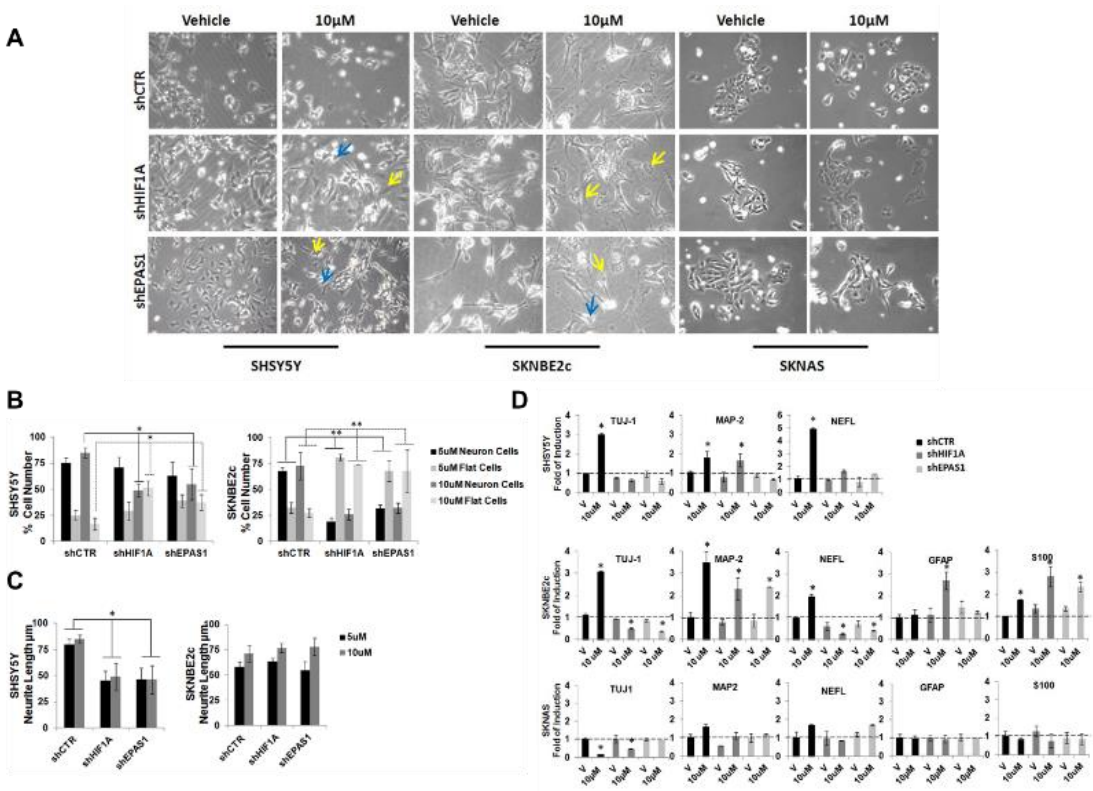

Figure 4.4.1. ATRA treatment combined with *HIF1A* or *EPAS1* silencing enhances the glial phenotype. (**A, B**) SHSY5Y, SKNBE2c, and SKNAS cells were silenced for *HIF1A* or *EPAS1* expression (sh*HIF1A*, sh*EPAS1*, respectively) and treated with 5 µM (not shown) and 10 µMATRA, or only with vehicle (**V**), for 6 days. Phenotypic changes were analyzed by counting the cells that showed the neuronal and flat-cell phenotypes, in six different fields for each experimental point. The data are expressed as percentages. Blue arrows, examples of neuronal cells; yellow arrows, examples of flat cells. (**C**) The mean neurite lengths of the counted cells (µm). (**D**) Gene expression analysis of TUJ-1, NEFL, GFAP and S100 performed using RT-PCR in the three NB cell lines. Data are means of three experiments (* $P \leq 0.05$; ** $P \leq 0.01$).

To determine whether this co-treatment might be more long-lived, cells were treated the with 10 µM ATRA for 25 days, and then it was assessed their differentiation status (Figure 4.5.1 A). Upon this extended 10 µM ATRA treatment, GFAP immunostaining was observed in the SHSY5Y and SKNBE2c sh*HIF1A* and sh*EPAS1* cells, but not in vehicle-treated cells (Figure 4.5.1 A *V*). In the ATRA-treated SHSY5Y and SKNBE2c shCTR cells, GFAP expression was very weak in the cytoplasm. The immunostaining of the glial marker GFAP in both of these cell lines supports the phenotypic changes in these SHSY5Y and SKNBE2c sh*HIF1A* and sh*EPAS1* cells. As shown in figure 4.5.1 B, the SHSY5Y shCTR cells preserved a neuronal-like phenotype, whereas the SHSY5Y sh*HIF1A* and sh*EPAS1* cells gained a highly fusiform phenotype and formed pseudoganglia, which are typical of primary neurons. In the SKNBE2c shCTR cells, there was a mixed population of thread-like and flat cells, while the SKNBE2c sh*HIF1A* and sh*EPAS1* cells showed glial phenotypes.

4.5 Combination of ATRA with *HIF1A* or *EPAS1* silencing results in senescence of NB cells

NB shCTR, sh*HIF1A*, and sh*EPAS1* cells were also treated with 5 µM and 10 µM ATRA for 40 days, and then analyzed them for their senescence state. These final cell populations were tested for senescence-associated β-galactosidase (Figure 4.5.1 C) [68]. Vehicle-treated NB sh*HIF1A* and sh*EPAS1* cells showed greater senescence compared to the vehicle-treated NB shCTR cells (Figure 4.5.1 D; except for the SHSY5Y sh*EPAS1* cells). This suggested that the decreased *HIF1A* and *EPAS1* expression in these NB cells might make them more prone to go into senescence, independent of the ATRA treatment. Furthermore, the combination of the ATRA treatment with the *HIF1A* or *EPAS1* gene silencing showed greater senescence in the SHSY5Y

(10 µM ATRA) and SKNBE2c (5 µM, 10 µM ATRA) cells, but not in the SKNAS cells (Figure 4.5.1 C-D).

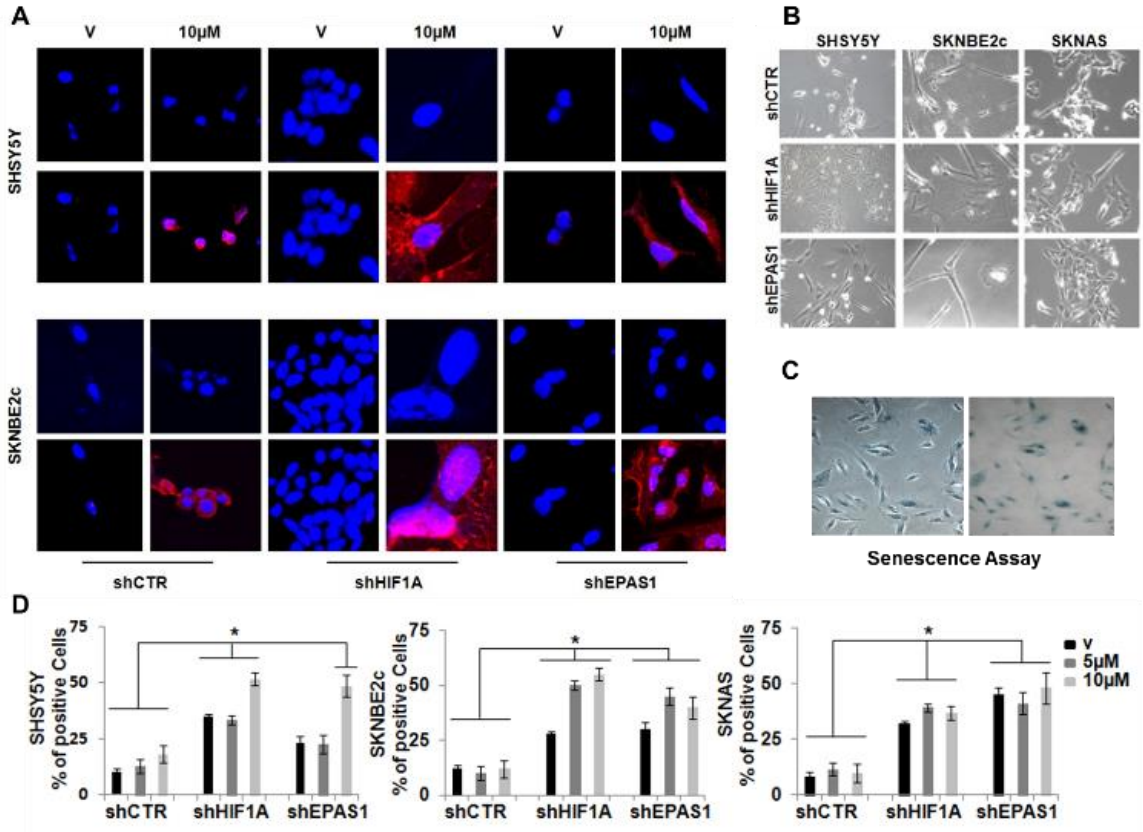

Figure 4.5.1. Long-term combination treatment of the NB cell lines. (**A**) After 25 days of ATRA treatment, *HIF1A* or *EPAS1* silenced and ATRA-treated SHSY5Y and SKNBE2c cells were immunostained with an antibody against GFAP. The settings of the confocal microscope were strictly maintained throughout the whole study. The panels are representative of three independent experiments. (**B**) SHSY5Y and SKNBE2c shCTR cells show thread-like structures that indicate neuronal differentiation; whereas the SHSY5Y and SKNBE2c sh*HIF1A* cells grow similar to ganglion structures, and the SHSY5Y and SKNBE2c sh*EPAS1* cells show a mixed population of flat and neuronal cells. The SKNAS cells did not show any morphological change. (**C, D**) After 40 days of treatment, the cells showed morphological evidence of senescence, which included the expression of senescence-associated-β -galactosidase (SA-β -Gal). Quantification was performed for the percentages of enlarged cells that showed SA-β -Gal expression. Data are means of three experiments (*P ≤ 0.05).

4.6 *HIF1A* affects chromatin state and gene expression regardless microenviroment.

To asses wheter HIF1A may affect chromatin state, SKNBE2c cell lines shCTR and sh*HIF1A* grown normoxia (NX) and hypoxia (HYP) condition were analysed evaluating their nuclei dimension, using LeicaApplicationSuite/AF software and a DMI4000B microscope (Leica Mycrosystem). Larger nuclei in hypoxia are indicative of chromatin decondensation [86]. Dapi staining in figure 4.6.1 shows a significative increase of nuclei size (represented in histogram) in *HIF1A* silenced cells compared to CTR cells grown in NX, while nuclei size in HYP do not seems to vary after *HIF1A* depletion. Moreover,

nuclei size are greater in cells grown in HYP compared to NX grown cells. These findings underline, as expected, that hypoxia and its related factors affect chromatin state, further suggesting that HIF1A is able to interfere with chromatin structure in an oxygen independent way.

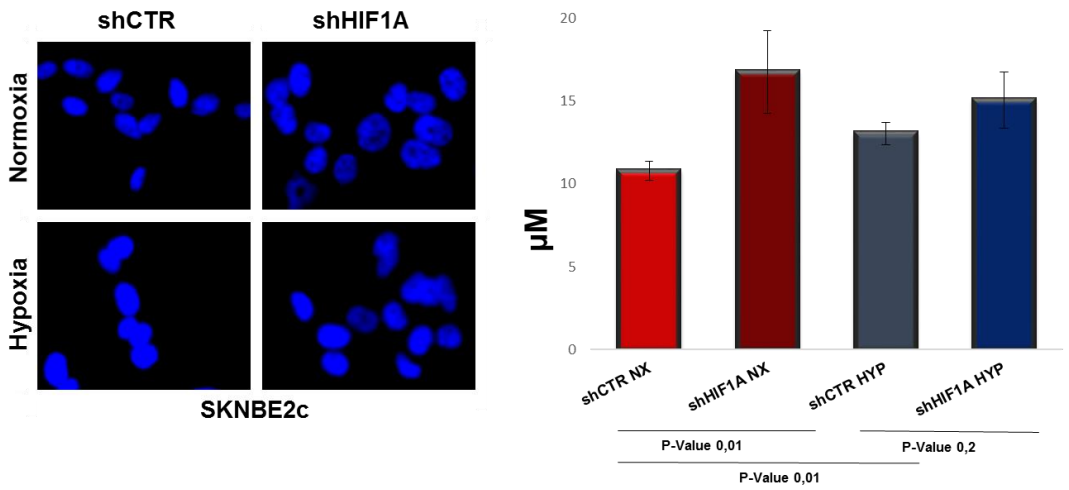

Figure 4.6.1 Nuclei dimentions in HIF1A silenced NB cell line in normoxia and hypoxia conditions. Dapi staining of *HIF1A* silencend SKNBE2c cells grown in hypoxia and normoxia conditions. Histograms show nuclei dimention in µM assesed with LeicaApplicationSuite/AF software and a DMI4000B microscope Leica Mycrosystem.

To provide genes and pathways differentially regulated by *HIF1A*, silenced SKNBE2c NB cell lines grown in NX and HYP (0,1 % O_2) conditions were subjected to RNA-seq esperiment. SKNBE2c cells have showed phenotypic and developmental intermediate features, (derived from their neural crest precursors) during retinoids treatments and this aspect makes them the best choise for our further studies, because best representing the eterogeneity of the tumor. Four experimental samples SKNBE2c shCTR NX, shCTR HYP, sh*HIF1A* NX and sh*HIF1A* HYP, each one in triplicates, were tried for RNA seq. For each samples RNA was prepared for the sequencing with HiSeq 2500 (illumina) as follows: purification, fragmentation, cDNA synthesis and libraries design (*Biogem facility*). Row data resulting from the sequencing were analysed with the set of open source software programs TopHat v2.0.14 and Cufflinks (Tuxedo) following the analysis pipeline (*Nature protocol* 2012). This data sets, allowed to generate “two gene sets”, that represents differential expression genes from sh*HIF1A* HYP compared to shCTR HYP and sh*HIF1A* NX compared to shCTR NX. RNA-seq data of differentialy expressed genes, were sorted by the measure of log2 fold change (≥+0,5 or ≤-0,5). The log2 fold

change represents the value of different expression between sh*HIF1A* genes versus shCTR genes (Figure 4.6.2).

The reliability of RNA-seq data was assesed by RT-PCR. Twelve genes were chosen from the comparison shHIF1A HYP vs shCTR HYP (Appendices 7.3) with value of log2 fold change ≤+2 and ≥ -2.

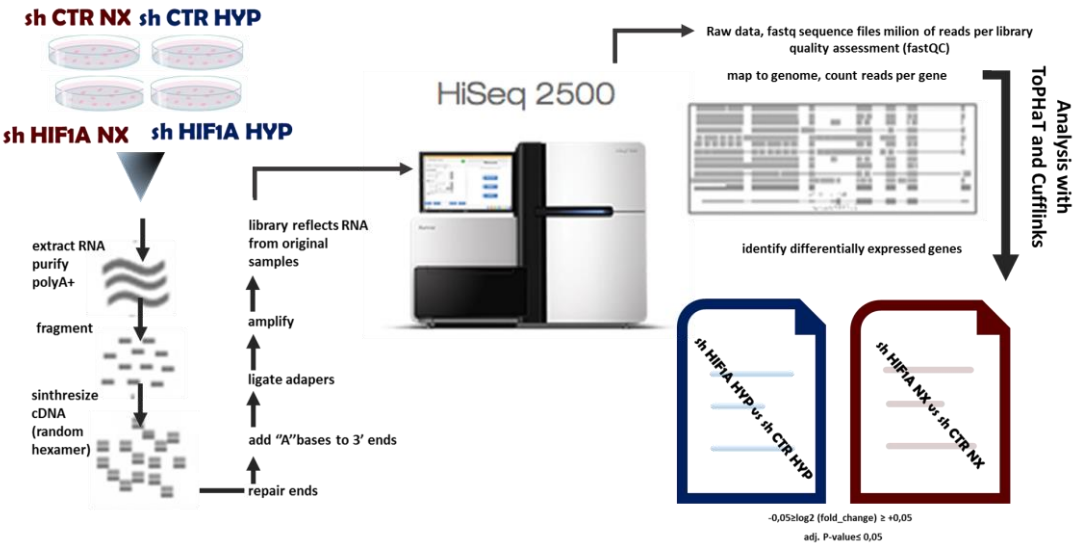

Figure 4.6.2 RNA-seq experiment. Overview of SKNBE2c shCTR and sh *HIF1A* grown in normoxia (NX) and hypoxia (HYP) condition. RNA-seq experiment (design, making libraries, sequencing, data analysis).

From the analysis of these "two gene sets" 2261 genes were found differentially regulated in the comparison sh*HIF1A* sh NX vs shCTR NX and 1839 genes comparing sh*HIF1A* HYP vs shCTR HYP. As observed in figure 4.6.3, gene ontology analysis of "two gene sets" (using the WEB-based GEne SeT AnaLysis Toolkit web tool-webGestalt) shows that *HIF1A* regulates the same pathways in both oxygen conditions; with the difference that there is an increase of metabolic activity in normoxia and of axon guidance pathway in hypoxia. *HIF1A* in normoxia is able to affect the expression of much more genes (2261) rather than in hypoxia conditions (1893), anyway the distribution's percentage of up and downregulated genes has the same trend between the different O_2 levels.

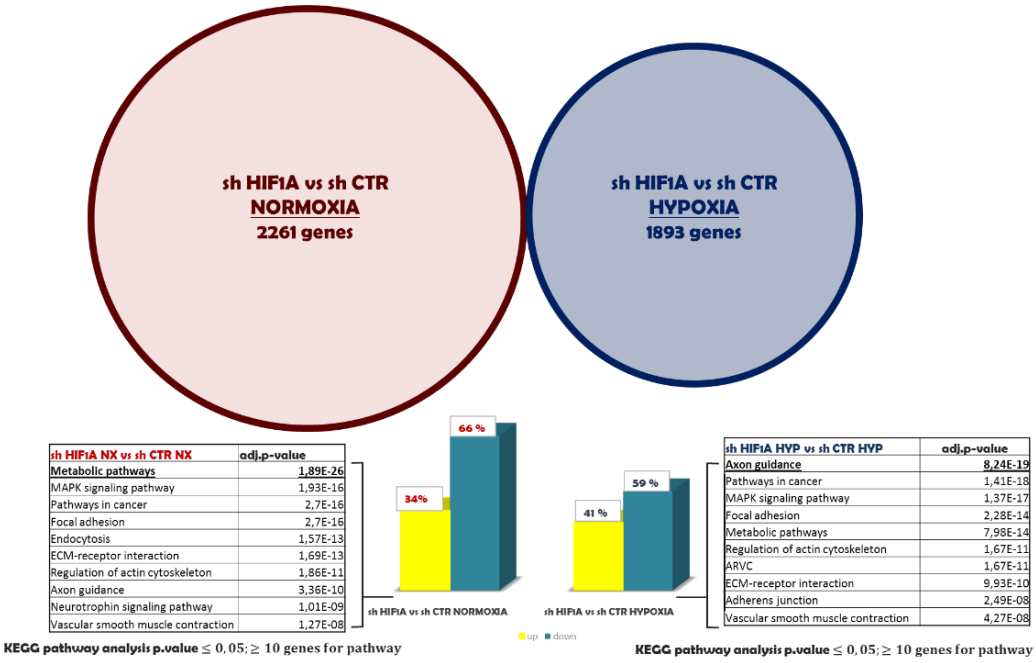

sh HIF1A NX vs sh CTR NX	adj.p-value
Metabolic pathways	1,89E-26
MAPK signaling pathway	1,93E-16
Pathways in cancer	2,7E-16
Focal adhesion	2,7E-16
Endocytosis	1,57E-13
ECM-receptor interaction	1,69E-13
Regulation of actin cytoskeleton	1,86E-11
Axon guidance	3,36E-10
Neurotrophin signaling pathway	1,01E-09
Vascular smooth muscle contraction	1,27E-08

sh HIF1A HYP vs sh CTR HYP	adj.p-value
Axon guidance	8,24E-19
Pathways in cancer	1,41E-18
MAPK signaling pathway	1,37E-17
Focal adhesion	2,28E-14
Metabolic pathways	7,98E-14
Regulation of actin cytoskeleton	1,67E-11
ARVC	1,67E-11
ECM-receptor interaction	9,93E-10
Adherens junction	2,49E-08
Vascular smooth muscle contraction	4,27E-08

Figure 4.6.3: RNA-seq data processing(I). In red circle *HIF1A* target genes regulated in normoxia, in blue circle *HIF1A* target genes regulated in hypoxia. Histograms represent the percentage of genes up (log2 fold chage ≥0,5) and down (log2 fold chage ≤-0,5) regulated in two gene sets. The table shows the results of KEEG pathway analysis p-value ≤0,05 and ≥10 genes for pathway.

The next step was to identify HIF1A target genes regulated in both O_2 conditions. To this aim the “two gene sets” (figure 4.6.4) (sh*HIF1A* vs shCTR hypoxia and sh*HIF1A* vs shCTR normoxia) were matched and three gene lists were obtained: 1) *HIF1A* target genes regulated “exclusively in hypoxia”,with 637 genes, 2) *HIF1A* target genes regulated “exclusively in normoxia” with 1405 genes and 3) a list of genes which are commonly regulated in hypoxia and normoxia with 1256 genes, named “*HIF1A*-target genes” (figure 4.4.5 A). To deeply investigate the function of *HIF1A* on gene regulation in normoxia and hypoxia, *HIF1A* target genes regulated “exclusively in normoxia” and “exclusively in hypoxia” were analyzed. As observed in figure 4.6.4 the number of *HIF1A* target genes regulated “exclusively in normoxia” are greather than the number of genes regylated “exclusively in hypoxia”. Furthermore, we observed a significative difference in gene numbers that are down and up regulated, in particular 72% NX vs 56 % HYP down regulated and 28% NX vs 44% HYP upregulated. KEGG pathway analysis (webGestalt) of the two “excluxive” gene sets revealed an enrichment of metabolic and cellular energy intake pathways in normoxia opposed to an enrichment of axon guidance and cancer pathways in hypoxia. These results underline a different *HIF1A* role in

normal and in low oxygen level conditions. Infact seems reasonable to suppose a *HIF1A* role in metabolic process in both conditions, with a switch versus the regulation of neuron differentiation pathway when *HIF1A* is depleted. Thus, *HIF1A* has a role in metabolic pathways in hypoxia, which is less revelant than its role in neuronal differentiatiation.

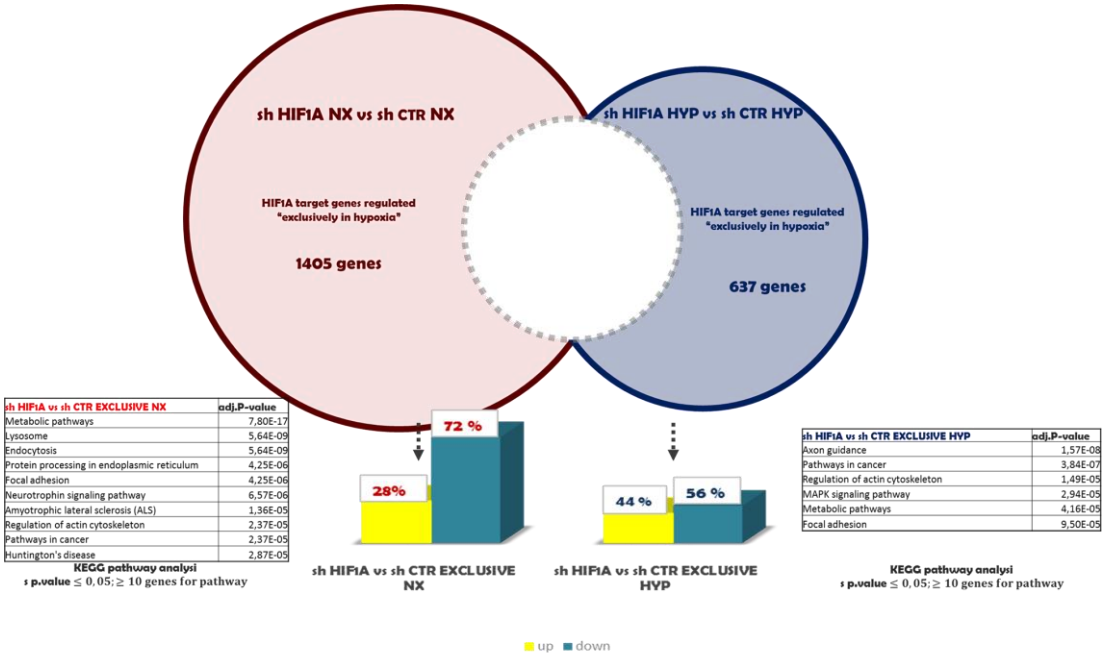

sh HIF1A vs sh CTR EXCLUSIVE NX	adj.P-value
Metabolic pathways	7,80E-17
Lysosome	5,64E-09
Endocytosis	5,64E-09
Protein processing in endoplasmic reticulum	4,25E-06
Focal adhesion	4,25E-06
Neurotrophin signaling pathway	6,57E-06
Amyotrophic lateral sclerosis (ALS)	1,36E-05
Regulation of actin cytoskeleton	2,37E-05
Pathways in cancer	2,37E-05
Huntington's disease	2,87E-05

KEGG pathway analysi
s p.value $\leq 0,05; \geq 10$ genes for pathway

sh HIF1A vs sh CTR EXCLUSIVE HYP	adj.P-value
Axon guidance	1,57E-08
Pathways in cancer	3,84E-07
Regulation of actin cytoskeleton	1,49E-05
MAPK signaling pathway	2,94E-05
Metabolic pathways	4,16E-05
Focal adhesion	9,50E-05

KEGG pathway analysi
s p.value $\leq 0,05; \geq 10$ genes for pathway

Figure 4.6.4: RNA-seq data processing(II) In red circle *HIF1A* target genes regulated "exclusively in normoxia, in blue circle *HIF1A* target genes regulated "exclusively in hypoxia. Histograms represent the percentage of genes up (log2 fold chage ≥0,5) and down (log2 fold chage ≤-0,5) regulated in two gene sets. Table shows KEEG pathway analysis p-value ≤0,05 and ≥10 genes for pathway.

In figure 4.6.5 are shown "*HIF1A*-target genes" commonly regulated by absence of *HIF1A* in both hypoxia and normoxia conditions. The expression values of these genes (about -7,2 and +4,7 log2 fold change) are shown in figure 4.6.5 B. Interestingly, as obeserved in dotplot each gene has the same regulation trend (up and down) in both O_2 conditions. This is not true for 19 genes (less than 1,6 %). Gene ontology analysis of "*HIF1A*-target genes" has revealed an enrichment in pathway of MAPK signaling, axon guidance and cancer (webGestalt). Particulary the same MAPK signaling and axon guidance pathaways have been found to be altered in NB patients with low *HIF1A* expression levels *(*in mentioned two NB microarray datasets) in figure 4.6.5 C.

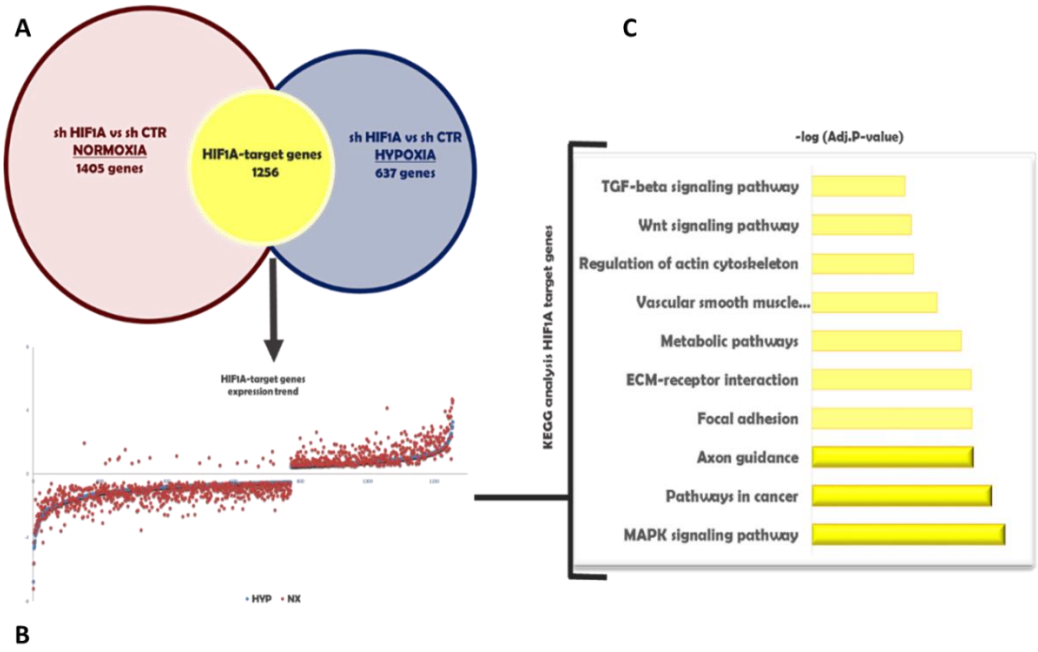

Figure 4.6.5: RNA-seq data processing(III). (A) In red circle *HIF1A* target genes regulated "exclusively in normoxia, in blue circle *HIF1A* target genes regulated "exclusively in hypoxia" and in yellow circle *HIF1A* target genes. (B) Dot plot shows regulation trend of *HIF1A* target genes (up≥0,5 and down≤-0,5), (C)table shows KEEG pathway analysis of *HIF1A*-target genes p-value ≤0,05and considerind ≥10 genes for pathway.

Various genes are mutated at relatively low frequency in NB but with potential biological functions. In order to asses whether *HIF1A* targets might be mutated in high-risk NB (HR-NB), "*HIF1A*-target list" was crossed with a list of significantly mutated genes in NB tissues (with non-silent somatic changes), derived from WES and DT-seq of 17 matched germline and HR-NB tissue pairs [27] [Table 7.3] (Figure 4.6.6 A).

The twelve genes resulting from this crossing were further filtred to find a proposable *HIF1A* target to use in cotreatment with RA. In particular the genes down-represented (negative value of log2 fold change) in absence of *HIF1A* (RNAseq data in SKNBE2c cells) were selected because the intent of this study is to propose *HIF1A* direct target to hit for improvement of NB therapies. These genes are: *FGFR1* (Fibroblast Growth Factor Receptor 1) *FZD1* (Frizzled Class Receptor 1) and *SYT13* (Synaptotagmin 13). Furthermore, the correlation of these gene expressions to NB patients survival was evaluated in two NB microarray datasets mentioned before (deposited in the R2 microarray web tool). As observed in Kaplan-Meier curve (Figure 4.6.6 B) *FGFR1* and *FDZ1* expression were associated with patients bad clinical outcome in both datasets. Contrary *SYT13* expression is associate with good clinical outcame

(high relaps free survival) in Versteeg dataset and with bad clinical outcame (with no significative P-value) in Seeger dataset.

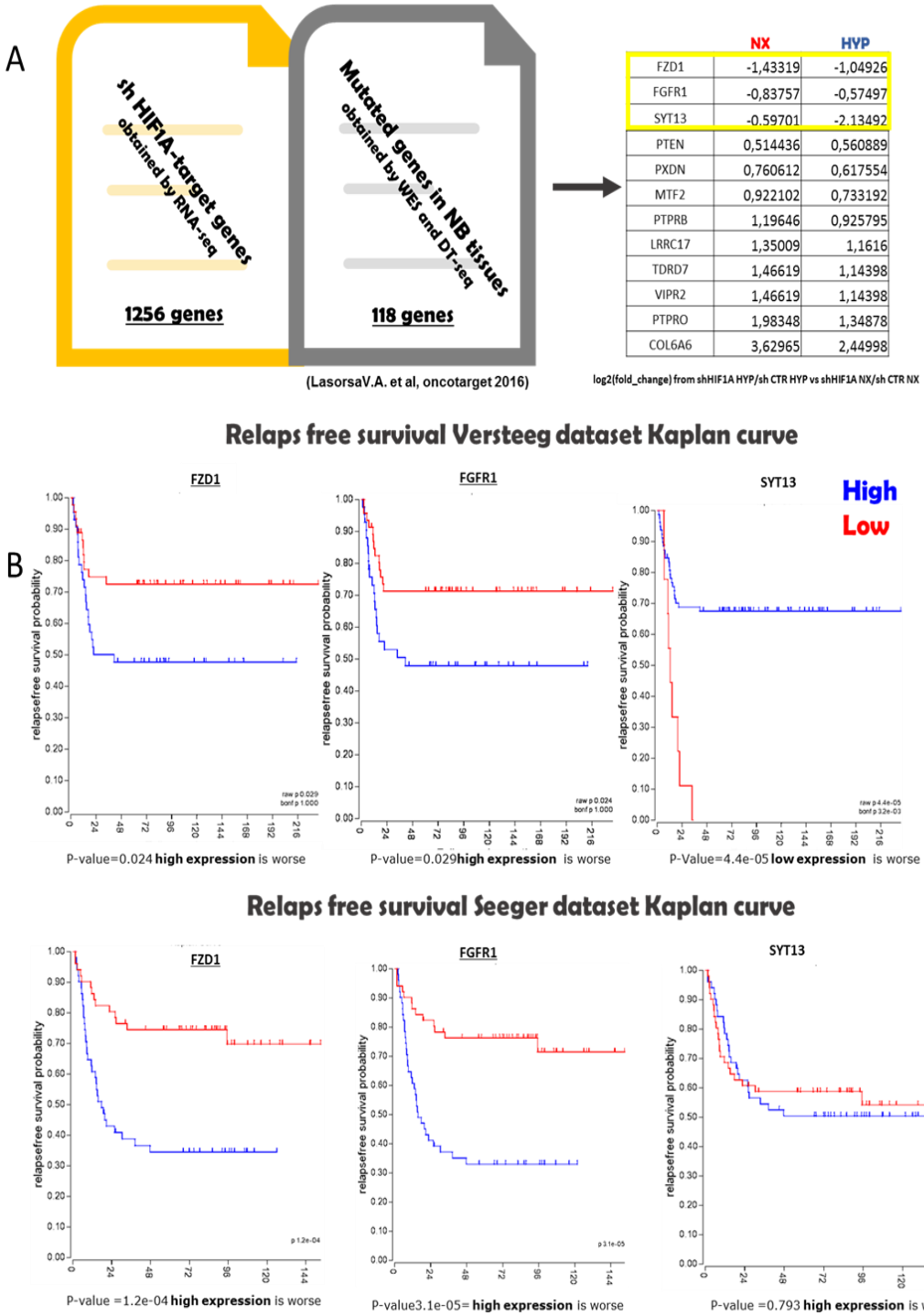

Figure 4.6.6"*HIF1A* target genes" found to be mutated in NB tissues: (A)Comparison of *HIF1A* target genes obtained by RNA-seq, and gene list of mutated gene in NB tissues obtained by WES and dt-seq.(B) Kaplan curve of relapse free survival of selected gene, expressed in Versteeg and Seeger microarray datasets r2 amc

From literature data both FGFR1 and FZD1 genes are involved in NB aggressivnes and differentiating stage [69,70] and cooperates with retinoids in tissue development and organogenesis [71,72]. Interesting tyrosine kinase receptor *FGFR1* has been found to be mutated in NB relaps [73]. The inhibition of tyrosine kinase receptors represents promising strategies to cure NB. Taken together these findings indicate *FGFR1* as the best candidate gene for differentiation therapy in combination with ATRA.

5. DISCUSSION

NB is a developmental malignancy arising within the neuronal ganglia of the peripheral sympathetic nervous system. In the last 25 years, the long-term survival for high-risk NB has improved, to reach about 50% [74,75]. So patients who have relapsed high-risk NB, remain a significant challenge for physicians and researchers, and on balance no curative treatment currently exists. So far, there are constant efforts for the development of new therapeutic strategies against metastatic NB, with the intention being to definitively prevent late recurrence. The clinical use of high doses retinoids after intensive chemoradiotherapy (with or without autologous bone marrow transplantation) significantly improves event-free survival for high-risk NB patients [1,34, 76]. However terapeutic failure that seems to be caused by the drug pharmacokinetics or by several biochemical factors highlights an emergent demand for novel combination strategies with retinoids to provide more therapeutic efficiency [77].

Hypoxia and HIFs regulate the proliferation and differentiation of different stem cell populations including embryonic, neural, and hematopoietic stem cells. Cancer stem cells (CSCs) exist as a distinct sub-population in solid tumors and hypoxia may enhance their stem cell-like features and make tumors more aggressive. In NB, hypoxia downregulates neuronal and neuroendocrine differentiation markers and upregulates genes expressed during normal neural crest development [57]. Low oxygen levels mediate post-transcriptional regulation of the HIF-1α and HIF-2α proteins, this might induce the expression of different genes for cell adaptation. The correlation between hypoxia and differentiating status grade would suggest that HIF and/or HIF-regulated pathways are one of the mechanisms that underline the unresponsiveness to differentiation therapy [57, 78].

HIF-1α is overexpressed in a wide spectrum of solid tumors even under normoxia conditions. The mechanisms that might regulate HIF-1α expression and ultimately lead to increased tumor growth and chemoradioresistance are different [79, 78]. Otherwise, HIF-2α is more tissue-specific, and it promotes the growth of clear-cell renal cell carcinoma (ccRCC) and NB cells, and it is

involved in the regulation of stem cell maintenance [49]. Therefore, there is increasing interest in the identification of the mechanisms of HIF-1α and HIF-2α up-regulation in solid tumors, to guide the choice of HIF inhibitors (e.g., transcription- or translation-based) that will be best-suited for treatment [81, 82].

In the present study is showed that *HIF1A* and *EPAS1* mRNA levels correlate with worse survival in high-risk NB patients, using two different NB microarray gene-expression datasets. In both of these datasets, were identified two patient subgroups with 'High' and 'Low' *HIF1A* and *EPAS1* expression levels. As a result of the gene ontology analysis, restricted to developmental genes that were differentially regulated between these two subgroups for both of the datasets, neuronal pathways were more represented in patients with 'Low' *HIF1A* or *EPAS1* expression, than in those with 'High' *HIF1A* or *EPAS1* expression. This finding suggests that low expression of *HIF1A* or *EPAS1* in tumors that are more differentiated, might promote an efficient NB cell response to differentiation therapy.

According to the literature, HIFs gene overexpression in NB solid tumors might be determined by several factors, as well as a hypoxic microenvironment. In proposed data is shown that the MAPK PI3K-AKT pathways were more represented in the patient subgroups with different *EPAS1* expression, which suggests that these pathways might orchestrate the regulation of the *EPAS1* mRNA in these tumors [64]. Moreover, it is addressed the hypothesis that IL-1B might up-regulate HIF-1α in patients with NB via a pathway that is dependent on nuclear factor kappa B (NFKB) [46]. Also it couldn't exclude that *HIF1A* and/or *EPAS1* expression in solid tumors is regulated by other factors, such as genetic/ epigenetic alterations, which were not determined in the this study.

In NB cell lines, low oxygen concentration stabilized HIF-1α and HIF-2α protein expression, whereas the *HIF1A* and *EPAS1* mRNA levels decreased. However, the increases in the HIF-2α protein levels during hypoxia were only modest in comparison to those for HIF-1α protein levels in the same cells. These protein increment in hypoxia might result in negative feedback on their mRNA production, thus suggesting that high *HIF1A* and *EPAS1* gene

expression under normoxic growth conditions might be determined by other factors that are not directly linked to the low oxygen concentration. *HIF1A* and *EPAS1* mRNA expression in normoxia might reflect the results obtained in-silico analysis of NB microarrays, so *HIF1A* and *EPAS1* silencing might represent a useful therapeutic approach for the treatment of solid tumors with high *HIF1A* and/or *EPAS1* mRNA levels.

In the present study, it was identified a new combination treatment that drives glial differentiation and senescence responses in NB cell lines. This treatment is based upon the use of *HIF1A* or *EPAS1* gene silencing to enhance ATRA-induced differentiation proprieties. This mechanism operates in certain cells (i.e., the SHSY5Y and SKNBE2c cells) but not in cells that are resistant to retinoids (i.e., the SKNAS cells). Achieved results show that single use of ATRA induces neurite outgrowth and up-regulation of neural markers, whereas in combination with *HIF1A* or *EPAS1* gene silencing it enhances the glial phenotype and promotes up-regulation of glial markers. Significantly, even with extended co-treatment these cells were driven into ganglion-like clusters, resembling less aggressive ganglioneuroma cells. Again it's possible to observe that upon ATRA treatment *EPAS1*-silenced cells (i.e., NB sh*EPAS1* cells) showed an intermediate phenotype between the unsilenced (i.e., the NB shCTR cells) and the *HIF1A*-silenced cells (i.e., the NB sh*HIF1A* cells) which suggests that *EPAS1* is not the main player in determining neuronal-glial transdifferentiation.

The individual *HIF1A* or *EPAS1* gene silencing was not sufficient to lead subdifferentiation into Schwann cells, as also for ATRA used as a single agent, which acts independent of Schwann cell differentiation. The combination treatments of *HIF1A* or *EPAS1* silencing in the presence of ATRA exclusively pushed the NB cells toward transdifferentiation of the neuronal cells into Schwann cells. These NB cell lines are characterized by markers of embryonic peripheral nervous system development. Therefore these findings suggest that *HIF1A* or *EPAS1* (or HIF-related pathways) sustain the activation of alternative pathways that can provide Schwann transdifferentiation in NB cells upon retinoid treatment. The conversion of NB cells into ganglionic and Schwann cells might have great clinical impact in differentiation therapeutic protocols.

Pro-senescence therapy has been argued as a promising therapeutic strategy for the treatment of cancers. Tumor relapse is the most significant barrier to effective therapy and compounds such as the retinoid agents that induce initial neuronal differentiation might be not enough in prevention of tumor recurrence. The proposed combination therapy can potentially help to reduce NB relapse through two main effects: (i) differentiation into a more benign phenotype; and (ii) induction of senescence. RA can cause senescence in some NB cells [83, 84] but it is currently not clear whether senescence represents a significant component of its clinical response. Evidence from the literature correlates senescence and hypoxia; hypoxia can inhibit or prevent senescence in cells, even if the pathways that are altered remain unknown [61]. In proposed NB cell system, results show that silencing of *HIF1A* or *EPAS1* expression is enough to increase the number of senescent cells independent of the ATRA responsiveness, and that the combination of ATRA with *HIF1A* or *EPAS1* silencing enhances senescent cells in RA-responsive cells.

Between HIFs, *HIF1A* is the most promising factor to be silenced to induce differentiation in cotreatment with RA, indeed as mentioned before low levels of *HIF1A* are correlated to enrichment of pathway of neuronal differentiation (axon guidance), in R2 deposited patients microarray datasets. This finding underlines the strong assosiation of *HIF1A* with differentiative grade of tumor, further supporting “our thesis” that pinpoints *HIF1A* as main driver of failure in NB differentiating therapies.

In solid tumor, there is a different expression of HIF-1α because of oxigen level and this peculiarity causes several problem in the use of direct drug compound to target it. This study proposes the identification of *HIF1A* target genes related to all tumor area, whose expression is activated or repressed by the presence of *HIF1A* regardless microenviroment, in order to offer new potential attack strategies in NB treatment. From the transcriptome analysis (RNA-seq) of *HIF1A* silenced cell line grown in normoxia and hypoxia conditions two gene sets (sh*HIF1A* HYP vs shCTR HYP and sh*HIF1A* NX vs shCTR NX) were listed, which represent *HIF1A* target genes in normoxia as in hypoxia condition. These results reveled a crucial role of *HIF1A* in normal oxygen conditions, something which, has never been looked at.

The absence of *HIF1A* involves approximately the same pathways (in NX and HYP), probably because there are several common genes between the two comparisons, except for an enrichment of metabolic pathway in normoxia and axon guidance pathway in hypoxia.

The analysis of *HIF1A* target genes regulated “exclusively in normoxia” reveals that *HIF1A* affects the expression of genes involved in metabolism and in cell energy uptake. Particulary the global gene regulation (72% down vs 28% up) in absence of *HIF1A* underlines the hypotesis that NB cells slow down their metabolic activity, thus becaming less proliferating and so less aggressive.

Gene ontology analysis of *HIF1A* target genes regulated “exclusively in hypoxia” shows an enrichment of axon guidance and cancer pathways, of note without global differences in their up and down gene regulation (56%down vs 44% up). This refects the same results obtained in NB patients with low *HIF1A* expression microrray datasets.

These new findings point out a role of *HIF1A* in normoxia conditions. In particular in normoxia *HIF1A* mainly ragulates cell energy intake and metabolic activity, whereas in hypoxia *HIF1A* lack is essential for neuronal differentiation pathway. *HIF1A*-regulated genes, regardless the microenvironment, are involved in signal transduction (MAPK signaling), neuronal differentiation and cancer pathways. These latest evidences are in line with previously data in NB patients with low *HIF1A* gene expression. Thus, these pathways or genes represent canditate targets instead of HIF1A which has been previously described, for developing a differentiating therapy in combination with ATRA.

As shown by WES analysis in last years, high risk NB are characterised by low incidence of somatic mutations. Anyway, the low frequencies of mutated genes has a grate impact on tumor development because mutations affect important biological processes (focal adhesions and regulation of actin cytoskeleton pathways) [27]. Targeting mutated genes represents an usefull tool for development of novel personalized therapies. Interesting twelve genes belonging to “*HIF1A target genes*” have been previosuly found mutated in NB patients. [27]. *FGFR1* from RNA-seq analysis is downregulated in NX and HYP conditions and its expression is correlated with bad survival in NB patients.

Furthermore FGFR1 is tyrosine kinase receptor and its inhibition may represents a promising strategies to cure NB.

6. CONCLUSIONS

Taken together, our findings provide the first evidence that *HIF1A* or *EPAS1* inhibition combined with ATRA treatment can convert NB cells into ganglionic and Schwann cells and might also generate a novel trigger for senescence in NB RA-responsive cells. Indeed, these data shed new light in the mechanisms underlying the neuronal–Schwann cell transdifferentiation process, which might represent a model for the development of novel therapeutic strategies for patients with high-risk NB [85].

Recent studies show FGFR1 mutations in NB relaps. From transcriptome analysis of silenced *HIF1A* NB cell line, FGFR1 has been identified as a putative druggable *HIF1A* target. Its regulation independently from microenvironment strenghts the hypothesis that FGFR1 is expressed in well-oxygenated and not-oxygenated areas in solid tumors and so represents the best therapeutic target to complitely eradicate the disease. The use of FGFR1 inhibitors into differentiation therapy protocols might offer therapeutic advantages for relapse prevention, which represents a significant barrier that needs to be surmounted in therapeutic approaches for patients with high-risk NB.

7. APPENDICES

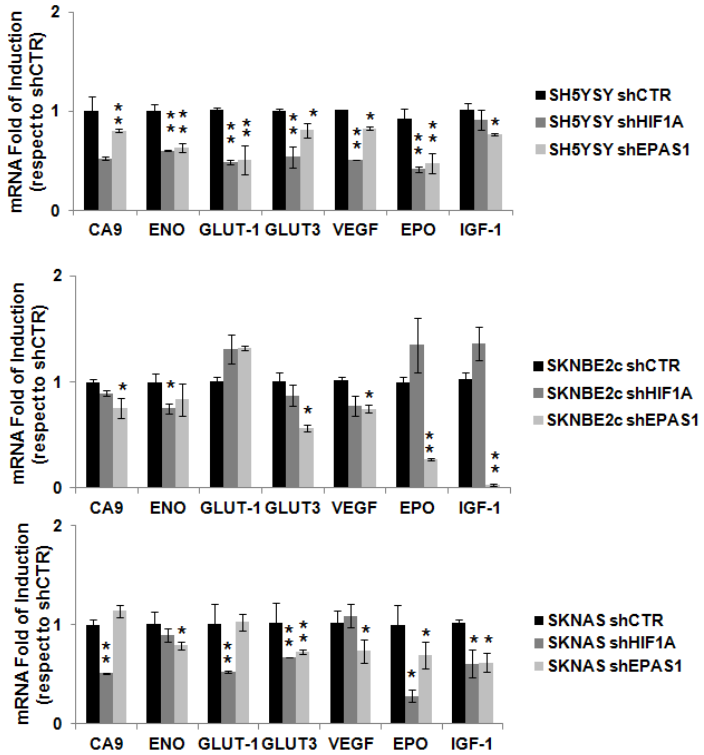

Figure 7.1. mRNA expression under *HIF1A* and *EPAS1* induction. The *HIF1A* and *EPAS1* induction of the expression of *CA9*, *ENO*, *GLUT-1*, *GLUT-3*, *VEGF*, *EPO*, *IGF-2* was evaluated by RT-PCR in the SHSY5Y (A), SKNBE2c (B) and SKNAS (C) cell lines previously silenced for *HIF1A* or *EPAS1* expression (i.e., sh*HIF1A* or sh*EPAS1*, respectively). The data are fold-changes of induction with respect to the shCTR unsilenced cells. The mean fold change of $2^{-(\text{average } \Delta\Delta CT)}$ was determined using the mean difference in the ΔC_T between the gene expression in the sh*HIF1A* or sh*EPAS1*cells and the ΔC_T for gene expression in the shCTR cells (as internal control). Data are means of three experiments (* P ≤0.05; ** P ≤0.01).

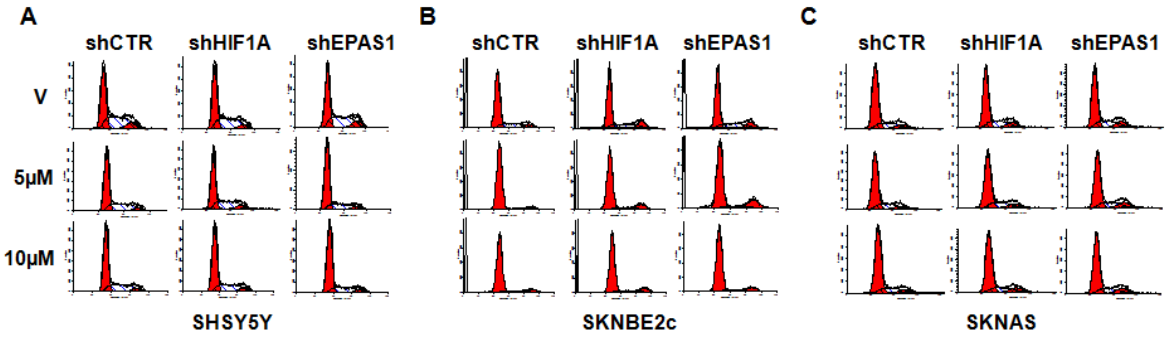

Figure 7.2. ATRA treatment: cell cycle. Unsilenced cells (shCTR) and HIF1A or EPAS1 silenced cells (i.e., shHIF1A or shEPAS1, respectively) treated for 6 days with 5 μM and 10 μM ATRA and then processed for flow cytometry using propidium iodide. Flow-histograms are shown for the SHSY5Y (A), SKNBE2c (B), SKNAS (C) cells.

Table 7.1. Differential gene expression between 'High' and 'Low' *EPAS1* mRNA expression levels.

Versteeg dataset			Seeger dataset		
Gene	**R-value**	**p-value**	**Gene**	**R-value**	**p-value**
UNC5C	0.494	0.0007	*CITED2*	0.598	1.65E-08
KDR	0.396	0.0381	*SH3GL3*	-0.473	0.0002
EYA4	0.396	0.0464	*EYA4*	0.462	0.0003
GPC3	0.383	0.0532	*SFRP1*	0.433	0.0012
GNA13	-0.400	0.0535	*INSM1*	0.418	0.0018
LAMA5	0.373	0.0604	*NRG1*	-0.420	0.0019
ESRRG	-0.369	0.0635	*SMAD1*	0.407	0.0025
EDA2R	-0.373	0.0688	*DLK1*	0.408	0.0028
TRPC5	-0.354	0.0711	*LY6H*	-0.380	0.0085
TNFAIP1	0.356	0.0720	*GREM1*	0.372	0.0112
SIX5	0.335	0.0721	*DCX*	-0.363	0.0154
LAMA3	0.340	0.0727	*GPR56*	-0.357	0.0164
LAMB1	0.339	0.0730	*CYP46A1*	-0.358	0.0164
GATA2	0.358	0.0733	*SEMA3D*	-0.359	0.0167
HAND1	0.360	0.0737	*NELL1*	0.343	0.0273
ANGPTL2	0.335	0.0740	*SEMA3A*	-0.337	0.0312
LRP5	0.337	0.0749	*POU4F1*	0.338	0.0318
ST8SIA4	-0.340	0.0756	*PAK3*	-0.333	0.0328
ELN	0.362	0.0758	*SMPD1*	-0.334	0.0333
TIMM8A	-0.335	0.0758	*NGFRAP1*	-0.329	0.0347
TLL2	-0.332	0.0759	*POU4F2*	0.330	0.0357
WIF1	-0.341	0.0761	*ITGA8*	-0.327	0.0366
SPP1	-0.342	0.0795	*HECA*	0.320	0.0461
ETS2	0.343	0.0796	*SMPD3*	-0.318	0.0470
DLL1	0.344	0.0799	*IL18*	-0.313	0.0510
TFAP2B	0.349	0.0821	*UNC5C*	0.314	0.0517
EBF4	0.344	0.0843	*DKK1*	0.314	0.0531
FOXO1	0.346	0.0858	*PKD2*	0.308	0.0587
EMD	-0.323	0.0904	*CHODL*	0.307	0.0593
ACVRL1	0.324	0.0920	*CDH11*	-0.306	0.0604
ENG	0.325	0.0924	*TBR1*	-0.304	0.0615
SEMA3D	-0.325	0.0955	*SLIT3*	0.302	0.0636
INSM1	0.319	0.0989	*DDX47*	0.302	0.0653
ACVR1	0.315	0.1001	*SPOCK2*	-0.295	0.0768
NPR3	0.319	0.1006	*SEMA6D*	-0.294	0.0773
MYH9	0.317	0.1015	*PAPSS1*	0.292	0.0778
OPHN1	-0.316	0.1017	*EXT2*	-0.295	0.0787
SFRP1	0.316	0.1033	*TRPC5*	-0.292	0.0798
TSHZ1	0.312	0.1099	*HDAC9*	0.290	0.0807
PRKAR1A	-0.306	0.1142	*LAMB1*	0.288	0.0838
AGT	0.308	0.1150	*ZEB2*	0.286	0.0899
COL18A1	0.305	0.1151	*PLXNA3*	-0.282	0.0986
SIX3	-0.306	0.1161	*KALRN*	-0.277	0.1143
FZD4	0.308	0.1172	*HRAS*	-0.276	0.1158
BEX1	-0.309	0.1174	*FGF14*	0.273	0.1233
EPHB4	0.307	0.1178	*ETS2*	0.273	0.1256
PKD2	0.302	0.1233	*PHGDH*	0.268	0.1265
KCNQ2	0.301	0.1262	*BTG1*	0.268	0.1269
FGFR3	0.300	0.1284	*DHCR24*	-0.269	0.1278
LFNG	0.298	0.1322	*PSME4*	0.267	0.1285
SPEG	0.296	0.1380	*ROBO3*	0.271	0.1287
AGPAT6	0.291	0.1421	*HHAT*	0.270	0.1295
FLII	0.291	0.1438	*CMKLR1*	-0.269	0.1296
NGRN	-0.294	0.1440	*STMN1*	-0.258	0.1306
HRAS	-0.290	0.1443	*RELN*	0.265	0.1313
SOSTDC1	-0.291	0.1460	*AES*	0.269	0.1315
COL4A2	0.286	0.1461	*CCL2*	-0.259	0.1321
NOTCH3	0.293	0.1462	*GAL*	0.265	0.1323
SLIT3	0.292	0.1473	*TWIST1*	0.259	0.1328
STAB1	0.286	0.1483	*SEMA6A*	-0.259	0.1335
LSR	0.286	0.1492	*SERPINI1*	0.264	0.1335
ERG	0.292	0.1494	*SMARCA1*	-0.263	0.1336
ADAM18	-0.284	0.1494	*ACVR1*	0.259	0.1343
GJA5	0.287	0.1497	*NME5*	-0.261	0.1350
DLL4	0.284	0.1503	*KLF3*	0.260	0.1353
SMAD1	0.288	0.1504	*PBXIP1*	0.261	0.1363
COL15A1	0.287	0.1507	*COL9A2*	-0.256	0.1370
TSHZ3	0.287	0.1520	*NGFR*	-0.260	0.1372
ERC2	-0.281	0.1521	*MARK2*	-0.262	0.1372
DAB2	0.283	0.1529	*NLGN1*	0.261	0.1375
ENPEP	0.281	0.1534	*PHYH*	0.256	0.1378
FRZB	0.280	0.1541	*EYA1*	0.254	0.1425
FZD8	0.282	0.1546	*PRKRA*	0.253	0.1446
SEMA5A	0.281	0.1554	*TCF12*	0.253	0.1448
ANGPT1	0.278	0.1613	*GRSF1*	0,252	0.1465
PRELP	0.278	0.1618	*TRIM3*	-0.251	0.1495
NPR1	0.277	0.1631	*TLE2*	0.249	0.1504
BDNF	-0.276	0.1634	*SEMA4D*	0.250	0.1512
TBX2	-0.272	0.1840	*CTNND2*	-0.249	0.1523
SNCA	-0.271	0.1877	*CDK5RAP3*	-0.248	0.1544
ZIC2	-0.270	0.1879	*SLIT2*	-0.246	0.1609
SVIL	0.270	0.1896	*SKIL*	-0.246	0.1626
NRP1	0.268	0.1897	*SEPP1*	-0.244	0.1679
ST8SIA2	0.268	0.1916	*RTN1*	-0.243	0.1710
SOX9	-0.269	0.1919	*CDKN1B*	0.243	0.1723
HOXC9	0.267	0.1944	*GAP43*	-0.241	0.1766
PLXND1	0.264	0.2080	*GADD45G*	-0.241	0.1770
FLNA	0.264	0.2101	*PFN1*	0.239	0.1832
MPPED2	-0.254	0.2170	*VCAN*	-0.238	0.1837
WFS1	0.255	0.2183	*IL7*	-0.238	0.1840
SEMA4C	0.254	0.2185	*PPARD*	0.236	0.1910
ID1	0.260	0.2186	*JMJD6*	-0.235	0.1946
HSPB2	0.261	0.2186	*UGDH*	0.235	0.1951
ZEB2	0.260	0.2187	*CHRM3*	0.234	0.1965
MMP2	0.261	0.2192	*STMN2*	-0.234	0.1979
VEZF1	-0.260	0.2193	*PTPRR*	0.233	0.1991
POFUT1	0.255	0.2199	*MYH6*	-0.232	0.1998
TUBD1	-0.257	0.2215	*SPRY2*	-0.232	0.2002

SNTG2	0.255	0.2218
ELK3	0.250	0.2220
FEZ1	-0.256	0.2223
COL6A3	0.255	0.2227
HDAC4	0.255	0.2228
GRSF1	0.256	0.2232
JAG1	0.258	0.2234
MAML3	0.250	0.2236
MYH11	0.257	0.2237
APAF1	0.258	0.2239
FGF5	-0.256	0.2240
CITED2	0.256	0.2243
SKI	0.250	0.2246
SIM2	-0.251	0.2250
THY1	0.257	0.2256
PPARD	0.250	0.2257
SOX11	-0.250	0.2259
PBXIP1	0.251	0.2268
AR	0.251	0.2271
MLF1	-0.252	0.2278
ITGB5	0.250	0.2278
FOXK1	0.251	0.2286
LMO1	0.246	0.2315
PLXNA1	0.245	0.2328
DLK1	0.247	0.2328
NPTN	-0.246	0.2333
TBX5	-0.245	0.2335
UNC5B	0.246	0.2341
SRF	0.245	0.2341
TSHZ2	0.247	0.2343
HTN3	-0.245	0.2345
HEYL	0.247	0.2350
SPATA18	-0.243	0.2436
NES	0.242	0.2439
NELL1	0.241	0.2450
ADAM10	0.241	0.2452
HOXD8	-0.242	0.2455
FLNB	0.242	0.2471
DGCR2	0.240	0.2492
SHC3	-0.240	0.2500
EYA1	0.239	0.2544
LHX6	0.238	0.2561
MEA1	-0.237	0.2562
PAPSS2	0.237	0.2573
SPARC	0.237	0.2580
NGFRAP1	-0.236	0.2611
POU4F2	0.235	0.2611
AHNAK	0.234	0.2612
ROBO4	0.235	0.2623
KLK6	-0.234	0.2627
QKI	-0.236	0.2627
DVL3	0.233	0.2635
COL1A1	0.236	0.2638
ITGA11	0.232	0.2641
RREB1	0.234	0.2645
FGF10	-0.233	0.2652
NTNG1	-0.232	0.2653
IGFBP4	0.232	0.2656
CCK	-0.232	0.2665
TRAF4	-0.232	0.2669
ANPEP	0.228	0.2673
NR5A2	0.228	0.2674
TLE3	0.232	0.2684
SERPINE2	0.228	0.2687
AFF3	0.228	0.2688
COL3A1	0.229	0.2688
FABP7	-0.229	0.2701
SNAI2	0.229	0.2712
MYT1	0.230	0.2722
CHUK	-0.229	0.2726
AEBP1	0.230	0.2736
SH3GL3	-0.229	0.2736
CALCRL	0.229	0.2739
COL1A2	0.229	0.2752
POU3F3	-0.226	0.2776
SLC30A1	0.226	0.2778
TGIF1	0.225	0.2811
VEGFC	0.225	0.2815
DLX2	-0.224	0.2864
INSR	0.223	0.2887
ITGA2	0.223	0.2895
TCL1A	0.222	0.2916
TFIP11	0.222	0.2922
DKK2	-0.221	0.2924
DCTN1	0.222	0.2925
SEMA5B	0.221	0.2931
DGKD	0.221	0.2955
DOPEY2	0.220	0.2978
MOV10	0.220	0.2989
DACH1	0.219	0.2995

TFIP11	0.231	0.2017
TP53BP2	0.231	0.2048
PAPSS2	0.226	0.2286
FGF9	-0.226	0.2293
ACP2	-0.225	0.2329
HBEGF	-0.224	0.2332
PCOLCE	0.223	0.2386
PPP1R9A	-0.223	0.2404
TLX3	0.221	0.2491
BRAF	-0.221	0.2503
NUMB	-0.219	0.2552
CREG1	-0.218	0.2559
SEMA3E	-0.218	0.2572
SH2B3	-0.217	0.2573
IFRD1	-0.217	0.2590
DIXDC1	0.218	0.2594
LEFTY2	-0.217	0.2602
CACNB2	-0.215	0.2606
NEO1	-0.215	0.2623
KRT19	-0.215	0.2628
PNMA1	-0.216	0.2635
TIMP1	-0.213	0.2677
NES	0.213	0.2682
DDX41	0.214	0.2690
PAX9	0.212	0.2723
CALCA	-0.210	0.2854
MFN2	-0.210	0.2865
DACH1	0.208	0.2924
TRO	-0.208	0.2954
THRA	-0.207	0.2971
TPP1	-0.207	0.2976
NRP2	-0.207	0.2994

Table7 2. Differential gene expression between 'High' and 'Low' *HIF1A* mRNA expression levels.

Versteeg dataset			Seeger dataset		
Gene	**R-Value**	**P-value**	**Gene**	**R-value**	**p-value**
JMJD6	0.582	0.00000	*GMFB*	0.396	0.0050
NTRK1	-0.515	0.00020	*KCNQ2*	-0.393	0.0051
ROR2	0.499	0.00035	*RELN*	0.397	0,0054
NRCAM	-0.490	0.00036	*PTHLH*	0.400	0.0055
SPRED2	0.486	0.00038	*ATXN3*	0.389	0.0055
B3GNT5	0.492	0.00040	*CNTFR*	-0.386	0.0059
HMX1	-0.479	0.00046	*APBA1*	-0.401	0.0060
SIX3	0.458	0.00125	*HDAC5*	-0.383	0.0063
RNF113A	0.455	0.00135	*NUMB*	0.418	0.0063
INSRR	-0.448	0.00168	*FRAT2*	-0.379	0.0068
DLX6	0.439	0.00191	*TCF25*	-0.376	0.0068
MAFF	0.440	0.00193	*ZNF267*	0.377	0.0071
PLXNC1	-0.443	0.00195	*BRSK2*	-0.402	0.0073
IL7	-0.436	0.00203	*MTR*	0.370	0.0076
RAPGEF5	-0.441	0.00205	*C1GALT1*	0.371	0.0076
SHC3	0.434	0.00212	*CUL7*	-0.372	0.0076
VPRBP	0.425	0.00275	*ATR*	0.428	0.0077
APBA1	-0.420	0.00281	*DRD2*	-0.366	0.0081
NR2F1	0.425	0.00286	*GLRB*	-0.405	0.0083
EIF2B2	0.426	0.00288	*LIF*	0.366	0.0084
ACHE	-0.421	0.00290	*APBA2*	-0.362	0.0089
TRERF1	-0.421	0.00301	*UGDH*	0.362	0.0091
RET	0.421	0.00307	*STMN3*	-0.360	0.0092
SOX6	-0.412	0.00381	*EGR3*	0.357	0.0099
RBBP7	0.409	0.00382	*CHUK*	0.351	0.0116
GPI	0.409	0.00390	*HMX1*	-0.351	0.0121
SCN8A	-0.412	0.00394	*SIAH1*	-0.352	0.0121
PRPS1	0.409	0.00405	*SOX15*	-0.349	0.0122
SH2D2A	-0.406	0.00422	*ELF3*	0.348	0.0124
AMIGO1	-0.404	0.00425	*MARK4*	-0.344	0.0140
CXCR4	0.405	0.00434	*SFRP4*	0.341	0.0155
PCOLCE	0.401	0.00477	*RBBP7*	0.337	0.0174
PHLDA2	0.398	0.00520	*NR2F1*	0.334	0.0178
INVS	0.395	0.00557	*SOX9*	0.328	0.0181
NRSN1	-0.396	0.00557	*C16orf80*	-0.335	0.0181
DLX5	0.395	0.00567	*GTF2IRD1*	-0.334	0.0181
GSS	0.390	0.00647	*NR5A2*	0.329	0.0181
PROK1	-0.387	0.00728	*EIF2AK3*	0.329	0.0181
SLIT1	0.385	0.00785	*LEPR*	0.330	0.0182
EXT2	0.383	0.00821	*MBNL1*	0.334	0.0185
HOXC4	-0.382	0.00826	*PRKAR1A*	0.331	0.0185
FREM1	-0.379	0.00902	*CRMP1*	-0.331	0.0186
HHAT	0.376	0.00977	*ACVR1B*	-0.332	0.0186
QKI	0.376	0.00990	*ARHGAP24*	0.330	0.0187
PLCE1	0.374	0.00998	*NTRK2*	0.325	0.0197
HES6	0.374	0.01001	*MAEA*	-0.325	0.0199
CITED1	0.375	0.01010	*DGCR2*	-0.320	0.0235
TSHZ2	-0.372	0.01022	*NCAM1*	-0.319	0.0236
KEAP1	0.373	0.01026	*INA*	-0.317	0.0250
KIF1B	-0.371	0.01035	*TNFSF11*	0.316	0.0254
SPEG	-0.370	0.01058	*PAFAH1B3*	-0.314	0.0260
RNF103	-0.369	0.01075	*BICC1*	0.315	0.0262
NHLH2	0.368	0.01080	*MEGF8*	-0.313	0.0267
CRABP1	0.367	0.01084	*TFAP2B*	-0.311	0.0272
SIX2	0.368	0.01089	*PDGFC*	0.312	0.0273
KRT19	-0.369	0.01093	*DPYSL3*	-0.312	0.0274
TEAD4	0.367	0.01101	*ARNT2*	-0.308	0.0300
FAM132B	0.366	0.01114	*CXCL1*	0.307	0.0301
EBF4	-0.364	0.01124	*SPEG*	-0.306	0.0308
TWIST1	0.364	0.01131	*CRKL*	-0.305	0.0319
VCAN	0.365	0.01132	*GATA2*	-0.304	0.0321
TMOD2	-0.364	0.01135	*AGT*	0.301	0.0358
ITGA8	-0.362	0.01165	*HOXD4*	0.297	0.0410
PCDHB12	-0.362	0.01166	*PLXNA1*	-0.296	0.0416
GRHL1	-0.359	0.01168	*AES*	-0.295	0.0419
LMO4	0.361	0.01180	*FLT1*	0.292	0.0454
APBA2	-0.360	0.01181	*BDNF*	0.291	0.0470
NDRG4	-0.359	0.01181	*PCDHB11*	-0.291	0.0473
PAPSS1	0.359	0.01190	*TNFRSF12A*	0.288	0.0499
CSRP2	0.360	0.01193	*BTG1*	0.288	0.0501
TGFB2	0.359	0.01196	*THBD*	0.285	0.0548
FZD7	0.361	0.01198	*HHEX*	0.284	0.0551
SEMA3F	0.356	0.01244	*FZD7*	0.283	0.0573
SPATA18	0.356	0.01255	*NEURL*	-0.282	0.0582
GDF11	-0.356	0.01262	*CALCA*	0.280	0.0603
PCDHB15	-0.353	0.01370	*CLPTM1*	-0.280	0.0603
MIB1	-0.350	0.01508	*TGFB3*	0.279	0.0617
MMP2	0.348	0.01611	*SPG7*	-0.277	0.0623
FEZ1	0.347	0.01673	*MATN3*	0.278	0.0629
CHST9	-0.346	0.01675	*NTRK1*	-0.277	0.0629
HESX1	0.346	0.01686	*PTEN*	0.278	0.0632
MSH6	0.344	0.01764	*PRMT1*	-0.275	0.0641
ZBTB16	-0.343	0.01803	*GRIK1*	0.275	0.0645
ZMYM4	-0.340	0.02018	*QKI*	0.274	0.0649
EBF1	-0.339	0.02060	*CTNNB1*	0.275	0.0650
TLL2	0.337	0.02113	*EYA2*	0.273	0.0650
FKBP4	0.338	0.02121	*DCN*	0.275	0.0652
NEURL	-0.337	0.02154	*SMPD3*	-0.273	0.0655
TBX20	-0.333	0.02430	*HSD11B1*	0.271	0.0690
PDGFRA	0.332	0.02441	*PTMS*	-0.269	0.0732
NINJ1	0.331	0.02511	*DOK4*	-0.268	0.0743
POU3F1	-0.331	0.02519	*GPR65*	0.268	0.0748
DACT1	0.330	0.02579	*SEMA3C*	0.267	0.0752
WNT3	0.328	0.02682	*FBN2*	0.267	0.0754
CYFIP1	0.327	0.02779	*SLC30A1*	0.266	0.0754
SPHK1	0.327	0.02805	*KEAP1*	-0.266	0.0758
PRRX2	0.324	0.02969	*LAMA2*	0.264	0.0783

SRF	0.324	0.02988
CHODL	0.323	0.03039
FOXC1	0.322	0.03078
NRP1	-0.322	0.03084
CTNND2	-0.322	0.03085
VANGL2	-0.320	0.03210
FZD2	0.320	0.03227
SHB	0.319	0.03269
ALK	0.319	0.03309
DDX1	0.318	0.03363
FGF14	0.317	0.03405
HUS1	0.316	0.03429
DRD2	-0.316	0.03460
GATA2	-0.316	0.03471
UGDH	0.315	0.03483
DNER	-0.315	0.03499
ZNF22	0.315	0.03528
CEBPB	0.312	0.03729
ARVCF	-0.310	0.04016
ARHGAP22	-0.309	0.04025
SOX4	-0.309	0.04025
SALL1	-0.310	0.04043
GRSF1	0.307	0.04287
PHGDH	0.307	0.04293
HEXB	0.303	0.04704
DRP2	0.303	0.04765
AQP4	-0.301	0.04915
SBF2	-0.301	0.04929
LIMD1	0.300	0.04944
STRBP	0.300	0.04959
HOXB4	0.300	0.04975
DSCAM	0.300	0.05010
CNTN4	0.298	0.05228
BMPR2	-0.298	0.05248
GJA1	0.297	0.05281
HOXA4	0.297	0.05304
NCL	0.296	0.05311
PRMT1	0.296	0.05342
TIMP1	0.296	0.05363
CNTFR	-0.295	0.05511
AATF	0.294	0.05521
MYCNOS	0.294	0.05527
DDX47	0.294	0.05534
PRELID1	0.293	0.05581
CA10	-0.290	0.06053
PMP22	-0.289	0.06185
LAMA3	-0.289	0.06264
EPHB1	0.287	0.06385
SNTG2	-0.287	0.06417
MACF1	-0.287	0.06435
CAPN3	-0.286	0.06543
FYN	-0.286	0.06618
PTTG1IP	0.285	0.06731
MYT1L	-0.284	0.06814
PITX1	0.284	0.06880
WWP1	-0.283	0.07059
WNT5B	0.282	0.07092
EXT1	0.280	0.07444
ADAMTS9	0.278	0.07654
APBB2	0.278	0.07687
SCG2	-0.279	0.07700
MTSS1	-0.278	0.07730
ACVR2A	-0.278	0.07756
MYCN	0.277	0.07900
EPHB2	0.276	0.07953
PNMA1	0.276	0.07987
KIAA1715	-0.275	0.08132
MYT1	-0.275	0.08245
BZW2	0.273	0.08489
ASB1	0.273	0.08519
PCDHA3	-0.273	0.08522
TFAP2B	-0.273	0.08538
NRGN	0.272	0.08649
SIX4	0.271	0.08873
NAIP	-0.270	0.08885
ELAVL3	0.270	0.09064
DZIP1	0.269	0.09146
EDF1	0.268	0.09412
CBLN1	0.267	0.09544
CALCRL	-0.267	0.09580
MST1R	-0.266	0.09648
RACGAP1	0.265	0.09821
KALRN	0.265	0.09825
MAEA	0.265	0.09849
CHERP	0.265	0.09858
HOXD3	0.265	0.09867
POMT1	-0.264	0.09871
ATR	0.263	0.10080
WNT4	-0.263	0.10086
PDPN	0.262	0.10108
JPH1	0.263	0.10115
FES	0.263	0.10140
SEMA6C	-0.262	0.10157
GAL	0.261	0.10264
IL8	0.261	0.10355
NMUR2	-0.260	0.10363
RORB	-0.261	0.10364
FMN2	-0.260	0.10413
ALDH3A2	-0.259	0.10482
SEMA3E	-0.259	0.10533
HAND2	-0.259	0.10580
CANX	0.258	0.10648

CA10	-0.263	0.0812
SEMA5A	0.261	0.0813
PHOX2B	-0.261	0.0820
SVIL	0.262	0.0821
CD164	0.261	0.0821
NDRG4	-0.262	0.0825
DIXDC1	-0.261	0.0828
EFNB3	-0.261	0.0833
FZD3	-0.257	0.0842
FYN	-0.259	0.0845
C4orf6	0.257	0.0850
CTNND2	-0.257	0.0850
ITGB1	0.259	0.0850
ZFP36L1	0.256	0.0854
EDAR	0.257	0.0855
TGFBR3	0.258	0.0861
MAPT	-0.258	0.0869
FUT8	0.255	0.0870
ARC	0.255	0.0883
LMO1	-0.254	0.0893
MT3	0.254	0.0895
VPRBP	0.253	0.0911
AHNAK	0.252	0.0921
GATA3	-0.249	0.1008
PBX1	-0.248	0.1017
GNAO1	-0.247	0.1045
GSS	0.247	0.1045
RYK	0.247	0.1048
WNT5A	0.246	0.1054
SCMH1	-0.242	0.1065
PLXNB2	-0.245	0.1067
SMAD1	-0.242	0.1069
TTPA	0.245	0.1070
MCL1	0.242	0.1072
SEMA3E	0.242	0.1073
TRO	-0.244	0.1074
THRA	-0.244	0.1075
GAS7	0.245	0.1075
TNFRSF11B	0.245	0.1076
PLXNB1	-0.243	0.1077
ARVCF	-0.242	0.1079
PDPN	0.244	0.1080
CREG1	0.241	0.1085
FGFR1	0.242	0.1086
ACVR1	0.243	0.1087
PBX3	-0.239	0.1093
HOXB7	0.239	0.1100
NFATC1	0.238	0.1100
SEMA7A	0.240	0.1103
HTATIP2	0.238	0.1103
SEMA3B	0.238	0.1104
BMPR1B	-0.240	0.1104
MYL6B	-0.240	0.1107
SGCB	-0.238	0.1111
DNM1L	-0.239	0.1113
DCTN1	-0.237	0.1118
TP53BP2	0.237	0.1124
AHCTF1	0.236	0.1126
LECT2	0.237	0.1127
HAND2	-0.236	0.1128
NTNG1	0.236	0.1129
PIAS4	-0.236	0.1129
ERC1	-0.235	0.1139
NPTX1	0.234	0.1151
RNF103	-0.233	0.1184
NR4A3	0.233	0.1186
LGR4	0.233	0.1192
NDP	0.233	0.1196
DOC2A	-0.231	0.1212
LHX3	0.231	0.1213
ADAM10	0.231	0.1215
PHC3	0.231	0.1215
CRIM1	0.231	0.1216
MPZ	0.229	0.1251
SEMA4C	-0.229	0.1264
LGALS3	0.226	0.1285
MKL2	0.226	0.1291
LECT1	0.227	0.1296
SRI	-0.228	0.1296
TMOD2	-0.227	0.1296
PCDHB6	-0.227	0.1299
NAPA	-0.227	0.1301
DHCR24	0.227	0.1305
EDA	0.225	0.1327
BIN1	-0.224	0.1336
TNFAIP1	-0.225	0.1338
MAPK12	-0.223	0.1360
LIMD1	0.223	0.1363
BMP1	-0.223	0.1365
MID1	-0,223	0.1371
GJA1	0.222	0.1377
APLP1	-0.222	0.1378
GHR	0.222	0.1384
EMP1	0.222	0.1386
ATP6AP1	-0.221	0.1409
CXCR4	0.220	0.1419
SMAD3	0.220	0.1421
MTSS1	-0.220	0.1421
NRCAM	-0.220	0.1422
AMOT	0.218	0.1451
PRKRA	-0.218	0.1452
NOTCH2	0.218	0.1454

TUBD1	0.258	0.10690
VAX2	0.258	0.10724
TRIM54	0.257	0.10741
NFE2	-0.258	0.10785
TGFB3	0.257	0.10817
MITF	0.257	0.10834
SOX11	0.256	0.10958
FGF11	0.256	0.10985
DLL3	0.255	0.11035
CRYGD	0.255	0.11046
EIF2B5	0.255	0.11086
PSME4	0.255	0.11089
CTNNBIP1	-0.254	0.11102
EIF2AK3	0.255	0.11105
ECE2	-0.254	0.11151
FGF2	0.254	0.11185
LAMA4	-0.253	0.11206
TP53	0.253	0.11258
ITGA2	0.253	0.11401
GFRA3	-0.252	0.11440
SMAD3	0.252	0.11445
FZD5	0.251	0.11733
BMPR1A	0.250	0.11872
UNC5D	-0.250	0.11934
ANGPTL4	0.250	0.11968
MEOX1	-0.250	0.11983
MCL1	0.249	0.11994
EGR3	0.249	0.12135
E2F5	0.248	0.12247
DHCR7	0.248	0.12280
CNTN2	0.247	0.12411
SOX9	0.247	0.12478
CFC1	0.247	0.12531
SH3GL1	0.246	0.12547
NEUROD1	0.246	0.12579
STMN2	-0.245	0.12747
FHL3	0.245	0.12760
SMAD5	-0.245	0.12762
FLNB	0.244	0.13045
HECA	-0.243	0.13439
ACSBG1	-0.242	0.13493
HOXD9	0.242	0.13546
EMD	0.242	0.13577
GLRB	-0.241	0.13690
HMGB3	0.241	0.13772
HTATIP2	0.240	0.14007
ENC1	0.239	0.14218
DACH1	0.239	0.14220
DLK1	0.239	0.14341
CLDN11	0.238	0.14426
ERCC2	0.238	0.14473
CENPF	0.237	0.14576
PBX3	0.237	0.14641
CHRDL2	0.236	0.14816
LAMA1	0.235	0.15238
IRS2	0.235	0.15245
ANGPT2	0.234	0.15342
YWHAH	-0.234	0.15371
PKD2	0.234	0.15382
PTCH1	0.234	0.15387
ANGPTL2	0.234	0.15408
GCNT2	-0.234	0.15436
AXIN2	0.233	0.15505
MTL5	-0.233	0.15528
BVES	0.233	0.15545
MAML3	-0.233	0.15555
FXR1	0.232	0.15627
RNH1	0.232	0.15674
MARK4	0.231	0.15887
COL11A2	-0.231	0.15937
NDE1	0.231	0.15940
FUT10	0.231	0.15940
LOX	0.231	0.15948
MXD1	-0.230	0.16084
CCNF	0.229	0.16404
ATRNL1	-0.229	0.16436
THRA	-0.229	0.16460
SIAH2	0.229	0.16487
EHF	-0.228	0.16603
LEFTY1	-0.228	0.16658
WDR5	0.227	0.16701
THBD	0.227	0.16735
HRAS	0.227	0.16750
PSEN2	0.227	0.16769
PBX1	-0.226	0.16781
NHLH1	0.226	0.16781
AZU1	-0.227	0.16786
MYH3	-0.225	0.17132
COL13A1	0.225	0.17218
ZNF256	0.223	0.17691
F2R	0.223	0.17706
HOXD10	0.223	0.17713
EYA2	0.224	0.17722
DIP2A	-0.223	0.17789
DAZAP1	0.223	0.17796
MNT	0.222	0.17908
KLF5	-0.222	0.17925
ZNF7	0.222	0.17966
TCF12	0.221	0.18073
ETV5	0.221	0.18075
MAPT	-0.221	0.18082
TIMM8A	0.221	0.18095

NES	-0.218	0.1456
HMGCR	0.218	0.1457
VLDLR	0.217	0.1479
RAI2	0.216	0.1480
NRL	0.216	0.1483
ANPEP	0.217	0.1487
ILK	-0.216	0.1489
GATA6	0.216	0.1491
PTN	0.214	0.1527
TAGLN3	-0.215	0.1528
MYT1	-0.214	0.1535
MAPK1	-0.214	0.1541
CTNNBIP1	-0.213	0.1567
PTS	-0.212	0.1596
EREG	0.212	0.1596
HAND1	-0.211	0.1604
GNRH1	0.210	0.1658
YWHAH	-0.210	0.1666
RASA1	0.209	0.1681
MDK	-0.208	0.1697
DRG1	-0.207	0.1704
NEUROD1	0.207	0.1706
POGK	-0.208	0.1706
DMD	0.208	0.1708
ZMYM4	-0.208	0.1709
DCLK1	-0.207	0.1710
CACNA1A	0.206	0.1712
STX2	-0.208	0.1713
F2	0.207	0.1713
SEMA4F	-0.206	0.1714
BMP10	0.206	0.1716
TOP1	0.206	0.1718
NRP2	-0.205	0.1725
BAX	-0.205	0.1730
TRIM3	-0.205	0.1733
NDUFV2	-0.205	0.1737
FOXO4	0.204	0.1752
ADAMTS9	0.204	0.1755
SEMA4D	-0.204	0.1757
IL8	0.204	0.1760
ROBO3	-0.203	0.1765
MYT1L	-0.202	0.1788
DKK1	0.202	0.1789
SPHK2	-0.203	0.1791
EGR2	0.201	0.1849
ANGPTL4	0.199	0.1926
WWP1	0.198	0.1942
FZD6	0.198	0.1952
PGF	0.198	0.1954
RACGAP1	0.198	0.1957
PTMA	0.197	0.1966
TMPRSS6	0.197	0.1972
TAL1	0.197	0.1977
DGAT1	-0.196	0.1980
PPAP2B	0.196	0.2009
PHLDA2	0.194	0.2022
OPHN1	0.193	0.2027
MPPED2	-0.194	0.2029
SOX2	0.194	0.2031
DICER1	0.194	0.2033
NF1	-0.193	0.2034
THBS1	0.194	0.2036
PIK3CB	0.193	0.2037
EBF2	0.192	0.2037
EXT1	0.192	0.2037
ZEB2	0.194	0.2039
MSX1	0.192	0.2039
OVOL2	0.194	0.2041
LUC7L	-0.193	0.2042
BMPR1A	0.192	0.2043
CASP7	0.193	0.2045
CDK5RAP1	0.194	0.2047
NGRN	-0.194	0.2054
TLX2	-0.191	0.2058
DGKD	-0.191	0.2061
MAP1S	-0.194	0.2061
FOXC1	0.191	0.2062
ZNF3	-0.191	0.2066
ISL1	-0.191	0.2069
EIF2B2	0.191	0.2070
SIX2	0.191	0.2071
CDK5	-0.190	0.2095
NGFR	0.189	0.2098
SPP1	0.189	0.2102
NDRG2	-0.189	0.2103
MYCNOS	0.189	0.2104
ITGB7	0.189	0.2104
SPON1	0.189	0.2109
ANGPTL3	0.188	0.2115
GNRHR	0.187	0.2139
JARID2	-0.188	0.2142
L1CAM	-0.187	0.2146
NR4A2	0.187	0.2161
ODAM	0.187	0.2163
OLIG2	0.186	0.2174
GADD45B	0.186	0.2184
FZD1	0.185	0.2207
SPHK1	0.185	0.2234
MMP19	0.184	0.2244
CDK5R1	-0.184	0.2257
MMP11	-0.184	0.2259
PHC1	-0.182	0.2288

CHD5	-0.221	0.18129
CHRD	-0.221	0.18142
ALDH5A1	0.220	0.18190
RYK	0.220	0.18253
ID2	0.220	0.18292
PROK2	0.219	0.18437
CHKB	-0.219	0.18504
COL4A4	-0.218	0.18784
ERBB3	-0.218	0.18786
WNT6	0.217	0.18948
ERBB4	0.218	0.18963
EIF2B4	0.217	0.19228
LAMB1	0.216	0.19279
LY6H	0.216	0.19313
EPO	-0.216	0.19340
TBX2	0.216	0.19380
C11orf73	0.215	0.19417
DNASE2	0.215	0.19449
RELA	0.215	0.19504
SMO	0.214	0.19955
LMO1	-0.214	0.19979
LETM1	0.213	0.19991
MAPK1	-0.214	0.19991
FOXD3	-0.213	0.20344
GLDN	0.212	0.20548
AFF3	-0.212	0.20557
IFRD1	-0.212	0.20582
PAK3	-0.212	0.20584
PKP2	-0.211	0.20686
PTP4A1	-0.211	0.20708
LGALS1	0.210	0.20986
CCM2	-0.210	0.20995
SORT1	0.210	0.21009
FZD6	0.210	0.21018
SH3GL2	0.209	0.21251
RPS6KA6	0.209	0.21293
ARC	0.209	0.21310
FGF1	0.208	0.21431
AES	-0.208	0.21493
TRIM3	-0.207	0.21732
PCDHA2	-0.207	0.21740
HTR2B	0.207	0.21764
ZEB2	-0.207	0.21784
HHIP	0.206	0.22235
TRAF6	0.206	0.22283
MYL4	-0.205	0.22319
ISL1	-0.205	0.22348
SPRY4	0.205	0.22373
WNT8A	-0.205	0.22432
HEMGN	-0.205	0,22473
PCP4	-0.204	0.22835
CREG1	0.203	0.22985
MYH6	-0.203	0.23100
SFRP4	0.203	0.23214
HOXA5	0.202	0.23392
CALCA	0.202	0.23402
CFDP1	0.201	0.23719
CDON	-0.201	0.23834
ELF3	-0.200	0.24000
VDR	0.200	0.24100
ID4	0.200	0.24133
NR4A3	0.198	0.24182
GAP43	-0.198	0.24220
E2F1	0.199	0.24239
HOXB8	0.199	0.24251
MEA1	0.198	0.24276
AMOT	-0.199	0.24276
TMPRSS6	-0.199	0.24283
DIXDC1	-0.199	0.24293
GREM1	-0.199	0.24305
DSCAML1	0.199	0.24309
SPRED1	0.198	0.24326
BMP3	-0.199	0.24358
NLGN1	0.199	0.24397
PAFAH1B3	0.197	0.24492
RAB23	0.197	0.24627
SEPP1	-0.197	0.24637
IL1RAPL2	-0.196	0.24655
UNC5B	0.197	0.24671
LDB1	0.196	0.24698
ACVR1B	-0.196	0.24703
NPTX1	0.196	0.24768
ODAM	0.196	0.24803
TIMELESS	0.194	0.24989
VEGFC	0.194	0.25038
POSTN	0.194	0.25040
PAX5	0.194	0.25075
EBP	0.194	0.25080
FOXO1	-0.195	0.25095
NFATC3	0.194	0.25102
RPS4X	0.194	0.25125
GLI2	0.195	0.25142
FGFR3	-0.195	0.25149
ZNF45	0.194	0.25159
ADCYAP1R1	0.195	0.25164
FGF13	-0.195	0.25168
GADD45G	-0.193	0.25180
AVIL	-0.193	0.25473
LGR4	0.192	0.25557
ROBO3	-0.192	0.25594
NANOG	-0.192	0.25829
ST6GAL2	0.191	0.26080
PIM1	0.183	0.2291
NHLH2	0.183	0.2299
PAX2	0.182	0.2305
MYL1	0.183	0.2306
MEF2C	0.182	0.2321
ZBTB17	-0.181	0.2322
WNT6	0.180	0.2369
CRYGC	-0.180	0.2375
MITF	0.180	0.2375
REG3A	0.180	0.2377
DPYSL4	-0.179	0.2397
FHL1	-0.179	0.2401
RNH1	-0.179	0.2402
RET	0.177	0.2460
KDR	0.177	0.2464
ELAVL1	0.178	0.2465
AGGF1	-0.177	0.2468
IL23A	-0.177	0.2469
GPM6B	0.177	0.2473
STIL	0.177	0.2475
NEUROD4	0.177	0.2476
DAZAP1	0.176	0.2479
DOPEY2	-0.175	0.2517
TRPS1	0.175	0.2523
XAB2	-0.175	0.2529
HEXB	0.174	0.2539
HPCAL4	-0.175	0.2539
SRF	0.174	0.2563
SPRED2	0.173	0.2595
GNA13	-0.172	0.2646
HEY1	0.172	0.2647
APBB2	0.172	0.2648
DCX	-0.171	0.2660
CHRDL1	0.171	0.2665
PDGFRA	0.171	0.2667
PDE3B	0.171	0.2672
CSPG5	-0.169	0.2759
BMP2	0.169	0.2761
IRS2	-0.169	0.2767
TPP1	0.169	0.2775
SIAH2	-0.168	0.2794
LRCH4	0.168	0.2795
ELK3	0.168	0.2810
ITGB4	0.167	0.2820
PRPS1	0.166	0.2865
TFIP11	-0.166	0.2868
SYK	0.166	0.2872
AR	0.166	0.2875
EBP	0.165	0.2877
PDLIM5	0.165	0.2877
SPP2	0.166	0.2878
MLL	-0.166	0.2879
MAP2K1	-0.165	0.2880
LMO4	0.165	0.2888
HOXA7	0.164	0.2902
KIF1B	-0.164	0.2911
ANGPTL2	0.164	0.2918
NRP1	-0.164	0.2920
UNC5C	-0.164	0.2920
FGF12	0.163	0.2931
RPS6KA3	0.163	0.2931
MKKS	-0.163	0.2933
LMO2	0.162	0.2936
PPT1	0.161	0.2936
ERBB3	0.163	0.2937
UBE3A	-0.162	0.2937
CHL1	0.163	0.2939
CYLC1	0.162	0.2940
CYR61	0.162	0.2943
ENPEP	0.162	0.2945
CSRP2	0.162	0.2947
JAG1	0.162	0.2948
FEZ1	-0.159	0.2949
SMAD4	-0.159	0.2949
GPC3	0.162	0.2949
EMP2	0.159	0.2954
FXR1	0.161	0.2955
VAMP5	0.161	0.2956
FBN1	0.159	0.2957
SPRY1	0.159	0.2957
SEMA4G	0.161	0.2957
LGI1	0.159	0.2957
MYH11	0.159	0.2959
MAFG	-0.161	0.2963
PLXNA3	-0.159	0.2964
ENPP1	0.158	0.2969
JAG2	-0.159	0.2971
UTRN	-0.158	0.2972
MARK2	-0.159	0.2975
VCAN	0.160	0.2978
ARHGAP22	-0.160	0.2978
CYLC2	0.158	0.2982
GAMT	-0.160	0.2986
SPIN1	-0.160	0.2988
ADAM22	-0.160	0.2988
NBN	0.160	0.2990
PITX1	0.157	0.2999

SVIL	0.191	0.26213
BDNF	0.190	0.26290
MTR	0.190	0.26325
ZEB1	-0.190	0.26433
LDB2	-0.190	0.26541
EFNB2	-0.189	0.26886
SNAI1	0.188	0.27120
DOK4	-0.188	0.27154
OBSCN	-0.187	0.27476
ITGB8	-0.188	0.27482
TOP2B	0.187	0.27491
PAFAH1B1	-0.186	0.27868
DGKD	-0.186	0.27880
DVL2	0.186	0.27905
HAND1	-0.186	0.27917
GPR56	0.186	0.27919
EGR2	0.186	0.27944
ADAM18	-0.186	0.27947
FGF18	0.186	0.27964
GNAO1	-0.185	0.28210
SPG7	-0.185	0.28298
CHRM1	-0.185	0.28317
VGLL2	-0.184	0.28560
CLC	-0.184	0.28590
MKL2	0.184	0.28608
HLF	-0.183	0.28769
STX2	-0.183	0.28931
ATP2B2	-0.182	0.29117
CEBPG	0.182	0.29260
ID3	0.181	0.29394
SEMA4C	0.182	0.29444
CYP46A1	-0.181	0.29458
ETV4	0.181	0.29479
POU6F1	-0.181	0.29506
PHF3	-0.181	0.29570
HPCAL4	-0.181	0.29581
BRSK2	-0.180	0.29652
LGALS3	0.180	0.29692
PCDHA10	-0.180	0.29782
AZI1	0.180	0.29806
EFNB1	0.180	0.29834
RPL29	0.180	0.29875
HOXC6	-0.179	0.29904
LEFTY2	-0.179	0.29926

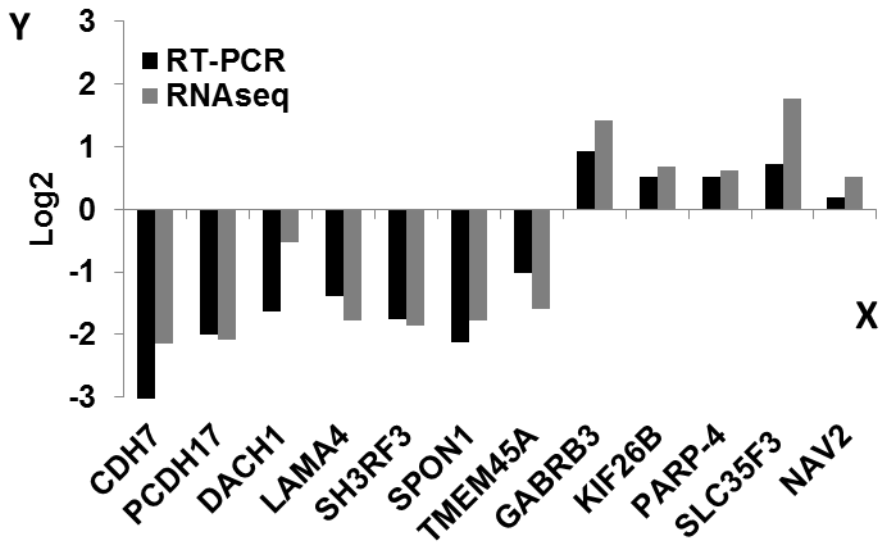

Figure 7.3. mRNA expression of "HIF1Atarget genes" reported as log2 fold change value obtained from rt-PCR and RNA-seq data analysis. Expression of CDH7, PCDH17, DACH1, LAMA4, SH3RF3, SPON1, TMEM45A, GABRB3, KIF26B, PARP-4, SLC35F3 and NAV2 was evaluated by RT-PCR in SKNBE2c sh HIF1A HYP and shCTR HYP. The fold-changes of shHIF1A vs shCTR is reported as log2 value.(Y axis). The log2 obtained from RT--PCR and from RNA-seq are shown in the graph in black and gray respectively (P-value ≤0.05). For both analysis the same mRNA samples (in triplicates) were used.

Table 7.3 (Lasorsa VA et al, oncotarget 2016) Results of prioritization of driver mutations combining data obtained by WES and DT-seq

Sample ID	Risk group	HUGO symbol	Sequence ontology	Sequence ontology protein sequence change	CHASM 3.2 cancer driver p-value (missense)	CHASM 3.2 cancer driver FDR (missense)	VEST 3.2 pathogenicity p-value (non-silent)	VEST 3.2 pathogenicity FDR (non-silent)	Composite p-value
NB1794	HR-Event3	ADCY3	MS	C125F	0,3592	0,65	0,0093	0,10	
NB1794	HR-Event3	ADCY6	MS	G486C	0,0012	0,05	0,0063	0,10	
NB2181	HR-Event3	AFF1	MS	S466Y	0,0114	0,25	0,0677	0,20	
NB2181	HR-Event3	AHNAK	FI	L5583fs	.	.	0,0060	0,10	
NB2181	HR-Event3	AKAP11	MS	E1339G	0,0242	0,35	0,0114	0,10	
NB2186	HR-Event3	ALK	MS	F1174L	0,00001	0,05	0,0116	0,10	8,09E-36
NB1506	HR-Event3	ALK	MS	F1245V	0,00001	0,05	0,0063	0,10	
NB1965	HR-Event3	ALK	MS	F1245C	0,00001	0,05	0,0060	0,10	
NB1229	High	ALK	MS	F1174L	0,00001	0,05	0,0116	0,10	
NB1355	Intermediate	ALK	MS	F1174L	0,00001	0,05	0,0116	0,10	
KELLY	High	ALK	MS	F1174L	0,00001	0,05	0,0116	0,10	
LAN-1	High	ALK	MS	F1174L	0,00001	0,05	0,0116	0,10	
SK-N-SH	High	ALK	MS	F1174L	0,00001	0,05	0,0116	0,10	
NB1506	HR-Event3	ALPK1	MS	A200T	0,0434	0,45	0,0142	0,10	
NB2136	HR-Event3	ANGPTL3	MS	L203P	0,0140	0,25	0,0061	0,10	
NB2100	HR-Event3	APTX	MS	H220Q	0,0008	0,05	0,0059	0,10	
NB1488	HR-Event3	ARHGEF10L	MS	W348C	0,2458	0,60	0,0111	0,10	3,28E-04
NB1875	High	ARHGEF10L	MS	G1058D	0,0692	0,50	0,0110	0,10	
NB2136	HR-Event3	ASPHD2	MS	P174H	0,2390	0,60	0,0138	0,10	
NB2181	HR-Event3	ATP8B4	MS	Y941C	0,0008	0,05	0,0127	0,10	
NB2437	HR-Event3	ATRX	SG	E1644X			0,0015	0,10	6,84E-03
SK_N_BE2	High	^ATRX	MS	N717K	0,7476	0,85	0,5182	0,65	
NB1488	HR-Event3	CD163	MS	G530R	0,0242	0,35	0,0087	0,10	
NB2181	HR-Event3	CDIPT	MS	R55H	0,0158	0,30	0,0062	0,10	
NB1506	HR-Event3	CH25H	FD	225_226del	.	.	0,0013	0,10	
NB1690	HR-Event3	CHD9	MS	S616P	0,00001	0,05	0,0197	0,10	2,54E-11
NB1229	High	CHD9	MS	F2295L	0,0030	0,10	0,0212	0,10	
NB1855	HR-Event3	CHD9	MS	R2284G	0,0008	0,05	0,0133	0,10	
SK-N-SH	High	CHD9	MS	R2554I	0,0092	0,25	0,0164	0,10	
NB2136	HR-Event3	CNNM4	MS	A271V	0,1696	0,55	0,0180	0,10	
NB1812	HR-Event3	COL5A2	MS	R916S	0,3548	0,65	0,0240	0,10	
NB2181	HR-Event3	COL6A6	MS	G359R	0,0756	0,50	0,0067	0,10	2,11E-06
NB1900	HR-Event3	COL6A6	MS	R719Q	0,0042	0,15	0,0120	0,10	
CHP126	High	COL6A6	MS	G1452E	0,1872	0,55	0,0083	0,10	
NB1690	HR-Event3	COLGALT2	MS	R196L	0,0148	0,25	0,0079	0,10	
NB2181	HR-Event3	CPLX2	MS	M55I	0,0932	0,55	0,0197	0,10	
NB2181	HR-Event3	CTNNAL1	MS	A420T	0,1382	0,55	0,0195	0,10	
NB2181	HR-Event3	DCHS1	MS	R2330C	0,2138	0,60	0,0183	0,10	
NB2136	HR-Event3	DCUN1D4	MS	E246K	0,0242	0,35	0,0056	0,10	
NB1995	HR-Event3	DHRS7	MS	R271G	0,2830	0,60	0,0172	0,10	
NB2161	HR-Event3	DMBT1	SG	S542X	.	.	0,0060	0,10	
NB1794	HR-Event3	DTHD1	MS	I405K	0,1098	0,55	0,0067	0,10	2,16E-04
NB1054	HR-Event3	DTHD1	MS	P489T	0,2000	0,60	0,0118	0,10	
NB1488	HR-Event3	DYSF	MS	L2R	0,2390	0,60	0,0225	0,10	
NB1488	HR-Event3	ERBB3	MS	C231Y	0,0056	0,15	0,0065	0,10	
NB2100	HR-Event3	FGFR1	MS	N457K	0,0000	0,05	0,1207	0,30	
NB1690	HR-Event3	FHOD3	MS	R1388L	0,0148	0,25	0,0284	0,15	
NB1488	HR-Event3	FZD1	MS	Q572L	0,1668	0,55	0,0176	0,10	6,84E-04
NB2794	HR-Event3	FZD1	SG	E314X			0,0152	0,10	
NB1488	HR-Event3	FZD7	MS	Y244H	0,0392	0,40	0,0108	0,10	
NB1914	HR-Event3	GABRB2	MS	F464L	0,2050	0,60	0,0084	0,10	1,47E-04
LAN-1	High	GABRB2	MS	R354S	0,0326	0,40	0,0062	0,10	
NB2136	HR-Event3	GBE1	MS	P440T	0,0058	0,15	0,0080	0,10	2,35E-04
CHP126	High	GBE1	MS	P552L	0,0146	0,25	0,0106	0,10	
NB1812	HR-Event3	GCNT4	MS	P132Q	0,1524	0,55	0,0086	0,10	
NB1794	HR-Event3	HADHB	MS	D357Y	0,0604	0,50	0,0069	0,10	
NB2181	HR-Event3	HECTD3	MS	R406C	0,0400	0,40	0,0106	0,10	
NB1767	HR-Event3	HIVEP1	MS	R1029I	0,1872	0,55	0,0154	0,10	
NB2136	HR-Event3	HNF4A	MS	G79S	0,2116	0,60	0,0066	0,10	
NB2136	HR-Event3	HTRA1	MS	A180T	0,0406	0,40	0,0199	0,10	4,21E-06
NB962	HR-Event3	HTRA1	FD	171_171del			0,0010	0,10	
STA-N-B7	High	HTRA1	MS	R197Q	0,1078	0,55	0,0190	0,10	
NB1488	HR-Event3	IKBKAP	MS	G1210D	0,0008	0,05	0,0065	0,10	
NB2181	HR-Event3	INTS1	MS	F1962C	0,3258	0,65	0,0231	0,10	
NB1488	HR-Event3	IPO5	MS	E1026K	0,0000	0,05	0,0065	0,10	5,03E-08
NB2122	HR-Event3	IPO5	MS	D251N	0,0010	0,05	0,2404	0,40	
NB1488	HR-Event3	ITSN1	MS	N1399D	0,0092	0,25	0,2845	0,45	
NB2186	HR-Event3	KAT8	FI	Q234fs	.	.	0,0009	0,10	
NB1952	HR-Event3	KCNK18	MS	E305K	0,0216	0,35	0,0057	0,10	
NB2181	HR-Event3	KCTD10	MS	G198R	0,1148	0,55	0,0076	0,10	
NB2181	HR-Event3	KDM1B	MS	V391A	0,0552	0,45	0,0183	0,10	
NB2181	HR-Event3	L1CAM	MS	R750H	0,0008	0,05	0,0101	0,10	
NB2181	HR-Event3	LINGO2	MS	G291A	0,0576	0,45	0,0134	0,10	
NB1488	HR-Event3	LLGL2	MS	A849D	0,2116	0,60	0,0123	0,10	
NB2136	HR-Event3	LRP6	MS	V528A	0,0042	0,15	0,0274	0,15	
NB2181	HR-Event3	LRRC17	MS	P351T	0,0886	0,50	0,0068	0,10	1,90E-04
STA-N-B7	High	LRRC17	MS	E146K	0,0756	0,50	0,0101	0,10	
NB2136	HR-Event3	MLL4	FD	G1198fs	.	.	0,0007	0,10	
NB1812	HR-Event3	MTF2	MS	S186P	0,0484	0,45	0,0095	0,10	
NB1506	HR-Event3	MYH7	MS	L557R	0,2194	0,60	0,0162	0,10	5,41E-04
CHP134	High	MYH7	MS	R1592Q	0,0434	0,45	0,0128	0,10	
NB1488	HR-Event3	MYLK2	MS	L291H	0,0140	0,25	0,0072	0,10	
NB2181	HR-Event3	NADK	II	G414delinsE	.	.	0,0219	0,10	
NB2136	HR-Event3	NAV1	FD	I833fs			0,0004	0,10	4,48E-05
NB2065	HR-Event3	NAV1	II	P50delinsPG			0,0257	0,10	
NB1812	HR-Event3	NAV3	MS	D876Y	0,0008	0,05	0,0091	0,10	3,15E-06
CHP134	High	NAV3	MS	D775H	0,0012	0,05	0,0074	0,10	
NB2388	HR-Event3	NBEAL1	MS	F2158L	0,0256	0,35	0,0078	0,10	
NB1952	HR-Event3	NCKAP1L	MS	C65F	0,0036	0,15	0,0062	0,10	
NB2181	HR-Event3	NEB	MS	P49525	0,0008	0,05	0,0164	0,10	1,33E-09
SK_N_BE2	High	NEB	MS	A3007T	0,0032	0,10	0,0173	0,10	
NB962	HR-Event3	NEB	SG	L1967X			0,0007	0,10	
KELLY	High	NEB	MS	Q3207P	0,1318	0,55	0,0151	0,10	
NB2136	HR-Event3	NELL1	MS	C350Y	0,0042	0,15	0,0055	0,10	
NB1767	HR-Event3	NIPBL	SG	E245X	.	.	0,0019	0,10	
NB1812	HR-Event3	OR1F1	MS	C127F	0,1808	0,55	0,0190	0,10	
NB1488	HR-Event3	OSBPL7	MS	Y69H	0,0236	0,35	0,0095	0,10	
NB2388	HR-Event3	PCDHGB1	MS	V590E	0,0804	0,50	0,0082	0,10	2,71E-04
IMR32	High	PCDHGB1	MS	G534C	0,0392	0,40	0,0122	0,10	
NB1506	HR-Event3	POLG	MS	T1072S	0,3806	0,65	0,0184	0,10	
NB2181	HR-Event3	PPA2	MS	K101T	0,3882	0,65	0,0233	0,10	
NB2181	HR-Event3	PREPL	MS	L644P	0,0266	0,35	0,0114	0,10	
NB2136	HR-Event3	PTEN	FD	I265fs	.	.	0,0003	0,10	
NB2122	HR-Event3	PTK2	MS	I860M	0,0276	0,35	0,0218	0,10	2,09E-06
NB2181	HR-Event3	PTK2	MS	R569L	0,0000	0,05	0,0054	0,10	
NB1767	HR-Event3	PTPRB	MS	W1571C	0,0376	0,40	0,0053	0,10	
NB1914	HR-Event3	PTPRO	MS	V467L	0,0036	0,15	0,0138	0,10	
NB2181	HR-Event3	PTPRQ	MS	D948V	0,0768	0,50	0,0248	0,10	
NB2181	HR-Event3	PXDN	MS	A414V	0,0392	0,40	0,0127	0,10	2,95E-04
SK-N-DZ	High	PXDN	MS	C1467S	0,2830	0,60	0,0086	0,10	
NB1488	HR-Event3	PYCR1	MS	Q142P	0,3882	0,65	0,0167	0,10	
NB1767	HR-Event3	RAD9B	MS	R26I	0,1618	0,55	0,0152	0,10	
NB1506	HR-Event3	RASGRF1	MS	G709S	0,0048	0,15	0,0166	0,10	
NB1887	Low	RET	SS	.	.	.	0,0172	0,10	
NB1488	HR-Event3	RPS13	MS	L28S	0,0710	0,50	0,0104	0,10	3,42E-04
NB1394	HR-Event3	RPS13	MS	Y38S	0,3258	0,65	0,0124	0,10	
NB2136	HR-Event3	RUNDC3B	MS	R91H	0,1362	0,55	0,0169	0,10	
NB1767	HR-Event3	SCN2A	MS	G642R	0,0326	0,40	0,0101	0,10	
NB1506	HR-Event3	SELENBP1	MS	P313L	0,0048	0,15	0,0140	0,10	
NB2181	HR-Event3	SH3TC2	MS	L759M	0,0074	0,20	0,0578	0,20	
NB2181	HR-Event3	SIAE	MS	L213P	0,0046	0,15	0,0053	0,10	
NB2186	HR-Event3	SIRPB2	MS	G123R	0,1770	0,55	0,0116	0,10	1,98E-04
NB3076	High	SIRPB2	MS	C180F	0,0616	0,50	0,0062	0,10	
NB1488	HR-Event3	SLC7A1	MS	M399I	0,5452	0,75	0,0078	0,10	
NB2181	HR-Event3	SLIT3	MS	G1138R	0,0630	0,50	0,0140	0,10	
NB2161	HR-Event3	SMAD5	SS	.	.	.	0,0119	0,10	
NB1488	HR-Event3	SMPD1	MS	P155S	0,1116	0,25	0,0370	0,15	
NB2181	HR-Event3	SOX18	MS	W319R	0,1246	0,55	0,0162	0,10	
NB1506	HR-Event3	SRA1	FI	V110fs	.	.	0,0060	0,10	
NB2181	HR-Event3	SRRD	MS	L159V	0,6512	0,80	0,0076	0,10	
NB1488	HR-Event3	STX6	MS	R132C	0,1008	0,55	0,0130	0,10	
NB2181	HR-Event3	SUGP1	MS	R608W	0,1588	0,55	0,0117	0,10	
NB1488	HR-Event3	SYT13	MS	P365T	0,3414	0,65	0,0162	0,10	
NB1690	HR-Event3	TAB3	MS	K640E	0,2712	0,60	0,0135	0,10	3,32E-04
NB2065	HR-Event3	TAB3	MS	V459I	0,0092	0,25	0,1081	0,30	
NB1816	HR-Event3	TBK1	MS	N42S	0,0140	0,25	0,7488	0,85	
NB2181	HR-Event3	TDRD7	MS	Y1090H	0,0094	0,25	0,0537	0,20	
KELLY	High	TENM4	MS	M2094I	0,0044	0,15	0,0092	0,10	
NB1488	HR-Event3	TNFRSF19	MS	C88Y	0,1332	0,55	0,0143	0,10	
NB1488	HR-Event3	TRIP10	MS	Y42S	0,0392	0,40	0,0064	0,10	
NB1488	HR-Event3	TSPAN9	MS	L226V	0,1204	0,55	0,0159	0,10	
NB1914	HR-Event3	TULP2	MS	S471L	0,0060	0,15	0,0066	0,10	
NB2161	HR-Event3	TYRO3	SS	.	.	.	0,0079	0,10	
NB2181	HR-Event3	UBR3	MS	S440Y	0,0986	0,55	0,0063	0,10	
NB1488	HR-Event3	UNC13B	SG	Q1396X	.	.	0,0006	0,10	
NB2161	HR-Event3	UNC79	MS	V1900G	0,0004	0,05	0,0067	0,10	
NB1794	HR-Event3	VIPR2	MS	C376S	0,3726	0,65	0,0070	0,10	
NB1952	HR-Event3	XIRP2	MS	R222W	0,1180	0,55	0,0218	0,10	
STA-N-B7	High	ZFHX3	MS	G699D	0,0902	0,50	0,0143	0,10	
NB1488	HR-Event3	ZKSCAN4	MS	L391F	0,2000	0,60	0,0218	0,10	
NB2388	HR-Event3	ZNF711	MS	S599T	0,0010	0,05	0,0263	0,15	
NB2181	HR-Event3	ZSCAN2	MS	F483C	0,0012	0,05	0,0071	0,10	

(MS: missense; SG: stop gain; FI: frameshift insertion; FD: frameshift deletion; II: Inframe Insertion; SS: splicing)

In yellow the potential cancer driver genes.

8.REFERENCES

1. London WB, Castleberry RP, Matthay KK, et al. 2005. Evidence for an age cutoff greater than 365 days for neuroblastoma risk group stratification in the Children's Oncology Group. J. Clin. Oncol. 2005 Sep 20;23(27):6459-65.23:6459–65

2. Carlsen NL. How frequent is spontaneous remission of neuroblastomas? Implications for screening. Br J Cancer 1990, 61(3):441-446.

3. Anderson DJ, Carnahan JF, Michelsohn A, Patterson PH. Antibody markers identify a common progenitor to sympathetic neurons and chromaffin cells in vivo and reveal the timing of commitment to neuronal differentiation in the sympathoadrenal lineage. J. Neurosci. 1991, 11, 3507–3519.

4. Brodeur GM, Pritchard J, Berthold F, et al. Revisions of the international criteria for neuroblastoma diagnosis, staging, and response to treatment. J Clin Oncol. 1993;11(8):1466–1477.

5. Cecchetto G, Mosseri V, De Bernardi B, et al. Surgical risk factors in primary surgery for localized neuroblastoma: the LNESG1 study of the European International Society of Pediatric Oncology Neuroblastoma Group. J. Clin. Oncol. 2005 Nov 20;23(33):8483-9

6. Cohn SL. Pearson AD, London WB et al. The International Neuroblastoma Risk Group (INRG) classification system: an INRG Task Force report. J. Clin. Oncol 2009.jan. 27:289–97

7. Brodeur GM, Seeger RC: Gene amplification in human neuroblastomas: basic mechanisms and clinical implications. Cancer Genet Cytogenet 1986, 19(1-2):101-111

8. Brodeur GM et al. Consistent N-myc copy number in simultaneous or consecutive neuroblastoma samples from sixty individual patients. Cancer Res 1987, 47(16):4248-4253.

9. Brodeur GM, Seeger RC, Schwab M, Varmus HE, Bishop JM. Amplification of N-myc in untreated human neuroblastomas correlates with advanced disease stage. Science 1984, 224(4653):1121-1124.

10. Schleiermacher G, Michon J, Ribeiro A, et al.: Segmental chromosomal alterations lead to a higher risk of relapse in infants with MYCN-non-amplified localised unresectable/disseminated neuroblastoma (a SIOPEN collaborative study). Br J Cancer 2011, 105 (12): 1940-8.

11. Defferrari R, Mazzocco K, Ambros IM, et al.: Influence of segmental chromosome abnormalities on survival in children over the age of 12 months with unresectable localised peripheral neuroblastic tumours without MYCN amplification. Br J Cancer 112 (2): 290-5, 201.

12. Brodeur GM: Neuroblastoma: biological insights into a clinical enigma. Nat Rev Cancer 2003, 3(3):203-216.

13. Spitz R, Betts DR, Simon T et al Favorable outcome of triploid neuroblastomas: a contribution to the special oncogenesis of neuroblastoma. Cancer Genet Cytogenet 2006, 167(1):51-56

14. Chen Y Takita J, Choi YL, et al: Oncogenic mutations of ALK kinase in neuroblastoma. Nature 2008, 455(7215):971-974.

15. Mosse YP, Laudenslager M, Longo L, et al: Identification of ALK as a major familial neuroblastoma predisposition gene. Nature 2008, 455(7215):930-935.

16. Capasso M, Diskin SJ, Totaro F, et al. Replication of GWAS-identified neuroblastoma risk loci strengthens the role of BARD1 and affirms the cumulative effect of genetic variations on disease susceptibility. Carcinogenesis. 2013 Mar;34(3):605-11. sis.

17. Nguyen LB, Diskin SJ, Capasso M, et al.Phenotype restricted genome-wide association study using a gene centric approach identifies threelow-risk neuroblastoma susceptibility loci. PLoS Genet. 2011;7(3):e1002026.

18. Maris JM, Mosse YP, Bradfield JP et al. Chromosome 6p22 locus associated with clinically aggressive neuroblastoma. N Engl J Med. 2008;358(24):2585–2593.

19. Wang K, Diskin SJ, Zhang H, et al. Integrative genomics identifies LMO1 as a neuroblastoma oncogene. Nature.2010;469(7329):216–220.

20. Bosse KR, Diskin SJ, Cole KA, et al. Common variation at BARD1 results in the expression of an oncogenic isoform that influences neuroblastoma susceptibility and oncogenicity. Cancer Res. 2012; 72(8):2068–2078.

21. Capasso M, Diskin S, Cimmino F et al Common genetic variants in NEFL influence gene expression and neuroblastoma risk. Cancer Res. 2014 Dec 1;74(23):6913-24.

22. Capasso M, Devoto M, Hou C, et al Common variations in BARD1 influence susceptibility to high-risk neuroblastoma. Nat Genet. 2009; 41(6):718–723.

23. Eleveld TF, Oldridge DA, Bernard V, et al.: Relapsed neuroblastomas show frequent RAS-MAPK pathway mutations. Nat Genet 2015; 47 (8): 864-71,.

24. Sausen M, Leary RJ, Jones S, et al. Integrated genomic analyses identify ARID1A and ARID1B alterations in the childhood cancer neuroblastoma. Nat Genet. 2013 ;45:12-17.

25. Pugh TJ, Morozova O, Attiyeh EF, et al. The genetic landscape of high-risk neuroblastoma. Nat Genet. 2013; 45:279-284.

26. Molenaar JJ, Koster J, Zwijnenburg DA, et al. Sequencing of neuroblastoma identifies chromothripsis and defects in neuritogenesis genes. Nature. 2012; 483:589-593.

27. Lasorsa VA,, Formicola D, Pignataro P,et al. Exome and deep sequencing of clinically aggressive neuroblastoma reveal somatic mutations that affect key pathways involved in cancer progression. Oncotarget. 2016 Apr 19;7(16):21840-52.

28. Kushner BH, LaQuaglia MP, Bonilla MA, et al.: Highly effective induction therapy for stage 4 neuroblastoma in children over 1 year of age. J Clin Oncol 1994 12 (12): 2607-13.

29. Marstrand, TT, Borup R, Willer A,. et al. A conceptual framework for the identification of candidate drugs and drug targets in acute promyelocytic leukemia. Leukemia 2010 24, 1265–75 .

30. Tan BT, Wang L, Li S, Long ZY, Wu YM, Liu Y. Retinoic acid induced the differentiation of neural stem cells from embryonic spinal cord into functional neurons in vitro. Int J Clin Exp Pathol. 2015 Jul 1;8(7):8129-35.

31. Comptour A, Rouzaire M, Belville C, Bouvier D, Gallot D, Blanchon L, Sapin V. Nuclear retinoid receptors and pregnancy: placental transfer, functions, and pharmacological aspects. Cell Mol Life Sci. 2016 Oct;73(20):3823-37. doi: 10.1007/s00018-016-2332-9.

32. Sidell N, Altman A, Haussler MR, Seeger RC.Effects of retinoid acid (RA) on the growth and phenotypic expression of several human neuroblastoma cell lines. Exp Cell. Res. 1983 148 21-30.

33. Yu AL, Gilman AL, Ozkaynak MF, et al.: Anti-GD2 antibody with GM-CSF, interleukin-2, and isotretinoin for neuroblastoma. N Engl J Med 363 (14): 1324-34, 2010

34. Cheung NK, Cheung IY, Kushner BH, et al.: Murine anti-GD2 monoclonal antibody 3F8 combined with granulocyte-macrophage colony-stimulating factor and 13-cis-retinoic acid in high-risk patients with stage 4 neuroblastoma in first remission. J Clin Oncol 30 (26): 3264-70, 2012.]

35. Vaupel, P., Mayer, A., & Hockel, M. (2004). Tumor hypoxia and malignant progression.Methods Enzymol 381, 335–35

36. Ghattass, K., Assah, R., El-Sabban, M. & Gali-Muhtasib, H. Targeting hypoxia for sensitization of tumors to radio- and chemotherapy. Curr Cancer Drug Targets. 13, 670–85 (2013).

37. Burroughs SK, Kaluz S, Wang D, et al. Hypoxia inducible factor pathway inhibitors as anticancer therapeutics. Future Med Chem. 5, 553–72 (2013).

38. Bersten DC, Sullivan, AE, Peet, DJ, Whitelaw, ML. (2013). bHLH-PAS proteins in cancer. Nat Rev Cancer 13, 827–841

39. Schofield CJ, Ratcliffe, PJ Oxygen sensing by HIF hydroxylases. Nat Rev Mol Cell Biol 2004 5, 343–354.

40. Ivan M., Kondo K., Yang H. et al., HIFalpha targeted for VHL-mediated destruction by proline hydroxylation: implications for O2 sensing. Science 2001; 292, 464–468.

41. Holmquist-Mengelbier L, Fredlund E, Lofstedt, T, et al. Recruitment of HIF-1alpha and HIF-2alpha to common target genes is differentially regulated in neuroblastoma: HIF-2alpha promotes an aggressive phenotype. Cancer Cell 2006 10, 413–423.

42. Tian, H, Hammer, RE, Matsumoto, AM, Russell, D.W, McKnight, SL Hypoxia-responsive transcription factor EPAS1 is essential for catecholamine homeostasis and protection against heart failure during embryonic development. Genes Dev 1998 12, 3320–3324.

43. Schnell, PO, Ignacak,M.L, Bauer, AL et al. Regulation of tyrosine hydroxylase promoter activity by the von Hippel–Lindau tumor suppressor protein and hypoxia-inducible transcription factors. J Neurochem 2003 85, 483–491.

44. Kumar, GK., Overholt, JL., Bright, GR et al. Release of dopamine and norepinephrine by hypoxia from PC-12 cells. Am J Phys 1998 274, C1592–C1600

45. Sandau, KB, Fandrey, J, Brune, B. Accumulation of HIF-1alpha under the influence of nitric oxide. Blood 2001 97, 1009–15

46. Hellwig-Burgel, T, Rutkowski K, Metzen, E, Fandrey J, Jelkmann, W. Interleukin-1beta and tumor necrosis factor-alpha stimulate DNA binding of hypoxia-inducible factor-1. Blood 1999 94, 1561–7

47. Feldser, D, Agani F, Iyer NV, et al. Reciprocal positive regulation of hypoxia-inducible factor 1alpha and insulin-like growth factor 2. Cancer Res 1999 59, 3915–8

48. Kietzmann, T, Mennerich, D, Dimova, EY. Hypoxia-Inducible Factors (HIFs) and Phosphorylation: Impact on Stability, Localization, and Transactivity. Front Cell Dev Biol 2016.

49. Pietras A., Johnsson, AS, Pahlman S. The HIF-2α-driven pseudo-hypoxic phenotype in tumor aggressiveness, differentiation, and vascularization. Curr. Top. Microbiol. Immunol 20 10; 345, 1–20

50. Johnson AB, Barton MC Hypoxia-induced and stress-specific changes in chromatin structure and function. Mutat Res 2007, 618:149-162.

51. Watson JA, Watson CJ, McCann A, Baugh J. Epigenetics 2010, The epicenter of the hypoxic response. Epigenetics, 5:293-296

52. Beyer S, Kristensen MM, Jensen KS, Johansen JV, Staller P. The histone demethylases JMJD1A and JMJD2B are transcriptional targets of hypoxia-inducible factor HIF.J Biol Chem. 2008 Dec 26;283 (52) : 36542-52 .

53. Kang MK, Mehrazarin S, Park NH, Wang CY. Epigenetic gene regulation by histone demethylases: emerging role in oncogenesis and inflammation. Oral Dis. 2016 Aug 11.

54. Cloos PA, Christensen J, Agger K, Helin K.Erasing the methyl mark: histone demethylases at the center of cellular differentiation and disease. Genes Dev 2008, 22:1115-1140.

55. Estaras C, Fueyo R, Akizu N, Beltran S, Martinez-Balbas MA. RNA polymerase II progression through H3K27me3-enriched gene bodies requires JMJD3 histone demethylase. Mol Biol Cell 2013, 24:351-360.

56. Axelson, H., Fredlund, E., Ovenberger, M., Landberg, G. & Pahlman, S. Hypoxia-induced dedifferentiation of tumor cells-a mechanism behind heterogeneity and aggressiveness of solid tumors. Semin Cell Dev Biol. 2005; 16, 554–63.

57. Jogi, A., Vallon-Christersson J, Holmquist L. et al. Human neuroblastoma cells exposed to hypoxia: induction of genes associated with growth, survival, and aggressive behavior. Exp Cell Res 2004. 295, 469–87.

58. Merrill, RA, Ahrens JM, Kaiser ME. et al. All-trans retinoic acid-responsive genes identified in the human SH-SY5Y neuroblastoma cell line and their regulated expression in the nervous system of early embryos. Biol Chem 2004; 385, 605–14.

59. Chambaut-Guérin AM, Hérigault, S, Rouet-Benzineb P, Rouher C. & Lafuma C. Induction of matrix metalloproteinaseMMP-9 (92-kDa gelatinase) by retinoic acid in human neuroblastoma SKNBE cells: relevance to neuronal differentiation. J Neurochem 2000; 74, 508–17

60. Zhang B, Metharom P, Jullie H. et al. The significance of controlled conditions in lentiviral vector titration and in the use of multiplicity of infection (MOI) for predicting gene transfer events. Genet Vaccines 2004.Ther. 2, 6

61. Clark, O., Daga, S. & Stoker, A. W. Tyrosine phosphatase inhibitors combined with retinoic acid can enhance differentiation of neuroblastoma cells and trigger ERK- and AKT-dependent, p53-independent senescence.Cancer Lett 2013; 328, 44–54

62. Livak KJ, Schmittgen TD. Analysis of relative gene expression data using real-time quantitative PCR and the 2-ΔΔCT Method. Methods 2001; 25, 402–8 (

63. Andrews S. (2010) Babraham Bioinformatics Institute (simon.andrews@bbsrc.ac.uk)

64. Conrad, PW., Freeman, TL., Beitner-Johnson D, Millhorn, DE. EPAS1 trans-activation during hypoxia requires p42/p44 MAPK. J Biol Chem 1999; 274, 33709–13.

65. Celay, J. Blanco I, Lázcoz P. et al. Changes in gene expression profiling of apoptotic genes in neuroblastoma cell lines upon retinoic acid treatment.PLoS One. 2013; 8, e62771.

66. Coltella N. Percio S, Valsecchi R et al. HIF factors cooperate with PML-RARα to promote acute promyelocytic leukemia progression and relapse. EMBO Mol Med 2014; 6, 640–50.

67. Meller, K. Gradient isolation of glial cells: evidence that flat epithelial cells are astroglial cell precursors. Cell Tissue Res 1987; .249,79–88.

68. Dimri GP, Lee X, Basile G. et al. A biomarker that identifies senescent human cells in culture and in aging skin in vivo. Proc Natl Acad Sci USA 1995; 92, 9363–7.

69. Li H, Wang Y, Chen Z. et al Novel multiple tyrosine kinase inhibitor ponatinib inhibits bFGF-activated signaling in neuroblastoma cells and suppresses neuroblastoma growth in vivo.), Oncotarget.2016.

70. Cantilena S, Pastorino F, Pezzolo A. et al. Frizzled receptor 6 marks rare, highly tumourigenic stem-like cells in mouse and human neuroblastomas Oncotarget. 2011 Dec;2(12):976-83.

71. Terranova C, Narla ST, Lee YW. et al Global Developmental Gene Programing Involves a Nuclear Form of Fibroblast Growth Factor Receptor-1 (FGFR1). PLoS One. 2015 Apr 29;10(4):e0123380. doi: 10.1371/journal.pone.0123380. eCollection 2015.

72. Elizalde C, Campa VM, Caro M. et al Distinct roles for Wnt-4 and Wnt-11 during retinoic acid-induced neuronal differentiation Stem Cells. 2011 Jan;29(1):141-53. doi: 10.1002/stem.562.

73. Eleveld TF, Oldridge DA, Bernard V et al. Relapsed neuroblastomas show frequent RAS-MAPK pathway mutations. Nat Genet. 2015; 47(8):864-71

74. Maris, J. M., Hogarty, M. D., Bagatell, R. & Cohn, S. L. Neuroblastoma. Lancet. 2007; 23, 2106–20.

75. Øra, I. & Eggert, A. Progress in treatment and risk stratification of neuroblastoma: impact on future clinical and basic research.

76. Matthay, KK. Villablanca JG, Seeger RC. et al. Treatment of high-risk neuroblastoma with intensive chemotherapy, radiotherapy, autologous bone marrow

transplantation, and 13-cis-retinoic acid. Children's Cancer Group. N Engl J Med. 1999; 341, 1165–73.

77. Giaccone G, Pinedo, HM. Drug Resistance. Oncologist 1996; 1, 82–87.

78. Axelson, H., Fredlund, E., Ovenberger, M., Landberg, G. & Påhlman, S. Hypoxia-induced dedifferentiation of tumor cells-a mechanism behind heterogeneity and aggressiveness of solid tumors. Semin Cell Dev Biol 2005; 16, 554–63.

79. Hussein, D., Estlin, E. J., Dive, C. & Makin, G. W. Chronic hypoxia promotes hypoxia-inducible factor-1alpha-dependent resistance to etoposide and vincristine in neuroblastoma cells. Mol Cancer Ther 2006; 5, 2241–50.

80. Wang, D. et al. Hypoxia promotes etoposide (VP-16) resistance in neuroblastoma CHP126 cells. Pharmazie 2010; 65, 51–6.

81. Kummar, S. Raffeld M, Juwara L. et al. Multihistology, target-driven pilot trial of oral topotecan as an inhibitor of hypoxia-inducible factor-1α in advanced solid tumors. Clin Cancer Res 2011; 17, 5123–31

82. Onnis, B., Rapisarda, A. & Melillo, G. Development of HIF-1 inhibitors for cancer therapy. J Cell Mol Med 2009;13, 2780–6

83. Park, S. H., Lim, J. S. & Jang, K. L. All-trans retinoic acid induces cellular senescence via upregulation of p16, p21, and p27.Cancer Lett 2011; 310, 232–9.

84. Kilic Eren, M. & Tabor, V. The role of hypoxia inducible factor-1 alpha in bypassing oncogene-induced senescence. PLoS One 2014; 9, e101064

85. Liu, S. Tian Y, Chlenski A. et al. 'Cross-talk' between Schwannian stroma and neuroblasts promotes neuroblastoma tumor differentiation and inhibits angiogenesis. Cancer Lett 2005; 228, 125–31

86. Watson J.A. Watson CJ, McCrohan AM. et al. Generation of an epigenetic signature by chronic hypoxia in postate cells Hum Mol Genet. 2009 Oct 1;18(19):3594-604.

9. LIST OF PUBLICATIONS

Proteomic Alterations in Response to Hypoxia Inducible Factor 2α in Normoxic Neuroblastoma Cells.
Cimmino F, Pezone L, **Avitabile M**, Persano L, Vitale M, Sassi M, Bresolin S, Serafin V, Zambrano N, Scaloni A, Basso G, Iolascon A, Capasso M.
J Proteome Res. 2016 Oct 7;15(10):3643-3655.

CD55 is a HIF-2α marker with anti-adhesive and pro-invading properties in Neuroblastoma.
Cimmino F, **Avitabile M**, Pezone L, Scalia G, Montanaro D, Andreozzi M, Terracciano L, Iolascon A, Capasso M.
Oncogenesis. 2016 Apr 4;5:e212.

Inhibition of hypoxia inducible factors combined with all-trans retinoic acid treatment enhances glial transdifferentiation of neuroblastoma cells
Cimmino F, Pezone L, **Avitabile M**, Acierno G, Andolfo I, Capasso M, Iolascon A
Sci Rep. 2015 Jun 9;5:11158.